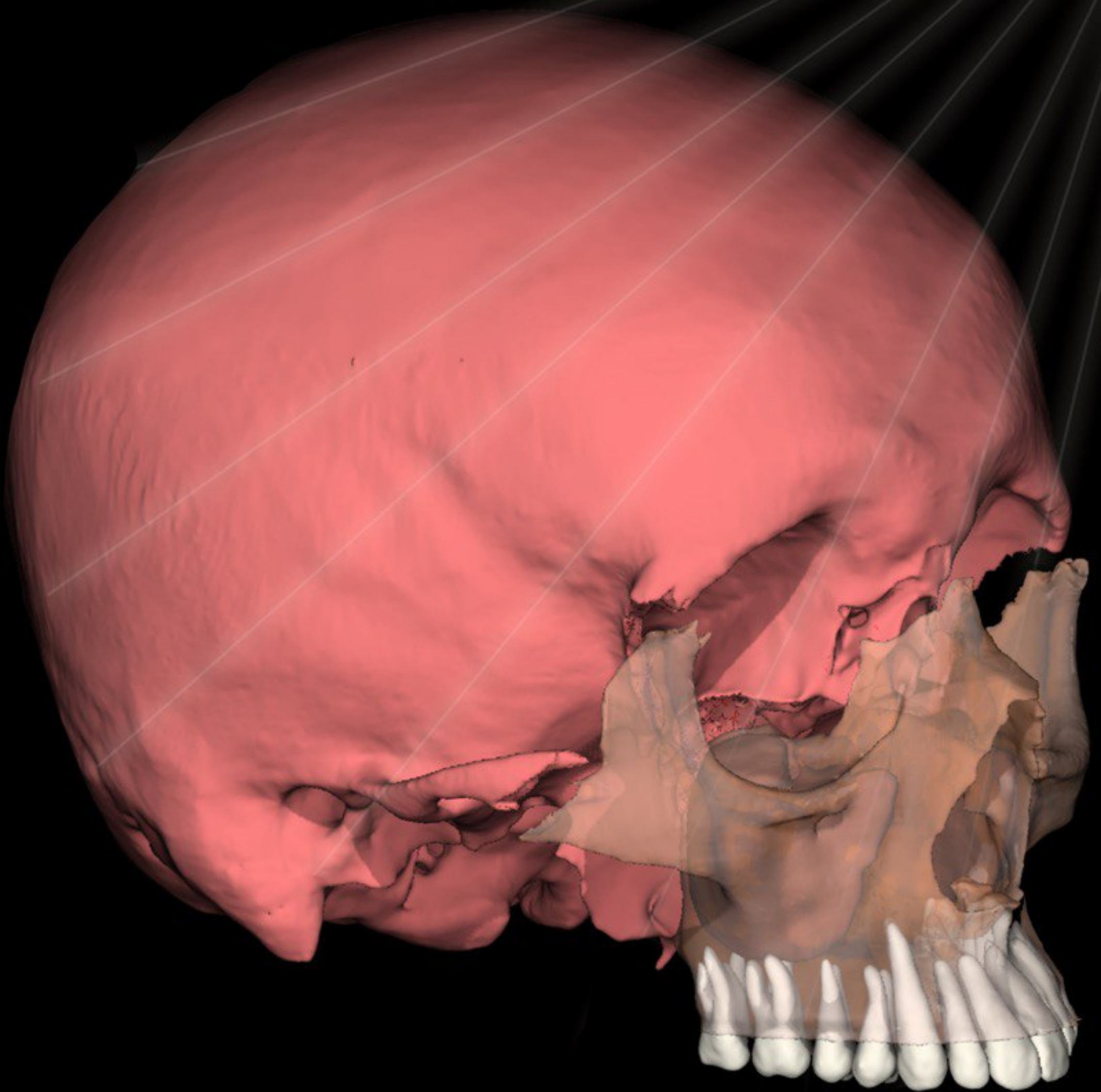


ARTIFICIAL INTELLIGENCE FOR SEGMENTATION OF MIDFACIAL STRUCTURES ON CBCT IMAGES



Nermin Morgan
2022

ARTIFICIAL INTELLIGENCE FOR SEGMENTATION OF MIDFACIAL STRUCTURES ON CBCT IMAGES

Nermin Morgan

Dissertation presented in
partial fulfilment of the
requirements for the
degree of Doctor in
Biomedical Sciences

Jury:

Supervisor: Prof. Dr. Reinhilde Jacobs

Chair examining committee: Prof. Dr. Steven Dymarkowski

Chair public defence: Prof. Dr. Tania Roskams

Jury members: Prof. Dr. Carine Carels

Prof. Ir. Peter Claes

Prof. Dr. Benjamin Salmon

Prof. Dr. Krisztián Nagy

December 2022

KUNSTMATIGE INTELLIGENTIE VOOR SEGMENTATIE VAN MIDDENGEZICHTSSTRUCTUREN OP CBCT-BEELDEN

Nermin Morgan

Proefschrift voorgedragen
tot het behalen van de
graad van Doctor in de
Biomedische
Wetenschappen

Jury:

Promotor: Prof. Dr. Reinhilde Jacobs

Voorzitter leescommissie: Prof. Dr. Steven Dymarkowski

Voorzitter openbare verdediging: Prof. Dr. Tania Roskams

Juryleden: Prof. Dr. Carine Carels

Prof. Ir. Peter Claes

Prof. Dr. Benjamin Salmon

Prof. Dr. Krisztián Nagy

December 2022

PREFACE

This doctoral thesis consists of 5 research articles, preceded by a scientific introduction and concluded by a general discussion, conclusion, and future perspectives. The research articles follow the standard scientific IMRAD structure (Introduction, Methods, Results, and Discussion), and were based on the following peer-reviewed publications:

Article 1

Preda F, **Morgan N**, Van Gerven A, Nogueira-Reis F, Smolders A, Wang X, Nomidis S, Shaheen E, Willems H, Jacobs R. Deep convolutional neural network-based automated segmentation of the maxillofacial complex from cone-beam computed tomography: A validation study. *J Dent.* 2022 Sep;124:104238. doi: 10.1016/j.jdent.2022.104238. Epub 2022 Jul 21. PMID: 35872223. (shared first-authorship)

Article 2

Morgan N, Van Gerven A, Smolders A, de Faria Vasconcelos K, Willems H, Jacobs R. Convolutional neural network for automatic maxillary sinus segmentation on cone-beam computed tomographic images. *Sci Rep.* 2022 May 7;12(1):7523. doi: 10.1038/s41598-022-11483-3. PMID: 35525857; PMCID: PMC9079060.

Article 3

Nogueira-Reis F, **Morgan N**, Nomidis S, Van Gerven A, Oliveira-Santos N, Jacobs R, Tabchoury CPM. Three-dimensional maxillary virtual patient creation by convolutional neural network-based segmentation on cone-beam computed tomography images. *Clin Oral Investig.* 2022 Sep 17. doi: 10.1007/s00784-022-04708-2. Epub ahead of print. PMID: 36114907.

Article 4

Morgan N, Shujaat S, Jazil O, Jacobs R. Three-dimensional quantification of skeletal midfacial complex symmetry. *Int J CARS* (2022). <https://doi.org/10.1007/s11548-022-02775-0>

Article 5

Morgan N, Cortellini S, Shujaat S, Nogueira-Reis F, Temmerman A, Quirynen M, , Jacobs R. Artificial intelligence-assisted evaluation of volumetric bone graft changes following maxillary sinus augmentation. *Journal of clinical periodontology*. (Submitted)

PERSONAL ACKNOWLEDGEMENTS

First and foremost, I would like to sincerely thank my supervisor, **Prof. Reinhilde Jacobs**, for her guidance, support, and patience throughout the PhD. She motivated me greatly, and without her encouragement and invaluable assistance, this PhD would not have been possible.

I wish to express my deep sense of gratitude to my colleague, **Dr. Sohaib Shujaat**. I greatly acknowledge his moral support and assistance during my PhD.

I would like to express my heartfelt thanks to my colleagues and friends at the **OMFS-IMPATh Research Group** for their steadfast encouragement and support.

Most of all, I would like to thank **my parents**, and **my sisters** for their love, support, and encouragement in the past 4 years.

Table of Contents

Preface.....	i
Personal acknowledgements.....	iii
Table of Contents.....	iv
List of Abbreviations.....	vi
General introduction.....	1
1. Digitalization in dentistry.....	1
1.1 CBCT data acquisition.....	5
1.2 Segmentation	6
1.2.1 Manual segmentation.....	6
1.2.2 Semi-automated segmentation.....	6
1.2.3 Automated segmentation.....	7
2. Midfacial structures.....	9
2.1 Midfacial skeletal complex.....	9
2.2 Maxillary sinus.....	9
3. Clinical applications.....	10
3.1 Symmetry assessment.....	10
3.2 Sinus graft follow-up.....	11
4. Aims and Hypotheses.....	12
5. References.....	14
Part 1- Automated segmentaion	24
Article 1 - Deep convolutional neural network-based automated segmentation of the maxillofacial complex from cone-beam computed tomography: A validation study	25
Article 2 - Convolutional neural network for automatic maxillary sinus segmentation on cone-beam computed tomographic images.....	47
Article 3 - Three-dimensional maxillary virtual patient creation by convolutional neural network-based segmentation on cone-beam computed tomography images	64

Part 2 – Clinical applications of automated segmentation.....	78
Article 4 - Three-dimensional quantification of skeletal midfacial complex symmetry.....	79
Article 5 - Artificial intelligence-assisted evaluation of volumetric bone graft changes following maxillary sinus augmentation	97
General discussion, conclusions, and future perspectives	114
Summary	124
Samenvatting	126
Scientific acknowledgements	128
Personal contributions.....	129
Conflicts of Interest	130
Curriculum Vitae and List of Publications	131

List of abbreviations

CAD/CAM	Computer-aided design/computer-aided manufacturing
3D	Three-dimensional
CT	Computed tomography
CBCT	Cone-beam computed tomography
MRI	Magnetic resonance imaging
FOV	Field of view
MPR	Multiplanar reconstructed
TMJ	Temporomandibular joint
2D	Two-dimensional
HU	Hounsfield units
AI	Artificial intelligence
DL	Deep learning
IQ	Intelligence quotient
ANN	Artificial neural network
CNN	Convolutional neural network
GPU	Graphics processing unit
ReLU	Rectified linear unit
MVP	Maxillary virtual patient
DSC	Dice similarity coefficient
DICOM	Digital Imaging and Communications in Medicine
STL	Standard Tessellation Language
HD	Hausdorff distance
IoU	Intersection over union
RMS	Root mean square
MSCT	Multi-slice computed tomography
ROI	Region of interest
TEM	Technical error of measurements
rTEM	Relative technical error of measurements
ICC	Intraclass correlation coefficient
DBBM	Deproteinized bovine bone mineral
L-PRF	Leukocyte and Platelet Rich Fibrin

General introduction

Aims & Hypotheses

1. Digitalization in dentistry

Digital dentistry refers to the incorporation of computer-controlled components and dental technologies for assisting dental professionals with patient communication, diagnostics, treatment planning, and follow-up evaluation. Some examples of devices and tools categorized under digital dentistry include, intraoral scanners, computer-aided design/computer-aided manufacturing (CAD/CAM) hardware and software programs, three-dimensional (3D) printers, virtual and augmented reality and digital radiographic devices (computed tomography [CT], cone-beam CT [CBCT], magnetic resonance imaging [MRI]). This digitization of workflows in clinical dentistry has overcome the limitations associated with traditional methods by offering improved precision of dental procedures, time-efficiency and higher standard of patient care^{1, 2}.

In recent years, digital technologies have been implemented in the majority of dentomaxillofacial workflows such as, restorative dentistry, orthodontics, dental implantology and maxillofacial reconstructive surgery³. The replacement of dental impression materials with intra-oral scanners has revolutionized fabrication of fixed and removable prostheses. With the use of CAD/CAM technology, it is now possible to deliver dental restorative treatment at a single visit with predictable outcomes⁴⁻⁹. In orthodontics, virtual planning with the application of digital models has enabled simulation of orthodontic treatment (Figures 1), virtual tooth set-up (Figure 2), tracking of treatment progress at follow-up and fabrication of orthodontic appliances via 3D printing¹⁰⁻¹². The digital workflows in dental implantology have facilitated 3D simulation of implant placement with high precision (Figure 3) and designing of surgical guides^{13, 14}. In maxillofacial reconstructive surgery, multimodal image registration (Figure 4) involving a combination of CBCT, intra-oral scan and/or facial soft tissue, and computer-assisted fabrication of surgical guides have improved outcomes of orthognathic and other reconstructive surgical procedures with a decrease in blood loss and less operation time. Furthermore, the incorporation of dynamic navigation systems in digital workflows of implantology and reconstructive surgery have improved the accuracy of surgical procedures compared to freehand approaches by providing real-time guidance^{15, 16}.

Although the steps involved in digital workflows may vary depending on the procedure being planned, certain commonalities are shared by these workflows, which include 3D CBCT-based data acquisition and segmentation, for creating a virtual model of the anatomical structures³.

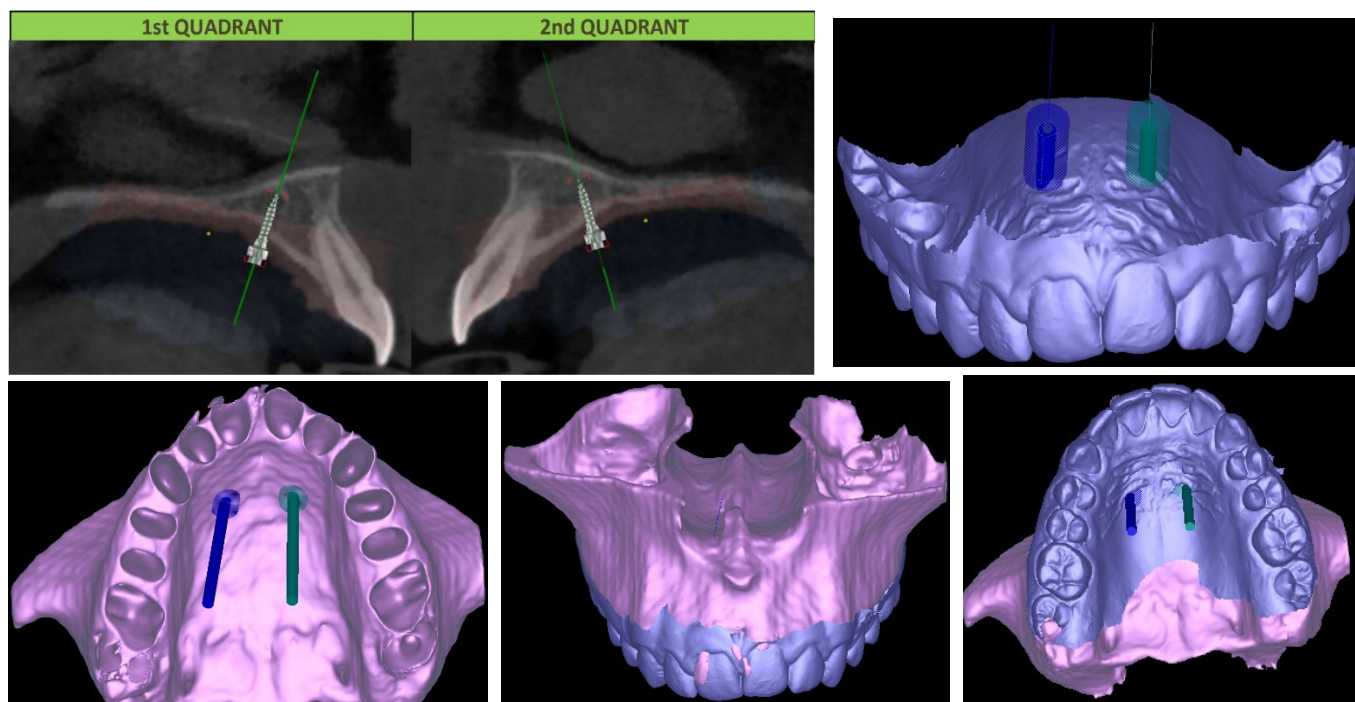


Figure 1. Digital workflow of mini-implant placement in maxilla: A) CBCT scan with inserted mini-implants in OnyxCeph^{3TM}, B) Intraoral scan, C) 3D virtual model of segmented maxilla from CBCT, D) registered intraoral and CBCT scans in Planmeca Romexis®.

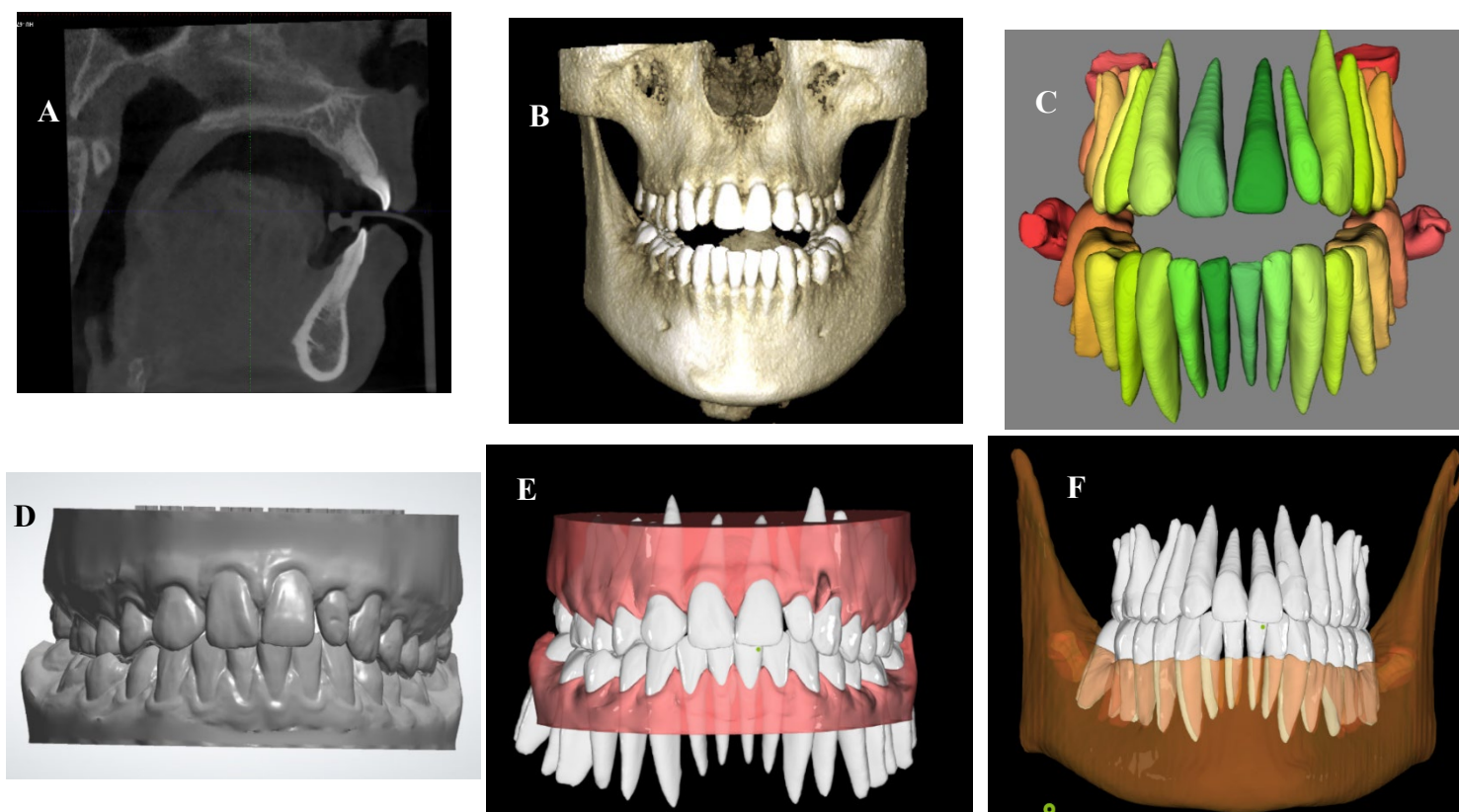


Figure 2. Digital workflow of orthodontic setup: A)&B) CBCT scan and 3D reconstructed model in Planmeca Romexis®, C) 3D virtual model of segmented teeth from CBCT ((creator.relu.eu, Relu BV), D) intraoral scan (3shape), E) segmented intraoral scan registered with segmented teeth (OnyxCeph^{3TM}), F) segmented mandible registered with intraoral scan(Relu platform).

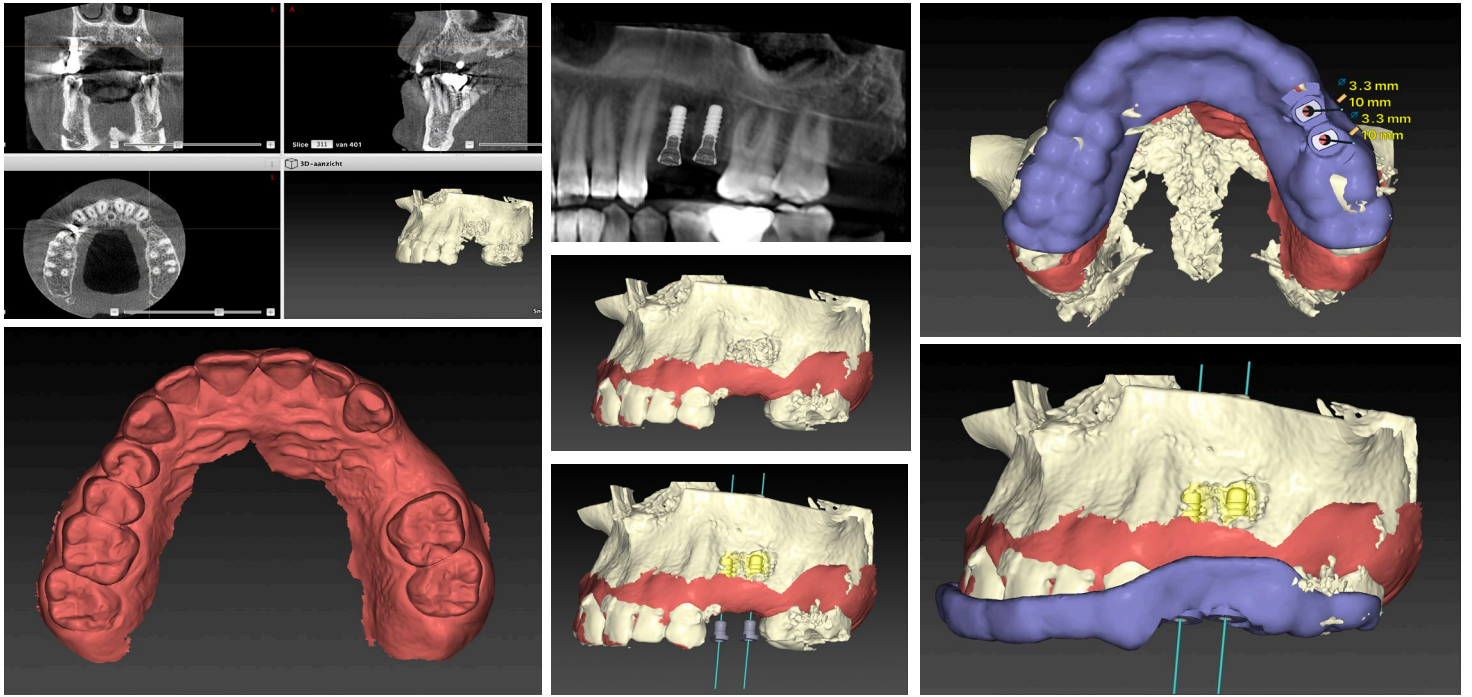


Figure 3. Digital workflow of virtual implant placement (yellow color) with surgical guide (purple color) planning in maxillary arch showing registered CBCT reconstructed model, intraoral scan (red color), and designed surgical guide (purple color) in Planmeca Romexis®.

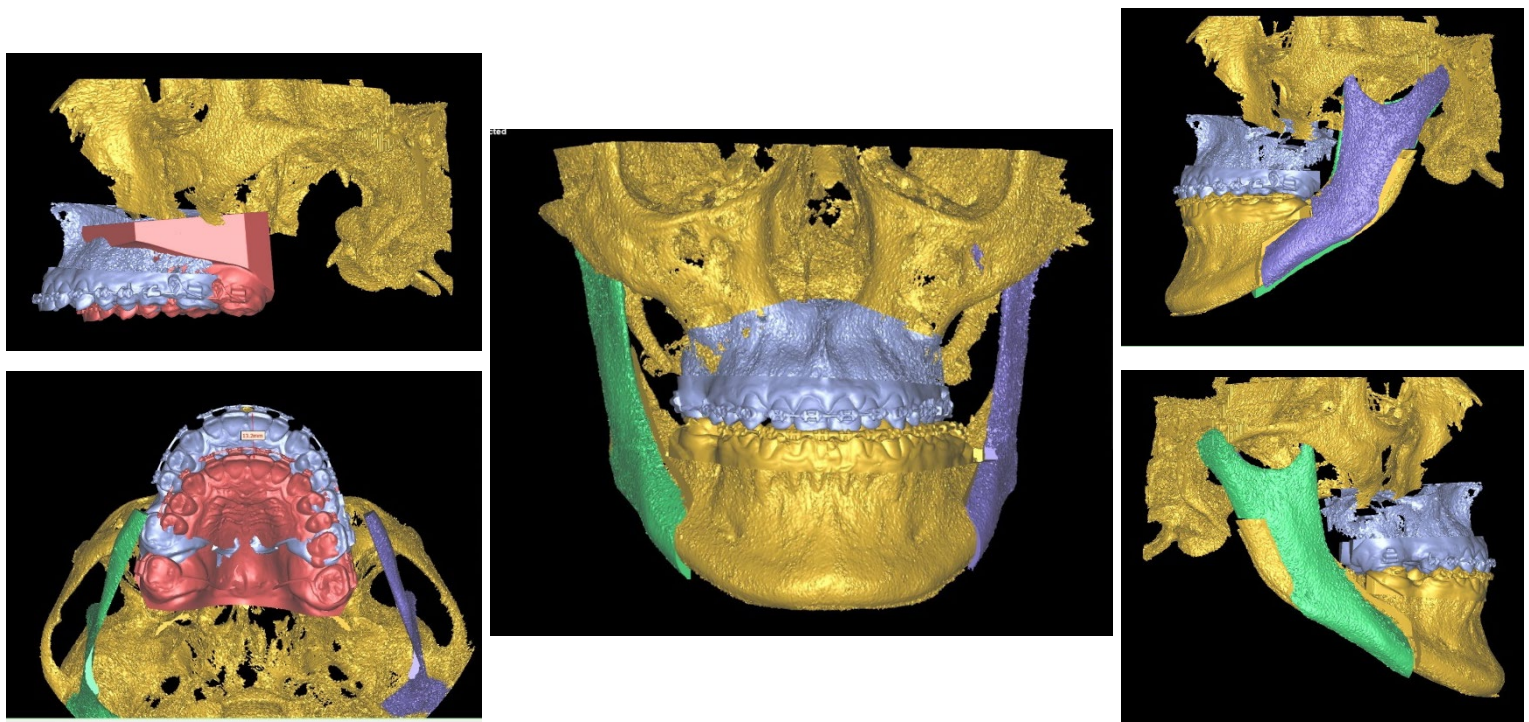


Figure 4. Digital workflow of bimaxillary advancement surgical planning showing CBCT reconstructed model (yellow color), registered intraoral scan (red color), and planned moved parts (blue and green colors) in 3D Surgery™, Dolphin.

1.1 CBCT data acquisition

Since the development of CBCT imaging in the early 1980s, it has been widely employed for diagnosis, pre-operative treatment planning, and post-operative follow-up evaluation in all fields of dentistry¹⁷. The conventional CT devices have almost become obsolete and replaced with CBCT imaging for dentomaxillofacial applications owing to the following reasons:

Size and cost: CBCT equipment has a much smaller size and physical footprint, and it costs around one-fourth to one-fifth the price of a CT device.

Variable field of view (FOV): The ability of CBCT devices to optimally collimate the primary x-ray beam and only cover the area of interest has made it possible to select patient-specific FOVs depending on the task at hand.

Fast acquisition: Scan time is drastically reduced to less than 30 seconds due to advancements in solid state detector frame rate, improved computer processing speed, and the ability of CBCT devices to capture all projection pictures in a single turn.

Sub-millimeter resolution: As an x-ray detector, most CBCT units use “mega pixel solid state devices” for high resolution imaging with voxel sizes ranging from 0.076 to 0.125 mm isotropically, which is optimal for radiologically examining fine dental details such as periodontal space, root canals, root resorption or fracture, and peri-implant bone defects.

Low patient radiation dose: In contrast to CT imaging, the absorbed dose from CBCT is highly reduced. A traditional CT exposes patients to 6-8 times more radiation compared to CBCT when scanning either maxilla or mandible¹⁸, while 18 times more for capturing both maxilla and mandible¹⁹.

Interactive analysis: Although CT data is digital, the images are normally made available to clinicians as hard copies on film transparencies. Furthermore, CT software packages for data reformatting require workstations with high computational power. In contrast, CBCT data is provided in digital format and data reconstruction can be performed using personal computers with low power. The CBCT raw datasets are also “isotropic” in nature, hence allowing image reorientation based on patient’s anatomic structures. In addition, the availability of user-friendly algorithms provides clinicians with the ability to interact with the images in real-time and easily perform dimensional assessments¹⁷.

Unique display modes for maxillofacial imaging: CBCT devices have more advanced image processing functions compared to CT imaging. In addition to reconstructing conventional multiplanar reconstructed (MPR) images in coronal, sagittal, and axial orthogonal planes, CBCT also provides

oblique MPR, curved oblique MPR, and cross-sectional MPR views. These views facilitate diagnostics and planning in dentomaxillofacial workflows by providing reconstructed images generally employed in a clinical setting, such as cephalometry, panoramic, and temporomandibular joint (TMJ) multiplanar images. Moreover, 3D volumetric surface generation of the anatomical region of interest is also possible using volume rendering techniques commonly based on maximum intensity projection.

Even though CBCT imaging has been regarded as a standard for dentomaxillofacial imaging, it is still prone to certain limitations, such as limited contrast resolution for soft tissue visualization and image degradation due to the presence of metal and motion artifacts.

1.2 Segmentation

The first and most essential step in the majority of digital dental workflows is segmentation, a process by which regions of interest are extracted from CBCT images for generating 3D models of the dentomaxillofacial structures. Any flaw in this step would negatively impact the final outcome. Segmentation techniques are usually divided into three categories: manual, semi-automatic, and automatic²⁰.

1.2.1 Manual segmentation

Manual segmentation refers to a slice-by-slice delineation of the region of interest on two-dimensional (2D) CBCT planes by an expert and acts as a clinical standard for segmentation. However, it is prone to certain limitations, such as labor-intensiveness, increased time-consumption, and observer variability^{21, 22}.

1.2.2 Semi-automated segmentation

Based on the aforementioned limitations, semi-automatic segmentation has been widely adopted for segmentation of CBCT images in dentomaxillofacial workflows, mostly via thresholding-based approaches^{23, 24}. These approaches function by selecting the most appropriate threshold level for the region of interest based on images pixel values, which is automatically expanded to the rest of slices. Hence, eliminating the need for slice-by-slice segmentation. However, this threshold level is selected based on the principle that the entire region of interest has a similar density. Therefore, the final segmentation lacks optimal delineation due to the presence of different structural densities, and manual post-processing is often required. Thin bony structures also require manual intervention to segment due to limited threshold selection values. In addition, presence of metal artifacts further makes it difficult to segment owing to a high intensity similarity of grey values between bone and artifacts²⁵.

These limitations are due to the fact that the currently available dentomaxillofacial segmentation software programs have been optimized based on CT data, which cannot be applied to CBCT scans due to the presence of uncalibrated absolute Hounsfield units (HU), beam hardening artifacts, noise, and low-contrast resolution²⁶⁻²⁸.

1.2.3 Automated segmentation

Artificial intelligence (AI) in the form of deep learning (DL) has been employed for automated segmentation to overcome the limitations associated with both manual and semi-automated segmentation approaches. The term “artificial intelligence” was first coined in 1956 by John Macarthy. It is broadly defined as the ability of computers and machines to mimic human intelligence quotient (IQ)²⁹. Machine learning is a subset of AI that builds algorithms and rules guided majorly by structured data and has the ability to capture intrinsic statistical patterns and structure by learning. It has been widely applied for problem-solving tasks, decision-making processes, and uncovering patterns and trends in data³⁰. DL is defined as a subset of machine learning which uses artificial neural networks (ANNs) that partially resemble neural networks of the human brain and rely on an enormous amount of structured and/or unstructured data as a core for solving complex problems. It surpasses its predecessor, machine learning, in performance by offering an improved ability to deal with high dimensional data with multiple predictor variables. Besides, DL can automatically learn feature hierarchies such as edges, shapes, and corners³¹, define what is important and predict the output³².

In deep learning, convolutional neural networks (CNNs) have demonstrated excellent performance in the field of image analysis. It employs multi-layer neural computational connections for image processing tasks such as classification and segmentation³¹. However, CNN-based deep learning approaches require a large amount of labeled data for training and a specialized graphics processing unit (GPU) for the construction of automated models. There is also an issue of model generalizability, where the trained model might not perform well with a dataset acquired with different devices having variable acquisition parameters. In addition, the training for segmentation is usually performed by a single observer; hence, the built model might have the same bias as the observer²⁰. In the midst of these limitations, the main advantages of deep-learning based automated segmentation are its high performance, consistency, and reproducibility.

U-Net, one of the most popular DL-based CNN architectures, has been widely employed for medical image segmentation tasks³³. It consists of a contracting path (encoder) and an expansive path (decoder), giving the U-shaped architecture. In addition, its contracting path follows a typical architecture of a CNN model that consists of repeated applications of convolutions, followed by a rectified linear unit (ReLU) and max pooling operations, while in the expansive path, pooling layers are replaced by upsampling layers to increase the resolution of the output³³ (Figure 5).

For volumetric segmentation of medical images, 3D U-Net, an extension of U-Net is commonly used, which replaces 2D operations with their 3D counterparts. This enables to directly take the entire 3D image as an input to train the model rather than taking each slice separately³⁴. Since their development, U-Net models have been successfully applied for various medical image segmentation tasks, such as segmentation of skin lesions on dermoscopy images³⁵, brain tumor on MR images³⁶, and heart on the diffusion tensor cardiac MR images³⁷.

Recently, in the field of dentomaxillofacial radiology, 3D U-Net architectures have been trained for the automated segmentation of craniofacial anatomical structures (mandible^{38, 39}, mandibular canal^{40, 41}, pharyngeal airway space⁴², teeth^{43, 44}), facilitating diagnosis and computer-guided treatment planning in dental implantology, traumatology, orthognathic surgery, and other reconstructive surgical procedures. However, no evidence exists related to the automated segmentation of midfacial structures.

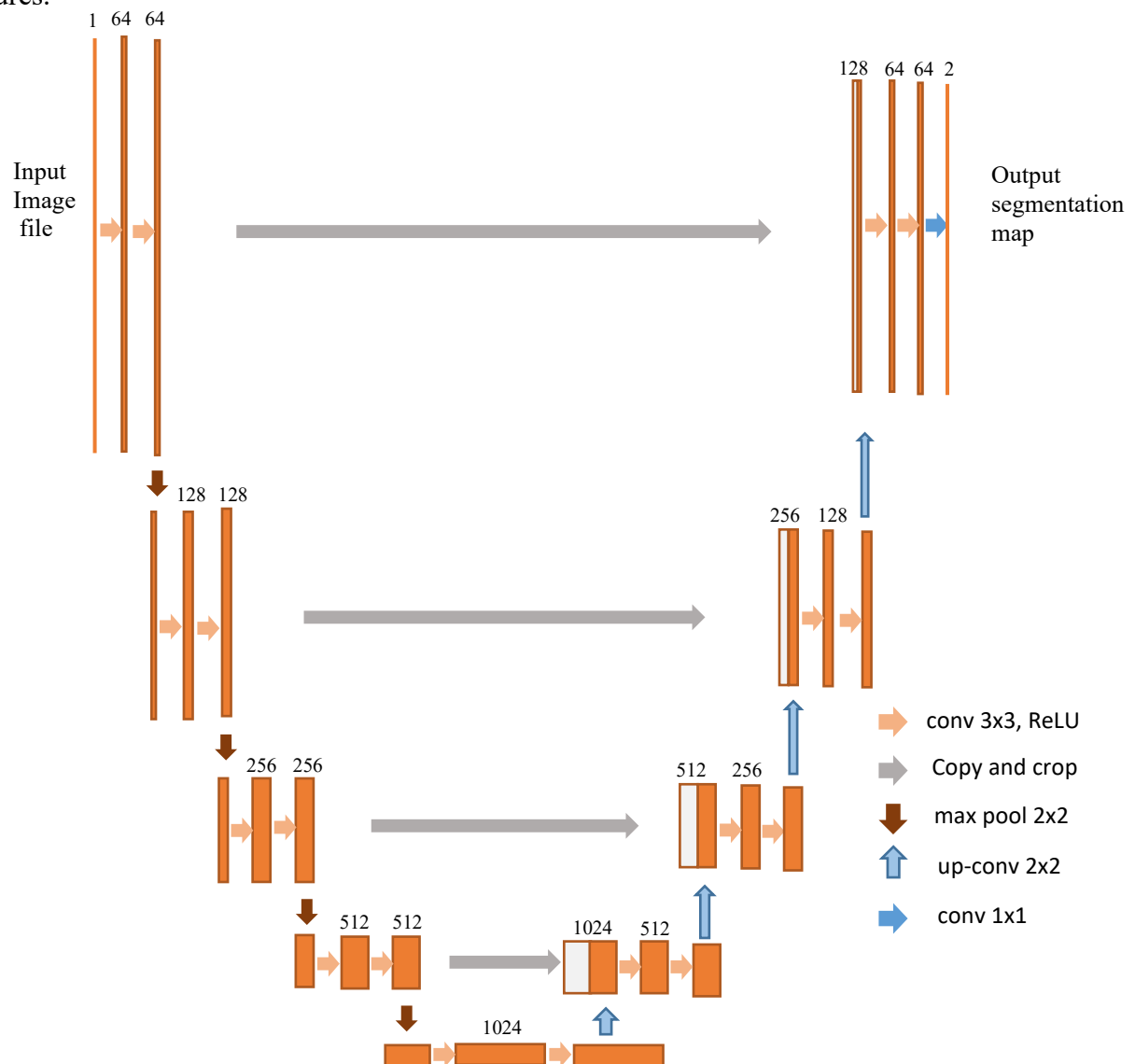


Figure 5. U-net architecture (example for 32x32 pixels in the lowest resolution). The orange boxes corresponds to a multi-channel feature map. The number of channels is denoted on top of the box. White boxes represent copied feature maps. The arrows denote the different operations.

2. Midfacial structures

The midface resembles a polyhedron-shaped box region of the facial region, which is maintained by a bony framework and separates the oral from orbital cavity. It can be subdivided into a bony component (midfacial skeletal complex) and air component (maxillary sinuses).

2.1 Midfacial skeletal complex

The midfacial skeletal complex is the middle portion of the osseous facial architecture, which contributes significantly to defining the facial form. It consists of maxilla, nasal skeleton, orbital rim, and zygoma (including the entire length of the zygomatic arches), which are bounded by frontomaxillary, frontozygomatic, and frontonasal suture lines. Clinically, the midfacial skeletal complex is a region of vital interest to segment for ensuring accurate diagnosis, patient-specific treatment planning (designing patient-specific osteotomy and repositioning guides, occlusal splints, fixation plates, and 3D printed models), and follow-up assessment of orthognathic and other maxillofacial reconstructive surgical procedures. Owing to the anatomical complexity and reduced bone thickness of the maxillary skeletal complex, it is one of the most difficult anatomical regions to segment with conventional approaches (manual/semi-automatic). Hence, resulting in a clinically significant over- and/or under-estimation of the segmented skeletal structure^{45, 46} and requiring a laborious amount of manual correction.

2.2 Maxillary sinuses

The pyramid-shaped maxillary sinus is the largest paranasal sinus, which lies in the body of the maxilla and is surrounded by the midfacial skeletal complex. An accurate segmentation of the maxillary sinus is also critical for various diagnostic and treatment planning tasks that require evaluation of sinus changes^{47, 48}. The most common surgical procedures requiring 3D sinus assessment through segmentation include surgical implant treatment, sinus augmentation^{49, 50}, and orthognathic surgery. Although the maxillary sinus is a well-defined cavity, its segmentation is difficult due to the presence of sinus thickening and its close proximity to the nasal passages and teeth roots.

3. Clinical applications of automated segmentation

In addition to introducing and validating automated approaches for midfacial structures segmentation, it is also important to explore their clinical applicability for improving the standard of patient care. In this context, automated segmentation of both the midfacial skeletal complex and maxillary sinus was applied for assessing facial symmetry and sinus graft changes, respectively.

3.1 Symmetry assessment

Facial skeletal symmetry is a balanced state where right and left hemifacial structures exhibit an identical mirror image of each side with equal similarity in shape, size, and position⁵¹⁻⁵³. It can also be defined as the positioning of bilateral anatomical structures at a similar distance from an arbitrary reference plane⁵⁴. However, perfect symmetry is rarely observed due to the presence of certain biological and environmental factors which can negatively influence the facial developmental process, thereby, leading to variations in the symmetry⁵⁵.

The normal range of variation in symmetry is expressed as relative symmetry^{56, 57} or fluctuating asymmetry⁵⁸, where a random difference exists between right and left sides⁵⁹. Minimal facial asymmetry within the normal range might be acceptable in a general population without the concern of aesthetic or functional problems⁶⁰. Nevertheless, it is essential to accurately quantify such an acceptable normal range, especially prior to the treatment planning of patients requiring orthodontic and/or surgical correction of facial asymmetry as well as functional and esthetic rehabilitation⁶⁰.

Facial hard tissue symmetry has been widely reported, yet a concern still exists related to the quantification of normal symmetry range⁶¹⁻⁶⁴. Furthermore, most prior studies have reported on the symmetry based on 2D linear and/or angular landmark-based methodology using panoramic radiography⁶⁵, lateral cephalometry^{66, 67} or photographs⁶⁸. As a 2D approach offers several limitations, such as image distortion, magnification, and structural superimposition, it cannot be considered a true representative of 3D facial structure^{69, 70}. Nowadays, 2D imaging techniques have been widely replaced with 3D CT and CBCT acquisition devices, which have proven to offer accurate and quantitative information related to the amount and localization of facial asymmetry in a normal population⁷¹⁻⁷³. Based on a systematic review⁵⁵, prior studies assessed the 3D symmetry of complete facial skeleton⁵⁴, zygoma⁷⁴⁻⁷⁷, and orbital structures using geometric morphometrics. This process involves surface segmentation followed by mirroring and registration to assess the symmetry.

The reason why such 3D morphometric methods are preferred over landmark-based dimensional measurements is because these account for the shape, size, and position of the segmented structures instead of solely relying on the landmark distances on orthogonal planes⁷⁸⁻⁸⁰. Saying that, no studies are available assessing the geometric morphometry of midfacial skeletal structures using AI-based automated segmentation techniques. Hence, it is important to apply CNN-based approaches to overcome the limitations associated with conventional manual/ semi-automated approaches for assessing symmetry.

3.2 Sinus graft follow-up

Maxillary sinus augmentation is aimed to reconstruct and increase the posterior maxillary bone volume by lifting the Schneiderian membrane and placing a bone graft in preparation for dental implant placement. To date, various graft materials have been successfully used for sinus augmentation, which are broadly classified into four categories: autograft⁸¹⁻⁸⁴, allograft⁸⁵⁻⁸⁷, xenograft⁸⁸⁻⁹¹, and alloplastic graft⁹²⁻⁹⁴.

Over time, these bone grafts undergo resorption at varying rates depending on the type of material and sinus re-pneumatization^{95,96}. This graft resorption could have a significant impact on the success and survival rate of the dental implant. Hence, accurate quantification of graft changes prior to and following implant placement is essential to determine whether adequate graft height, width, and volume remain at follow-up.

Post-surgical radiographic examination of sinus changes at follow-up is well-established in literature^{82, 97-110}. Previously, 2D periapical and panoramic radiography have been used to measure the vertical and horizontal bone graft height changes^{103, 105, 107, 109, 111}. However, such techniques are unable to provide 3D changes in bone morphology and volume. Hence, these have been replaced with CBCT^{102, 103, 110} imaging, which allow a more accurate and true 3D representation of graft changes. The changes at follow-up are quantified by segmenting either maxillary sinuses or bone grafts from the CBCT datasets and calculating the volumetric or dimensional differences at different post-operative time-intervals^{49, 112-114}. The method of choice for segmentation is either manual or semi-automatic, which could be impacted by operator-inconsistency, threshold level, and CBCT pixel values. In addition, it is difficult to extract the graft from the neighboring bone, particularly following healing when there is no clear demarcation between the graft and native bone¹⁰². Hence, sinus segmentation could be a better alternative for interpreting sinus changes. The application of such deep learning-based approaches might enable a more precise and consistent volumetric quantification of sinus/graft changes and further improve the standard of care.

4. Aims and Hypotheses

The overall aim of the PhD project is twofold. Firstly, to validate a CNN-based deep learning tool for automated 3D segmentation of midfacial skeletal structures and maxillary sinus on CBCT images. Secondly, to evaluate the performance of digital clinical workflows for midfacial skeletal symmetry and sinus/graft changes assessment following incorporation of an automated segmentation tool.

This doctoral thesis is divided into two main parts, each with its respective objectives.

Part 1 Automated segmentation

Recently, CNNs have proven to provide excellent performance in the field of 3D image analysis. However, a lack of evidence exists considering the CNN-based automated segmentation of the midfacial structures. Furthermore, no automated approach specialized in segmenting different structures with variable densities simultaneously has been proposed in the literature, which could pave the way towards the creation of a virtual patient. Both individual and simultaneous segmentation of anatomical structures as a single unit could be useful for a multitude of clinical applications in general dentistry and maxillofacial surgery.

The objectives were:

- To validate CNN-based deep learning tool for automated segmentation of the midfacial skeletal complex on CBCT images.
- To validate CNN-based deep learning tool for automated segmentation of the maxillary sinus on CBCT images.
- To assess the qualitative and quantitative performance of an integrated tri-CNN model for the creation of a maxillary virtual patient (MVP) consisting of the maxillary skeletal complex, maxillary sinuses, and teeth.

The hypothesis was that:

A CNN-based deep learning approach for automated individual and simultaneous anatomical structural segmentation could act as an accurate, consistent, and time-efficient tool, with the possibility of replacing conventional manual and semi-automated approaches.

Part 2 Clinical applications of automated segmentation

(A) Symmetry assessment

Skeletal structural segmentation is the most vital step in the symmetry assessment protocol. To our knowledge, no protocol exists for quantifying skeletal symmetry with the application of CNN-based segmentation approaches.

The objective was:

- To investigate symmetry of the midfacial skeletal complex in skeletal class I patients using a 3D CNN-based automated segmentation tool.

The hypothesis was that:

The automation of the segmentation step and provision of midfacial complex symmetry data would enhance the precision and time-efficiency of the symmetry evaluation process for further clinical applicability in patients requiring mirroring for reconstructive surgery.

(B) Sinus graft follow up

Post-surgical evaluation of the bone graft following sinus augmentation is essential for ensuring its optimal stability and a high success rate of implant treatment. To our knowledge, no study exists applying CNN-based automated sinus segmentation for assessing graft changes at follow-up.

The objective was:

- To quantify volumetric bone graft changes following sinus augmentation at a follow-up period of 6 months using a CNN-based maxillary sinus segmentation approach.

The hypothesis was that:

The application of automated maxillary sinus segmentation could lay a platform towards simplification of digital workflow for graft follow-up assessment.

5. References

1. Lin, Y.-M., *Digitalisation in Dentistry: Development and Practices*, in *The Digitization of Business in China: Exploring the Transformation from Manufacturing to a Digital Service Hub*, Y.-C. Kim and P.-C. Chen, Editors. 2018, Springer International Publishing: Cham. p. 199-217.
2. Shujaat, S., M.M. Bornstein, J.B. Price, and R. Jacobs, *Integration of imaging modalities in digital dental workflows - possibilities, limitations, and potential future developments*. Dentomaxillofacial Radiology, 2021. **50**(7): p. 20210268-20210268.
3. Vandenberghe, B., *The digital patient - Imaging science in dentistry*. J Dent, 2018. **74 Suppl 1**: p. S21-s26.
4. Park, J.S., Y.J. Lim, B. Kim, M.J. Kim, and H.B. Kwon, *Clinical Evaluation of Time Efficiency and Fit Accuracy of Lithium Disilicate Single Crowns between Conventional and Digital Impression*. Materials (Basel), 2020. **13**(23).
5. Clark, W.A., B. Brazile, D. Matthews, J. Solares, and I.J. De Kok, *A Comparison of Conventionally Versus Digitally Fabricated Denture Outcomes in a University Dental Clinic*. J Prosthodont, 2021. **30**(1): p. 47-50.
6. Stanley, M., A.G. Paz, I. Miguel, and C. Coachman, *Fully digital workflow, integrating dental scan, smile design and CAD-CAM: case report*. BMC Oral Health, 2018. **18**(1): p. 134.
7. Fasbinder, D., *Using digital technology to enhance restorative dentistry*. Compend Contin Educ Dent, 2012. **33**(9): p. 666-8, 670, 672 passim.
8. Kollmuss, M., S. Kist, J.E. Goeke, R. Hickel, and K.C. Huth, *Comparison of chairside and laboratory CAD/CAM to conventional produced all-ceramic crowns regarding morphology, occlusion, and aesthetics*. Clin Oral Investig, 2016. **20**(4): p. 791-7.
9. Martins, A.V., R.C. Albuquerque, T.R. Santos, L.M. Silveira, R.R. Silveira, G.C. Silva, and N. Silva, *Esthetic planning with a digital tool: A clinical report*. J Prosthet Dent, 2017. **118**(6): p. 698-702.
10. Christensen, L.R., *Digital workflows in contemporary orthodontics*. APOS Trends in Orthodontics, 2017. **7**: p. 12 - 18.
11. Camardella, L.T., E.K. Rothier, O.V. Vilella, E.M. Ongkosuwito, and K.H. Breuning, *Virtual setup: application in orthodontic practice*. J Orofac Orthop, 2016. **77**(6): p. 409-419.
12. Brown, M.W., L. Koroluk, C.C. Ko, K. Zhang, M. Chen, and T. Nguyen, *Effectiveness and efficiency of a CAD/CAM orthodontic bracket system*. Am J Orthod Dentofacial Orthop, 2015. **148**(6): p. 1067-74.
13. Lin, C.C., C.Z. Wu, M.S. Huang, C.F. Huang, H.C. Cheng, and D.P. Wang, *Fully Digital Workflow for Planning Static Guided Implant Surgery: A Prospective Accuracy Study*. J Clin Med, 2020. **9**(4).

14. Van der Groen, T., K. Lee, and B. Archer, *Eliminating Stone Models in Orthognathic Surgery: A Complete Digital Workflow*. Journal of Oral and Maxillofacial Surgery, 2020. **78**(10): p. e79.
15. Block, M.S., R.W. Emery, D.R. Cullum, and A. Sheikh, *Implant Placement Is More Accurate Using Dynamic Navigation*. J Oral Maxillofac Surg, 2017. **75**(7): p. 1377-1386.
16. Shujaat, S., M.M. Bornstein, J.B. Price, and R. Jacobs, *Integration of imaging modalities in digital dental workflows - possibilities, limitations, and potential future developments*. Dentomaxillofac Radiol, 2021. **50**(7): p. 20210268.
17. White, S.C. and M.J. Pharoah, *White and Pharoah's Oral Radiology: Principles and Interpretation*. 2018: Elsevier Health Sciences.
18. Tsiklakis, K., C. Donta, S. Gavala, K. Karayianni, V. Kamenopoulou, and C.J. Hourdakakis, *Dose reduction in maxillofacial imaging using low dose Cone Beam CT*. Eur J Radiol, 2005. **56**(3): p. 413-7.
19. Kapila, S., *Cone beam computed tomography in orthodontics : indications, insights, and innovations*. 2014, Ames, Iowa: Wiley-Blackwell.
20. Starmans, M.P.A., S.R. van der Voort, J.M. Castillo Tovar, J.F. Veenland, S. Klein, and W.J. Niessen, *Chapter 18 - Radiomics: Data mining using quantitative medical image features*, in *Handbook of Medical Image Computing and Computer Assisted Intervention*, S.K. Zhou, D. Rueckert, and G. Fichtinger, Editors. 2020, Academic Press. p. 429-456.
21. Heye, T., E.M. Merkle, C.S. Reiner, M.S. Davenport, J.J. Horvath, S. Feuerlein, S.R. Breault, P. Gall, M.R. Bashir, B.M. Dale, A.P. Kiraly, and D.T. Boll, *Reproducibility of Dynamic Contrast-enhanced MR Imaging. Part II. Comparison of Intra- and Interobserver Variability with Manual Region of Interest Placement versus Semiautomatic Lesion Segmentation and Histogram Analysis*. Radiology, 2013. **266**(3): p. 812-821.
22. Parmar, C., E. Rios Velazquez, R. Leijenaar, M. Jermoumi, S. Carvalho, R.H. Mak, S. Mitra, B.U. Shankar, R. Kikinis, B. Haibe-Kains, P. Lambin, and H.J. Aerts, *Robust Radiomics feature quantification using semiautomatic volumetric segmentation*. PLoS One, 2014. **9**(7): p. e102107.
23. Withey, D.J. and Z.J. Koles. *Medical Image Segmentation: Methods and Software*. IEEE.
24. Renard, F., S. Guedria, N.D. Palma, and N. Vuillerme, *Variability and reproducibility in deep learning for medical image segmentation*. Scientific Reports, 2020. **10**(1): p. 13724-13724.
25. Liu, Q., H. Deng, C. Lian, X. Chen, D. Xiao, L. Ma, X. Chen, T. Kuang, J. Gateno, P.-T. Yap, and J.J. Xia, *SkullEngine: A Multi-stage CNN Framework for Collaborative CBCT Image Segmentation and Landmark Detection*. 2021. p. 606-614.
26. Boucher, N., M. Mupparapu, and K. Matsumoto, *Cone Beam Computerized Tomography Imaging for Orthodontic Diagnosis*. 2021, Springer International Publishing: Cham. p. 55-91.

27. Chang, Y.-B., J.J. Xia, P. Yuan, T.-H. Kuo, Z. Xiong, J. Gateno, and X. Zhou, *3D segmentation of maxilla in cone-beam computed tomography imaging using base invariant wavelet active shape model on customized two-manifold topology*. Journal of X-ray science and technology, 2013. **21**(2): p. 251-282.
28. Pauwels, R., R. Jacobs, S.R. Singer, and M. Mupparapu, *CBCCT-based bone quality assessment: are Hounsfield units applicable?* Dento maxillo facial radiology, 2015. **44**(1): p. 20140238-20140238.
29. Park, W.J. and J.B. Park, *History and application of artificial neural networks in dentistry*. Eur J Dent, 2018. **12**(4): p. 594-601.
30. Mupparapu, M., C.W. Wu, and Y.C. Chen, *Artificial intelligence, machine learning, neural networks, and deep learning: Futuristic concepts for new dental diagnosis*. Quintessence Int, 2018. **49**(9): p. 687-688.
31. Lee, J.G., S. Jun, Y.W. Cho, H. Lee, G.B. Kim, J.B. Seo, and N. Kim, *Deep Learning in Medical Imaging: General Overview*. Korean J Radiol, 2017. **18**(4): p. 570-584.
32. Burt, J.R., N. Torosdagli, N. Khosravan, H. RaviPrakash, A. Mortazi, F. Tissavirasingham, S. Hussein, and U. Bagci, *Deep learning beyond cats and dogs: recent advances in diagnosing breast cancer with deep neural networks*. Br J Radiol, 2018. **91**(1089): p. 20170545.
33. Ronneberger, O., P. Fischer, and T. Brox. *U-Net: Convolutional Networks for Biomedical Image Segmentation*. in *Medical Image Computing and Computer-Assisted Intervention – MICCAI 2015*. 2015. Cham: Springer International Publishing.
34. Çiçek, Ö., A. Abdulkadir, S.S. Lienkamp, T. Brox, and O. Ronneberger, *3D U-Net: Learning Dense Volumetric Segmentation from Sparse Annotation*, in *Medical Image Computing and Computer-Assisted Intervention* S. Ourselin, et al., Editors. 2016, Springer International Publishing: Cham. p. 424-432.
35. Lin, B.S., K. Michael, S. Kalra, and H.R. Tizhoosh. *Skin lesion segmentation: U-Nets versus clustering*. in *2017 IEEE Symposium Series on Computational Intelligence (SSCI)*. 2017.
36. Zhang, J., X. Lv, Q. Sun, Q. Zhang, X. Wei, and B. Liu, *SDResU-Net: Separable and Dilated Residual U-Net for MRI Brain Tumor Segmentation*. Curr Med Imaging, 2020. **16**(6): p. 720-728.
37. Ferreira, P.F., R.R. Martin, A.D. Scott, Z. Khaliq, G. Yang, S. Nielles-Vallespin, D.J. Pennell, and D.N. Firmin, *Automating in vivo cardiac diffusion tensor postprocessing with deep learning-based segmentation*. Magn Reson Med, 2020. **84**(5): p. 2801-2814.
38. Egger, J., B. Pfarrkirchner, C. Gsaxner, L. Lindner, D. Schmalstieg, and J. Wallner, *Fully Convolutional Mandible Segmentation on a valid Ground- Truth Dataset*. Annu Int Conf IEEE Eng Med Biol Soc, 2018. **2018**: p. 656-660.

39. Verhelst, P.-J., A. Smolders, T. Beznik, J. Meewis, A. Vandemeulebroucke, E. Shaheen, A. Van Gerven, H. Willems, C. Politis, and R. Jacobs, *Layered deep learning for automatic mandibular segmentation in cone-beam computed tomography*. Journal of Dentistry, 2021. **114**: p. 103786.
40. Kwak, G.H., E.J. Kwak, J.M. Song, H.R. Park, Y.H. Jung, B.H. Cho, P. Hui, and J.J. Hwang, *Automatic mandibular canal detection using a deep convolutional neural network*. Sci Rep, 2020. **10**(1): p. 5711.
41. Lahoud, P., S. Diels, L. Niclaes, S. Van Aelst, H. Willems, A. Van Gerven, M. Quirynen, and R. Jacobs, *Development and validation of a novel artificial intelligence driven tool for accurate mandibular canal segmentation on CBCT*. Journal of Dentistry, 2022. **116**: p. 103891-103891.
42. Shujaat, S., O. Jazil, H. Willems, A. Van Gerven, E. Shaheen, C. Politis, and R. Jacobs, *Automatic segmentation of the pharyngeal airway space with convolutional neural network*. Journal of Dentistry, 2021. **111**: p. 103705.
43. Xu, X., C. Liu, and Y. Zheng, *3D Tooth Segmentation and Labeling Using Deep Convolutional Neural Networks*. IEEE Trans Vis Comput Graph, 2019. **25**(7): p. 2336-2348.
44. Lahoud, P., M. EzEldeen, T. Beznik, H. Willems, A. Leite, A. Van Gerven, and R. Jacobs, *Artificial Intelligence for Fast and Accurate 3-Dimensional Tooth Segmentation on Cone-beam Computed Tomography*. Journal of Endodontics, 2021. **47**(5): p. 827-835.
45. Scarfe, W.C., B. Azevedo, S. Toghyani, and A.G. Farman, *Cone Beam Computed Tomographic imaging in orthodontics*. Aust Dent J, 2017. **62 Suppl 1**: p. 33-50.
46. Yang, W.F. and Y.X. Su, *Artificial intelligence-enabled automatic segmentation of skull CT facilitates computer-assisted craniomaxillofacial surgery*. Oral Oncol, 2021. **118**: p. 105360.
47. Andersen, T.N., T.A. Darvann, S. Murakami, P. Larsen, Y. Senda, A. Bilde, C.V. Buchwald, and S. Kreiborg, *Accuracy and precision of manual segmentation of the maxillary sinus in MR images-a method study*. Br J Radiol, 2018. **91**(1085): p. 20170663.
48. Giacomini, G., A.L.M. Pavan, J.M.C. Altemani, S.B. Duarte, C. Fortaleza, J.R.A. Miranda, and D.R. de Pina, *Computed tomography-based volumetric tool for standardized measurement of the maxillary sinus*. PLoS One, 2018. **13**(1): p. e0190770.
49. Berberi, A., L. Bouserhal, N. Nader, R.B. Assaf, N.B. Nassif, J. Bouserhal, and Z. Salameh, *Evaluation of Three-Dimensional Volumetric Changes After Sinus Floor Augmentation with Mineralized Cortical Bone Allograft*. J Maxillofac Oral Surg, 2015. **14**(3): p. 624-9.
50. Starch-Jensen, T. and J.D. Jensen, *Maxillary Sinus Floor Augmentation: a Review of Selected Treatment Modalities*. J Oral Maxillofac Res, 2017. **8**(3): p. e3.
51. Baudouin, J.Y. and G. Tiberghien, *Symmetry, averageness, and feature size in the facial attractiveness of women*. Acta Psychol (Amst), 2004. **117**(3): p. 313-32.

52. Akhil, G., K.P. Senthil Kumar, S. Raja, and K. Janardhanan, *Three-dimensional assessment of facial asymmetry: A systematic review*. J Pharm Bioallied Sci, 2015. **7**(Suppl 2): p. S433-7.
53. Damstra, J., Z. Fourie, M. De Wit, and Y. Ren, *A three-dimensional comparison of a morphometric and conventional cephalometric midsagittal planes for craniofacial asymmetry*. Clinical Oral Investigations, 2012. **16**(1): p. 285-294.
54. Duran, G.S., F. Dindaroğlu, and P. Kutlu, *Hard- and soft-tissue symmetry comparison in patients with Class III malocclusion*. Am J Orthod Dentofacial Orthop, 2019. **155**(4): p. 509-522.
55. Morgan, N., I. Suryani, S. Shujaat, and R. Jacobs, *Three-dimensional facial hard tissue symmetry in a healthy Caucasian population group: a systematic review*. Clin Oral Investig, 2021. **25**(11): p. 6081-6092.
56. Thiesen, G., M.P.M. Freitas, E.A. Araújo, B.F. Gribel, and K.B. Kim, *Three-dimensional evaluation of craniofacial characteristics related to mandibular asymmetries in skeletal Class I patients*. Am J Orthod Dentofacial Orthop, 2018. **154**(1): p. 91-98.
57. Thiesen, G., B.F. Gribel, M.P.M. Freitas, D.R. Oliver, and K.B. Kim, *Mandibular asymmetries and associated factors in orthodontic and orthognathic surgery patients*. The Angle Orthodontist, 2018. **88**(5): p. 545-551.
58. Gateño, J., T.L. Jones, S.G.F. Shen, K.C. Chen, A. Jajoo, T. Kuang, J.D. English, M. Nicol, J.F. Teichgraber, and J.J. Xia, *Fluctuating asymmetry of the normal facial skeleton*. International Journal of Oral and Maxillofacial Surgery, 2018. **47**(4): p. 534-540.
59. Graham, J.H., S. Raz, H. Hel-Or, and E. Nevo, *Fluctuating Asymmetry: Methods, Theory, and Applications*. Symmetry, 2010. **2**(2): p. 466-540.
60. Yoon, S.-J., R.-F. Wang, H.J. Na, and J.M. Palomo, *Normal range of facial asymmetry in spherical coordinates: a CBCT study*. Imaging Sci Dent, 2013. **43**(1): p. 31-36.
61. Haraguchi, S., K. Takada, and Y. Yasuda, *Facial asymmetry in subjects with skeletal Class III deformity*. Angle Orthod, 2002. **72**(1): p. 28-35.
62. Maria Yanez-Vico, R., A. Iglesias-Linares, D. Torres-Lagares, J. Luis Gutierrez-Perez, and E. Solano-Reina, *Three-dimensional evaluation of craniofacial asymmetry: an analysis using computed tomography*. Clinical Oral Investigations, 2011. **15**(5): p. 729-736.
63. Severt, T.R. and W.R. Proffit, *The prevalence of facial asymmetry in the dentofacial deformities population at the University of North Carolina*. Int J Adult Orthodon Orthognath Surg, 1997. **12**(3): p. 171-6.
64. Zheng, X., L. Wang, B. Zhang, X. Bai, K. Qin, Y. Tian, R. Zhao, S. Liu, J. Wang, and Z. Zhao, *Accuracy of two midsagittal planes in three-dimensional analysis and their measurement in patients with skeletal mandibular deviation: a comparative study*. Br J Oral Maxillofac Surg, 2018. **56**(7): p. 600-606.

65. Kambylafkas, P., E. Murdock, E. Gilda, R.H. Tallents, and S. Kyrkanides, *Validity of panoramic radiographs for measuring mandibular asymmetry*. Angle Orthod, 2006. **76**(3): p. 388-93.
66. Terajima, M., A. Nakasima, Y. Aoki, T.K. Goto, K. Tokumori, N. Mori, and Y. Hoshino, *A 3-dimensional method for analyzing the morphology of patients with maxillofacial deformities*. Am J Orthod Dentofacial Orthop, 2009. **136**(6): p. 857-67.
67. Trpkova, B., N.G. Prasad, E.W. Lam, D. Raboud, K.E. Glover, and P.W. Major, *Assessment of facial asymmetries from posteroanterior cephalograms: validity of reference lines*. Am J Orthod Dentofacial Orthop, 2003. **123**(5): p. 512-20.
68. Berssenbrügge, P., N.F. Berlin, G. Kebeck, C. Runte, S. Jung, J. Kleinheinz, and D. Dirksen, *2D and 3D analysis methods of facial asymmetry in comparison*. J Craniomaxillofac Surg, 2014. **42**(6): p. e327-34.
69. Bergersen, E.O., *Enlargement and distortion in cephalometric radiography: compensation tables for linear measurements*. Angle Orthod, 1980. **50**(3): p. 230-44.
70. Joen M. Iannucci, L.J.H., *DENTAL RADIOGRAPHY : Principles and Techniques*. 2017, Elsevier. p. 257.
71. García-Sanz, V., C. Bellot-Arcís, V. Hernández, P. Serrano-Sánchez, J. Guarinos, and V. Paredes-Gallardo, *Accuracy and Reliability of Cone-Beam Computed Tomography for Linear and Volumetric Mandibular Condyle Measurements. A Human Cadaver Study*. Scientific reports, 2017. **7**(1): p. 11993-11993.
72. Kim, E.J., E.J. Ki, H.M. Cheon, E.J. Choi, and K.H. Kwon, *3-Dimensional analysis for class III malocclusion patients with facial asymmetry*. J Korean Assoc Oral Maxillofac Surg, 2013. **39**(4): p. 168-74.
73. Moro, A., P. Correria, R. Boniello, G. Gasparini, and S. Pelo, *Three-dimensional analysis in facial asymmetry: comparison with model analysis and conventional two-dimensional analysis*. J Craniofac Surg, 2009. **20**(2): p. 417-22.
74. Gibelli, D., M. Cellina, S. Gibelli, A.G. Oliva, G. Termine, V. Pucciarelli, C. Dolci, and C. Sforza, *Assessing symmetry of zygomatic bone through three-dimensional segmentation on computed tomography scan and "mirroring" procedure: A contribution for reconstructive maxillofacial surgery*. J Craniomaxillofac Surg, 2018. **46**(4): p. 600-604.
75. Gong, X., Y. He, Y. He, J.G. An, Y. Yang, and Y. Zhang, *Quantitation of zygomatic complex symmetry using 3-dimensional computed tomography*. J Oral Maxillofac Surg, 2014. **72**(10): p. 2053.e1-8.
76. Ho, J., R. Schreurs, S. Aydi, R. Rezai, T.J.J. Maal, A.J. van Wijk, L.F.M. Beenen, L. Dubois, D.M.J. Milstein, and A.G. Becking, *Natural variation of the zygomaticomaxillary complex symmetry in normal individuals*. J Craniomaxillofac Surg, 2017. **45**(12): p. 1927-1933.

77. Mao, S.H., Y.H. Hsieh, P.Y. Chou, V.B. Shyu, C.T. Chen, and C.H. Chen, *Quantitative Determination of Zygomaticomaxillary Complex Position Based on Computed Tomographic Imaging*. Ann Plast Surg, 2016. **76 Suppl 1**: p. S117-20.
78. Benazzi, S. and S. Senck, *Comparing 3-Dimensional Virtual Methods for Reconstruction in Craniomaxillofacial Surgery*. Journal of Oral and Maxillofacial Surgery, 2011. **69**(4): p. 1184-1194.
79. Khalifa, G.A., N.A. Abd El Moniem, S.A. Elsayed, and Y. Qadry, *Segmental Mirroring: Does It Eliminate the Need for Intraoperative Readjustment of the Virtually Pre-Bent Reconstruction Plates and Is It Economically Valuable?* J Oral Maxillofac Surg, 2016. **74**(3): p. 621-30.
80. Schramm, A., M.M. Suarez-Cunqueiro, M. Rücker, H. Kokemueller, K.H. Bormann, M.C. Metzger, and N.C. Gellrich, *Computer-assisted therapy in orbital and mid-facial reconstructions*. Int J Med Robot, 2009. **5**(2): p. 111-24.
81. Johansson, L.A., S. Isaksson, C. Lindh, J.P. Becktor, and L. Sennerby, *Maxillary sinus floor augmentation and simultaneous implant placement using locally harvested autogenous bone chips and bone debris: a prospective clinical study*. J Oral Maxillofac Surg, 2010. **68**(4): p. 837-44.
82. Klijn, R.J., G.J. Meijer, E.M. Bronkhorst, and J.A. Jansen, *A meta-analysis of histomorphometric results and graft healing time of various biomaterials compared to autologous bone used as sinus floor augmentation material in humans*. Tissue Eng Part B Rev, 2010. **16**(5): p. 493-507.
83. Nkenke, E. and F. Stelzle, *Clinical outcomes of sinus floor augmentation for implant placement using autogenous bone or bone substitutes: a systematic review*. Clin Oral Implants Res, 2009. **20 Suppl 4**: p. 124-33.
84. Schmitt, C.M., H. Doering, T. Schmidt, R. Lutz, F.W. Neukam, and K.A. Schlegel, *Histological results after maxillary sinus augmentation with Straumann® BoneCeramic, Bio-Oss®, Puros®, and autologous bone. A randomized controlled clinical trial*. Clin Oral Implants Res, 2013. **24**(5): p. 576-85.
85. Annibali, S., M.P. Cristalli, G. La Monaca, I. Bignozzi, A. Scarano, R. Corrado, and L. Lo Muzio, *Human maxillary sinuses augmented with mineralized, solvent-dehydrated bone allograft: a longitudinal case series*. Implant Dent, 2011. **20**(6): p. 445-54.
86. Bavetta, G. and M.E. Licata, *The use of human allogenic graft (HBA) for maxillary bone regeneration: review of literature and case reports*. Curr Pharm Des, 2012. **18**(34): p. 5559-68.
87. Irinakis, T., *Efficacy of injectable demineralized bone matrix as graft material during sinus elevation surgery with simultaneous implant placement in the posterior maxilla: clinical evaluation of 49 sinuses*. J Oral Maxillofac Surg, 2011. **69**(1): p. 134-41.

88. Özkan, Y., B. Akoğlu, and Y. Kulak-Özkan, *Maxillary sinus floor augmentation using bovine bone grafts with simultaneous implant placement: a 5-year prospective follow-up study*. *Implant Dent*, 2011. **20**(6): p. 455-9.
89. Scarano, A., A. Piattelli, V. Perrotti, L. Manzon, and G. Iezzi, *Maxillary sinus augmentation in humans using cortical porcine bone: a histological and histomorphometrical evaluation after 4 and 6 months*. *Clin Implant Dent Relat Res*, 2011. **13**(1): p. 13-8.
90. Sivoilella, S., E. Bressan, E. Gnocco, M. Berengo, and G.A. Favero, *Maxillary sinus augmentation with bovine bone and simultaneous dental implant placement in conditions of severe alveolar atrophy: a retrospective analysis of a consecutively treated case series*. *Quintessence Int*, 2011. **42**(10): p. 851-62.
91. Testori, T., G. Iezzi, L. Manzon, G. Fratto, A. Piattelli, and R.L. Weinstein, *High temperature-treated bovine porous hydroxyapatite in sinus augmentation procedures: a case report*. *Int J Periodontics Restorative Dent*, 2012. **32**(3): p. 295-301.
92. Boyne, P.J., L.C. Lilly, R.E. Marx, P.K. Moy, M. Nevins, D.B. Spagnoli, and R.G. Triplett, *De novo bone induction by recombinant human bone morphogenetic protein-2 (rhBMP-2) in maxillary sinus floor augmentation*. *J Oral Maxillofac Surg*, 2005. **63**(12): p. 1693-707.
93. Laurencin, C., Y. Khan, and S.F. El-Amin, *Bone graft substitutes*. *Expert Rev Med Devices*, 2006. **3**(1): p. 49-57.
94. Triplett, R.G., M. Nevins, R.E. Marx, D.B. Spagnoli, T.W. Oates, P.K. Moy, and P.J. Boyne, *Pivotal, randomized, parallel evaluation of recombinant human bone morphogenetic protein-2/absorbable collagen sponge and autogenous bone graft for maxillary sinus floor augmentation*. *J Oral Maxillofac Surg*, 2009. **67**(9): p. 1947-60.
95. Hatano, N., Y. Shimizu, and K. Ooya, *A clinical long-term radiographic evaluation of graft height changes after maxillary sinus floor augmentation with a 2:1 autogenous bone/xenograft mixture and simultaneous placement of dental implants*. *Clin Oral Implants Res*, 2004. **15**(3): p. 339-45.
96. Hürzeler, M.B., A. Kirsch, K.L. Ackermann, and C.R. Quiñones, *Reconstruction of the severely resorbed maxilla with dental implants in the augmented maxillary sinus: a 5-year clinical investigation*. *Int J Oral Maxillofac Implants*, 1996. **11**(4): p. 466-75.
97. Krennmair, G., M. Krainhöfner, H. Maier, M. Weinländer, and E. Piehslinger, *Computerized tomography-assisted calculation of sinus augmentation volume*. *Int J Oral Maxillofac Implants*, 2006. **21**(6): p. 907-13.
98. Riachi, F., N. Naaman, C. Tabarani, N. Aboelsaad, M.N. Aboushelib, A. Berberi, and Z. Salameh, *Influence of material properties on rate of resorption of two bone graft materials after sinus lift using radiographic assessment*. *Int J Dent*, 2012. **2012**: p. 737262.

99. Zijdeveld, S.A., E.A. Schulten, I.H. Aartman, and C.M. ten Bruggenkate, *Long-term changes in graft height after maxillary sinus floor elevation with different grafting materials: radiographic evaluation with a minimum follow-up of 4.5 years*. Clin Oral Implants Res, 2009. **20**(7): p. 691-700.
100. Gray, C.F., T.W. Redpath, R. Bainton, and F.W. Smith, *Magnetic resonance imaging assessment of a sinus lift operation using reoxidised cellulose (Surgicel) as graft material*. Clin Oral Implants Res, 2001. **12**(5): p. 526-30.
101. Wanschitz, F., M. Figl, A. Wagner, and E. Rolf, *Measurement of volume changes after sinus floor augmentation with a phycogenic hydroxyapatite*. Int J Oral Maxillofac Implants, 2006. **21**(3): p. 433-8.
102. Dellavia, C., S. Speroni, G. Pellegrini, A. Gatto, and C. Maiorana, *A new method to evaluate volumetric changes in sinus augmentation procedure*. Clin Implant Dent Relat Res, 2014. **16**(5): p. 684-90.
103. Hallman, M., M. Hedin, L. Sennerby, and S. Lundgren, *A prospective 1-year clinical and radiographic study of implants placed after maxillary sinus floor augmentation with bovine hydroxyapatite and autogenous bone*. J Oral Maxillofac Surg, 2002. **60**(3): p. 277-84; discussion 285-6.
104. Diserens, V., E. Mericske, and R. Mericske-Stern, *Radiographic analysis of the transcrestal sinus floor elevation: short-term observations*. Clin Implant Dent Relat Res, 2005. **7**(2): p. 70-8.
105. Ozyuvaci, H., B. Bilgiç, and E. Firatli, *Radiologic and histomorphometric evaluation of maxillary sinus grafting with alloplastic graft materials*. J Periodontol, 2003. **74**(6): p. 909-15.
106. Kirmeier, R., C. Arnetzl, T. Robl, M. Payer, M. Lorenzoni, and N. Jakse, *Reproducibility of volumetric measurements on maxillary sinuses*. Int J Oral Maxillofac Surg, 2011. **40**(2): p. 195-9.
107. Reinert, S., S. König, A. Bremerich, H. Eufinger, and M. Krimmel, *Stability of bone grafting and placement of implants in the severely atrophic maxilla*. Br J Oral Maxillofac Surg, 2003. **41**(4): p. 249-55.
108. Johansson, B., A. Grepe, K. Wannfors, P. Aberg, and J.M. Hirsch, *Volumetry of simulated bone grafts in the edentulous maxilla by computed tomography: an experimental study*. Dentomaxillofac Radiol, 2001. **30**(3): p. 153-6.
109. Szabó, G., L. Huys, P. Coulthard, C. Maiorana, U. Garagiola, J. Barabás, Z. Németh, K. Hrabák, and Z. Suba, *A prospective multicenter randomized clinical trial of autogenous bone versus beta-tricalcium phosphate graft alone for bilateral sinus elevation: histologic and histomorphometric evaluation*. Int J Oral Maxillofac Implants, 2005. **20**(3): p. 371-81.
110. Klijn, R.J., G.J. Meijer, E.M. Bronkhorst, and J.A. Jansen, *Sinus floor augmentation surgery using autologous bone grafts from various donor sites: a meta-analysis of the total bone volume*. Tissue Eng Part B Rev, 2010. **16**(3): p. 295-303.

111. Diss, A., D.M. Dohan, J. Mouhyi, and P. Mahler, *Osteotome sinus floor elevation using Choukroun's platelet-rich fibrin as grafting material: a 1-year prospective pilot study with microthreaded implants*. Oral Surg Oral Med Oral Pathol Oral Radiol Endod, 2008. **105**(5): p. 572-9.
112. Klein, G.G., V.P. Curvello, R.A. Dutra, S.P. Simeão, P.L. Santos, J.L. Gulinelli, and H.N. Filho, *Bone Volume Changes After Sinus Floor Augmentation with Heterogenous Graft*. Int J Oral Maxillofac Implants, 2016. **31**(3): p. 665-71.
113. Kim, E.S., S.Y. Moon, S.G. Kim, H.C. Park, and J.S. Oh, *Three-dimensional volumetric analysis after sinus grafts*. Implant Dent, 2013. **22**(2): p. 170-4.
114. Temmerman, A., J. Van Dessel, S. Cortellini, R. Jacobs, W. Teughels, and M. Quirynen, *Volumetric changes of grafted volumes and the Schneiderian membrane after transcrestal and lateral sinus floor elevation procedures: A clinical, pilot study*. J Clin Periodontol, 2017. **44**(6): p. 660-671.

Part 1

Automated segmentation

Deep convolutional neural network-based automated segmentation of the maxillofacial complex from cone-beam computed tomography: A validation study

Preda F.¹

Morgan N.^{1,2} (*shared first-authorship*)

Van Gerven A.³

Nogueira-Reis F.^{1,4}

Smolders A.³

Wang X.¹

Nomidis S.³

Shaheen E.¹

Willems H.³

Jacobs R.^{1,5}

¹ OMFS IMPATH Research Group, Department of Imaging & Pathology, Faculty of Medicine, KU Leuven & Oral and Maxillofacial Surgery, University Hospitals Leuven, Kapucijnenvoer33, BE-3000 Leuven, Belgium

² Department of Oral Medicine, Faculty of Dentistry, Mansoura University, 35516 Mansoura, Dakahlia, Egypt

³ Relu BV, Kapeldreef 60, BE-3000 Leuven, Belgium

⁴ Department of Oral Diagnosis, Division of Oral Radiology, Piracicaba Dental School, University of Campinas (UNICAMP), Av. Limeira 901, Piracicaba, São Paulo 13414-903, Brazil

⁵ Department of Dental Medicine, Karolinska Institutet, Box 4064, 141 04 Huddinge, Stockholm, Sweden

Published in *Journal of Dentistry* 2022 Sep;124:104238.

Abstract

Objectives

The present study investigated the accuracy, consistency, and time-efficiency of a deep CNN-based model for automated maxillofacial bone segmentation from CBCT images.

Materials and methods

A dataset of 144 scans was acquired from two CBCT devices and randomly divided into three subsets: training set ($n = 110$), validation set ($n = 10$) and testing set ($n = 24$). A 3D U-Net (CNN) model was developed, and the achieved automated segmentation was compared with a manual approach.

Results

The average time required for automated segmentation was 39.1s, with a 204-fold decrease in time consumption compared to manual segmentation (132.7 min). The model was highly accurate for identification of the bony structures of the anatomical region of interest, with a dice similarity coefficient (DSC) of 92.6%. Additionally, the CNN model was 100% consistent, providing identical segmentation results if a similar scan was processed without any variability. The inter-observer consistency for expert-based minor correction of the automated segmentation observed an excellent DSC of 99.7%.

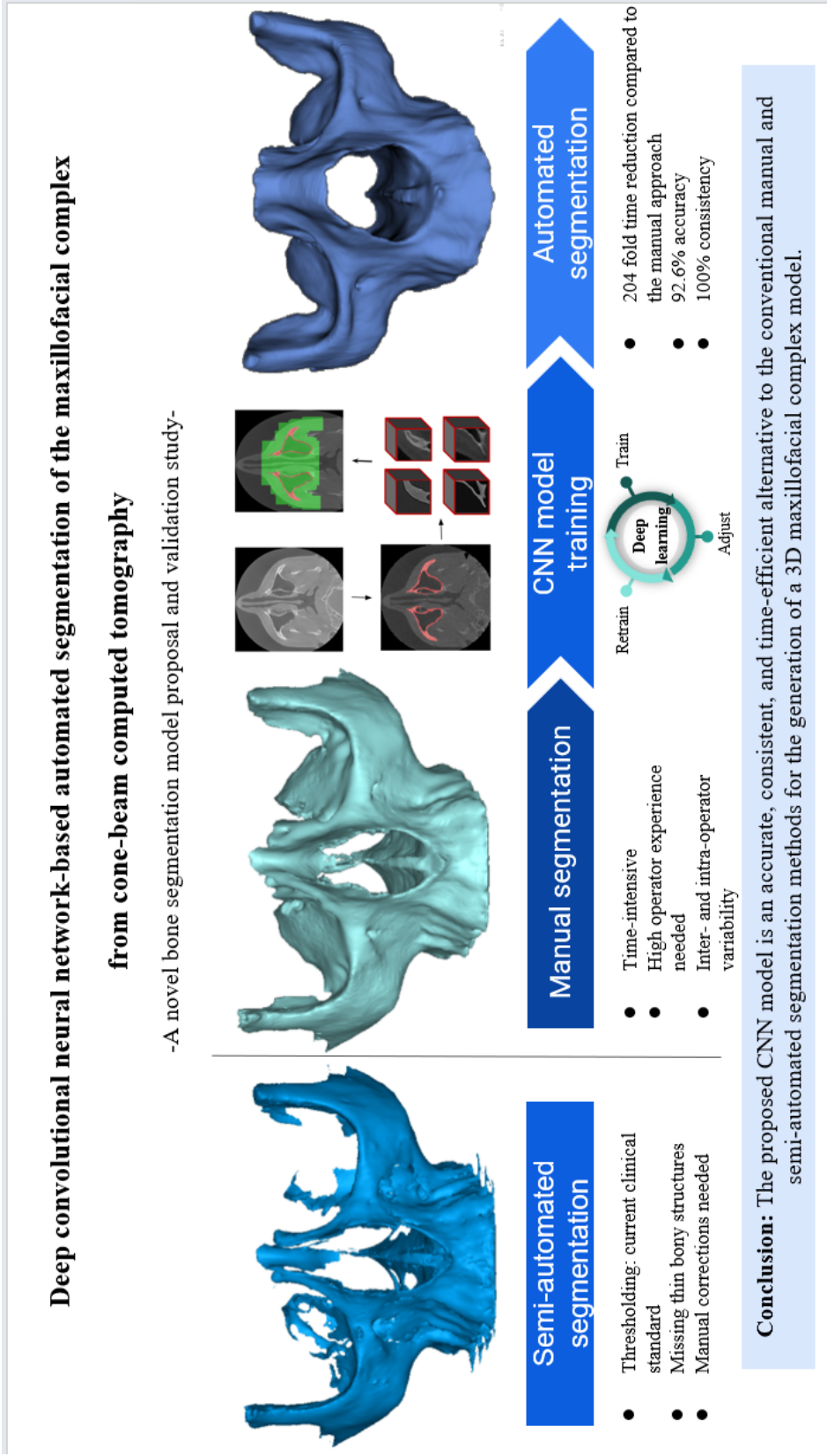
Conclusions

The proposed CNN model provided a time-efficient, accurate, and consistent CBCT-based automated segmentation of the maxillofacial complex.

Clinical significance

Automated segmentation of the maxillofacial complex could act as a potent alternative to the conventional segmentation techniques for improving the efficiency of digital workflows. This approach could deliver accurate and ready-to-print 3D models that are essential to patient-specific digital treatment planning for orthodontics, maxillofacial surgery, and implant placement.

Keywords: Bone segmentation, Deep learning, Neural network model, Computer generated 3D imaging, Digital dentistry.



1. Introduction

The integration of digital technology within each step of a dental workflow has transformed dentistry, where the contemporary 2D approaches are gradually becoming obsolete and being superseded by advanced 3D digital tools. In the era of precision dental medicine, digitalization has been widely applied in the majority of dental workflows^{1,2}. Although a consensus exists around the potential benefits of using 3D digital tools for enhancing the quality of care, their universal acceptability is partially hindered by the laborious nature of certain steps requiring considerable expertise in both clinical dentistry and medical image processing tools for various tasks, such as 3D radiographic data segmentation and integration, virtual treatment planning, and CAD/CAM^{3,4}.

The first and most essential step in the digital workflow of the majority of digital dental workflows is known as segmentation, which involves the generation of 3D models of the dentomaxillofacial structures. The most commonly applied methodologies for segmentation are either thresholding or template-based and semi-automatic in nature⁵⁻⁷ (Figure 1A). These techniques are prone to certain limitations, such as missing thin bony structures, excessive time-consumption⁸, a steep learning curve, observer variability, and the need for manual refinement. In the presence of metal artifacts from high-density materials, an extensive amount of manual post-processing is required by a trained operator owing to a high intensity similarity of grey values between bone and artifacts⁹. Furthermore, the currently available dentomaxillofacial segmentation software programs have been optimized based on CT data, which cannot be applied to CBCT scans due to the presence of uncalibrated absolute Hounsfield units (HU), beam hardening artifacts, inhomogeneity, noise, and low-contrast resolution¹⁰⁻¹². All these factors negatively affect the quality of the scan and the accuracy of bone segmentation.

Considering the limitations of the conventional segmentation methods, recent applications of deep CNNs have outperformed the previously available algorithms for modelling of the dentomaxillofacial region¹³⁻¹⁷. These CNNs have been successfully applied with promising results for the CBCT-based automated segmentation of the teeth, upper airway, inferior alveolar nerve canal, mandible, and maxillary sinus¹⁸⁻²³. However, a lack of evidence exists considering the CNN-based automated segmentation of the maxillofacial complex.

The maxillofacial complex holds a unique position in the workflows of orthognathic and reconstructive surgery, dental implantology, and orthodontics for ensuring an accurate diagnosis, patient-specific treatment planning (designing and manufacturing patient-specific osteotomy and repositioning guides, orthodontic devices, spacers, occlusal splints, fixation plates/implants, and 3D printed models), and follow-up assessment. It is one of the most difficult anatomical regions to

segment with conventional approaches owing to the anatomical complexity and reduced bone thickness, which often leads to a clinically significant under- and/or over-estimation of the segmented skeletal structure^{24,25} hence requiring a laborious amount of manual corrections. Therefore, it is important to assess whether CNN-based automated segmentation of the maxillofacial complex can simplify the segmentation process by offering an accurate and observer-independent alternative to the present conventional approaches.

The present study aimed to investigate the performance of a deep CNN-based model for automated maxillofacial complex bone segmentation from CBCT images. We hypothesized that a deep CNN approach would offer a more accurate, consistent, and time-efficient segmentation of the maxillofacial complex compared to the manual segmentation as the reference standard.

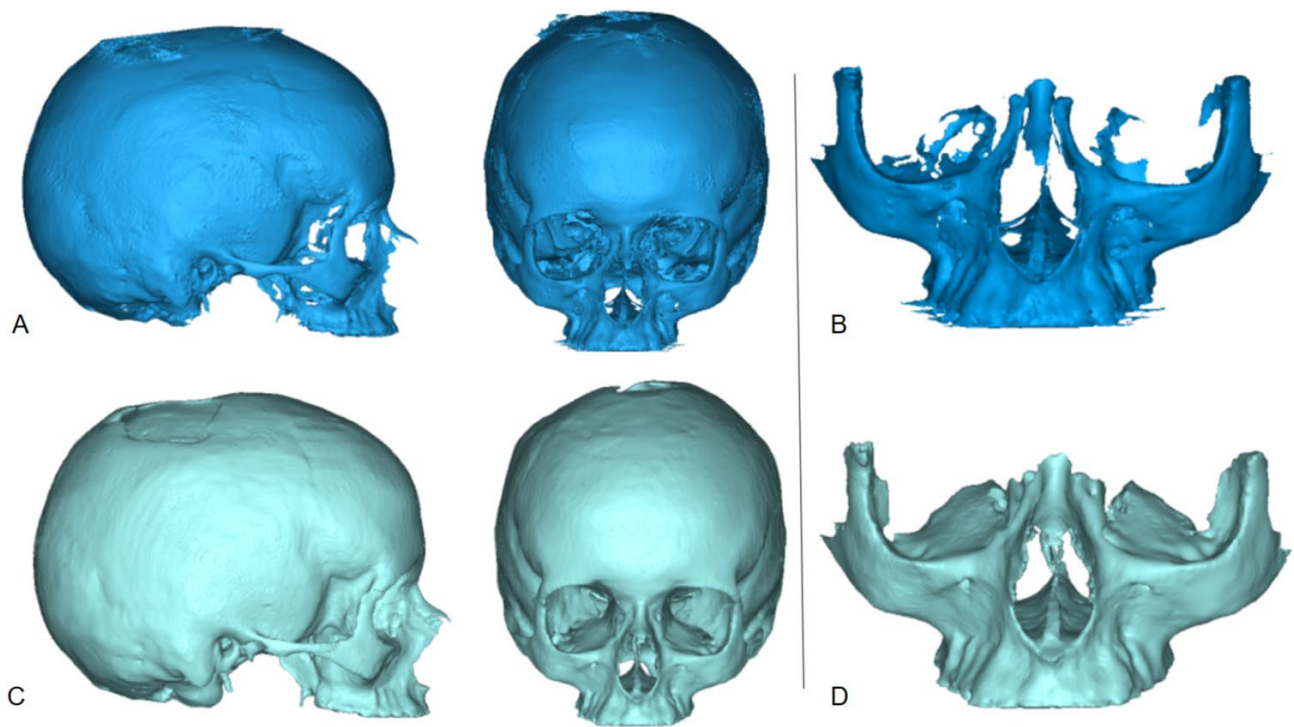


Fig. 1. Semi-automatic segmentation (thresholding-based) of the (A) upper skull (lateral and frontal view) and (B) maxillofacial complex with corresponding manual segmentation (C and D).

2. Materials and methods

This study was performed in accordance with the Declaration of Helsinki on medical research. Ethical approval was acquired from the Medical Ethics Committee of University Hospitals, KU Leuven, Leuven, Belgium (Reference No.: S57587). Informed consent was not required as patient information was anonymized. The study was carried out in line with the recommendations of Schwendicke et al. for reporting on artificial intelligence in dental research²⁶.

2.1. Dataset

A total of 144 scans were acquired from two CBCT devices, NewTom®VGI Evo (QR, Verona, Italy) and 3D Accuitomo® 170 (J. Morita, Kyoto, Japan), with variable scanning parameters (Table 1).

Inclusion criteria consisted of adult patients with permanent dentition. Scans of patients having dental implants, coronal/root fillings, sinus pathology, or having orthodontic brackets were also included. Patients with a history of maxillofacial trauma, orthognathic and maxillofacial reconstructive surgery, syndromic or degenerative diseases, and cleft lip and palate were excluded. The sample size was calculated based on previously comparable studies^{19,22} using a priori power analysis in G* power 3.1, assuming a paired two-sided t-test to compare intervention groups (neural network and observers) on the test dataset with a power of 80% and a significance level of 5%.

Table 1. CBCT scanning parameters.

Device	Number of scans	Field of view (cm)	Voxel size (mm)
NewTom V Gievo (QR, Verona, Italy)	83	24 x 19	0.30
		16 x 16	0.25
		15 x 12	0.10
		10 x 10	
		8 x 8	
3D Accuitomo 170 (J. Morita, Kyoto, Japan)	61	17 x 12	0.25
		14 x 10	0.20
		10 x 10	0.125
		10 x 5	
		8 x 8	

The CBCT images were exported in Digital Imaging and Communication in Medicine (DICOM) format and were randomly distributed into 3 subsets: a training set ($n = 110$), for CNN model training and fitting based on the labelled ground truth; a validation set ($n = 10$), for hyperparameter optimization and selection of an ideal model architecture; and a testing set ($n = 24$), to evaluate the model's performance including comparison with manual expert segmentation, used as a benchmark.

2.2. Ground truth labelling

2.2.1 *Upper skull*

A dataset of 30 CBCT scans acquired from NewTom device with full field of view (FOV 24x19 cm) were labelled manually in Mimics Innovation Suite (version 23.0, Materialise N.V., Leuven, Belgium) in order to train a preliminary model for segmentation of the upper skull (all the hard tissues of the head with the exception of the mandible) (Figure 1C). After importing the DICOM files into Mimics software, the manual segmentation was performed using multiple slices edit with automatic interpolation and a live wire function for delineation and fine-tuning of the upper skull's bony contours. The crowns of the teeth were cropped and removed to isolate the bony region of interest. All contours were checked in three orthogonal planes (sagittal, axial, and coronal) and in 3D volume rendering. Finally, the created mask of the upper skull was exported in Standard Tessellation Language (STL) file format for further processing in the CNN pipeline. Three experienced observers (an orthodontist, a maxillofacial radiologist, and one oral surgeon) performed this task, and the final segmentation was reassessed in a slice-by-slice manner by all the observers and corrections were performed if needed.

2.2.2. *Maxillofacial complex*

The preliminary model for automated segmentation of the upper skull indicated the need for refinement, specifically in the maxillofacial region. Moreover, this region is commonly included in the majority of the CBCT's FOVs and acts as a region of interest for maxillofacial surgeons, radiologists, and orthodontists, depending on the task at hand²⁷. Hence, the initial 30 cases were manually adjusted to confine the maxillofacial complex, including the palatine, maxillary, zygomatic, nasal, and lacrimal bones, defining the zygomaticotemporal, zygomaticofrontal, pterygomaxillary, pterygopalatine, frontomaxillary, and frontonasal sutures (Figure 1D). An additional dataset of 80 scans from both devices (NewTom and Accuitomo) was added to further train the model. Out of these, 32 scans were manually segmented as described above. Later, the manual segmentation of the remaining 48 scans was partially supported by the trained CNN model itself, which still required some modifications. These 48 scans were added in three training stages, allowing for gradual improvement of the model while decreasing the time needed for the manual segmentation with each stage. This step was performed by three observers (an orthodontist and two maxillofacial radiologists) and one of them rechecked all the segmentations to ensure that the agreed protocol was followed in relation to the anatomical extent and level of accuracy.

2.3 AI network architecture and training

Two CNN models were used in the pipeline with 3D U-Net architecture²⁸. Each network consisted of four contracting encoders and three expansive decoder blocks made up of two convolutions, followed by a rectified linear unit (ReLU) activation and group normalization²⁹ with eight feature maps. All convolutions had a kernel size of 3x3x3, 1 stride, and 1 dilation. A max pooling operation was applied after each encoder, reducing the spatial information by a factor of 2 in all dimensions.

The U Nets were trained as a binary classifier with a weighted Binary Cross Entropy Loss:

$$L_{BCE} = y_n * \log(p_n) + (1 - y_n) * \log(1 - p_n)$$

For each voxel n , where y_n is the ground truth value (0 or 1) and p_n refers to the predicted probability of the network. The training dataset was pre-processed using a two-step technique. Firstly, scans were resampled to an identical voxel size. Secondly, the full-size scans were down-sampled to a fixed size (96x96x96) at a lower resolution to overcome the memory limitations of the GPU (Figure 2). Two 3D U-Nets used for the segmentation operate at different fixed scan resolutions. The rough segmentation is performed on a voxel size of 1.5 mm/voxel (low resolution), while the subsequent fine segmentation on a voxel size of 0.23 mm/voxel (high resolution). At the end of the pipeline, both the scan and the AI predictions are resampled to the original scan resolution.

Subsequently, scans were imported into the primary 3D U-Net, which was specifically trained to segment low resolution scans. This rough segmentation was used to suggest 3D patches and clip only the patches belonged to the maxillofacial complex. These patches were in turn given to the second U-Net, finely segmented and then merged to produce a full resolution segmentation map. Thereafter, binarization was applied, and the largest connected component remained. Then, a marching cubes algorithm was applied to the binary image, and the predicted segmentation map was turned into an STL in a separate processing step. The resultant mesh was smoothed by a windowed-sinc function interpolation kernel that was run for 20 iterations with a passband value of 0.1 to create a 3D model suitable for different clinical applications^{20,22}.

The model parameters were optimized via Adam³⁰ with an initial learning rate of 1.25e-4 which was halved seven times during 300 epochs. Random spatial augmentations such as scaling, elastic deformation, and rotation were applied during training³¹. To prevent overfitting, early stopping was applied on the validation set. For accessibility, the CNN model was deployed to “Virtual Patient Creator” (creator.relu.eu, ReLu BV, Version October 2021), an online interactive imaging platform.

The users can upload CBCT images and obtain the automated segmentation of dentomaxillofacial structures (Figure 3). The segmentation can be downloaded as an STL file and used externally. Full details regarding the hardware used are provided as supplementary material.

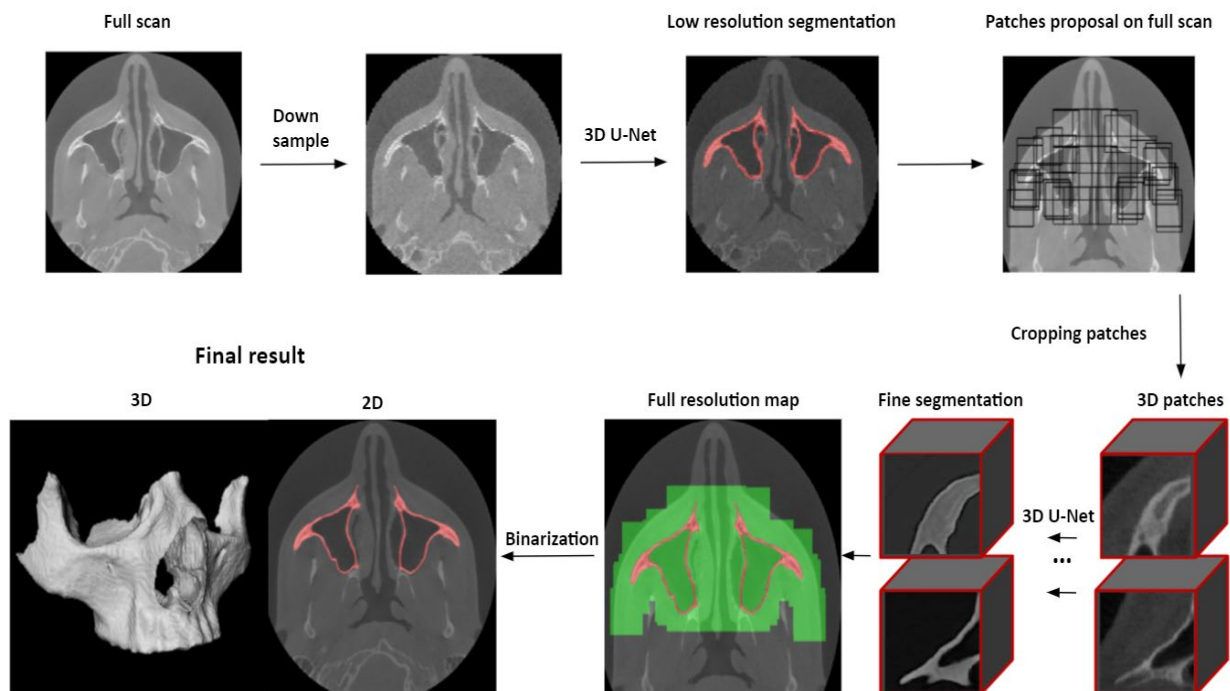


Fig. 2. 3D U-Net convolutional neural network pipeline for automated segmentation of the maxillofacial complex.

2.4 Testing of CNN pipeline

Testing of the CNN pipeline was carried out via the Virtual Patient Creator platform. The acquired automated segmentation was analysed visually by three operators. The types of identified flaws and their extent were documented and classified as follows;

- a- Excellent segmentation (no correction required),
- b- Very good segmentation (minor correction needed, with no clinical significance such as slight under- or over-segmentation of the ROI apart from the maxillary sinus walls or palate),
- c- Good segmentation (minor correction needed, having some clinical significance such as slight under- or over-segmentation of the ROI apart from the maxillary sinus walls or palate, slight over-segmentation of the foraminal margins),
- d- Insufficient segmentation (significant over- or under-segmentation with repetition needed)

Following classification, the AS was downloaded in STL format and manually corrected by two operators using Mimics software, if needed. The adjusted segmentation was denoted as “corrected segmentation (CS)”.

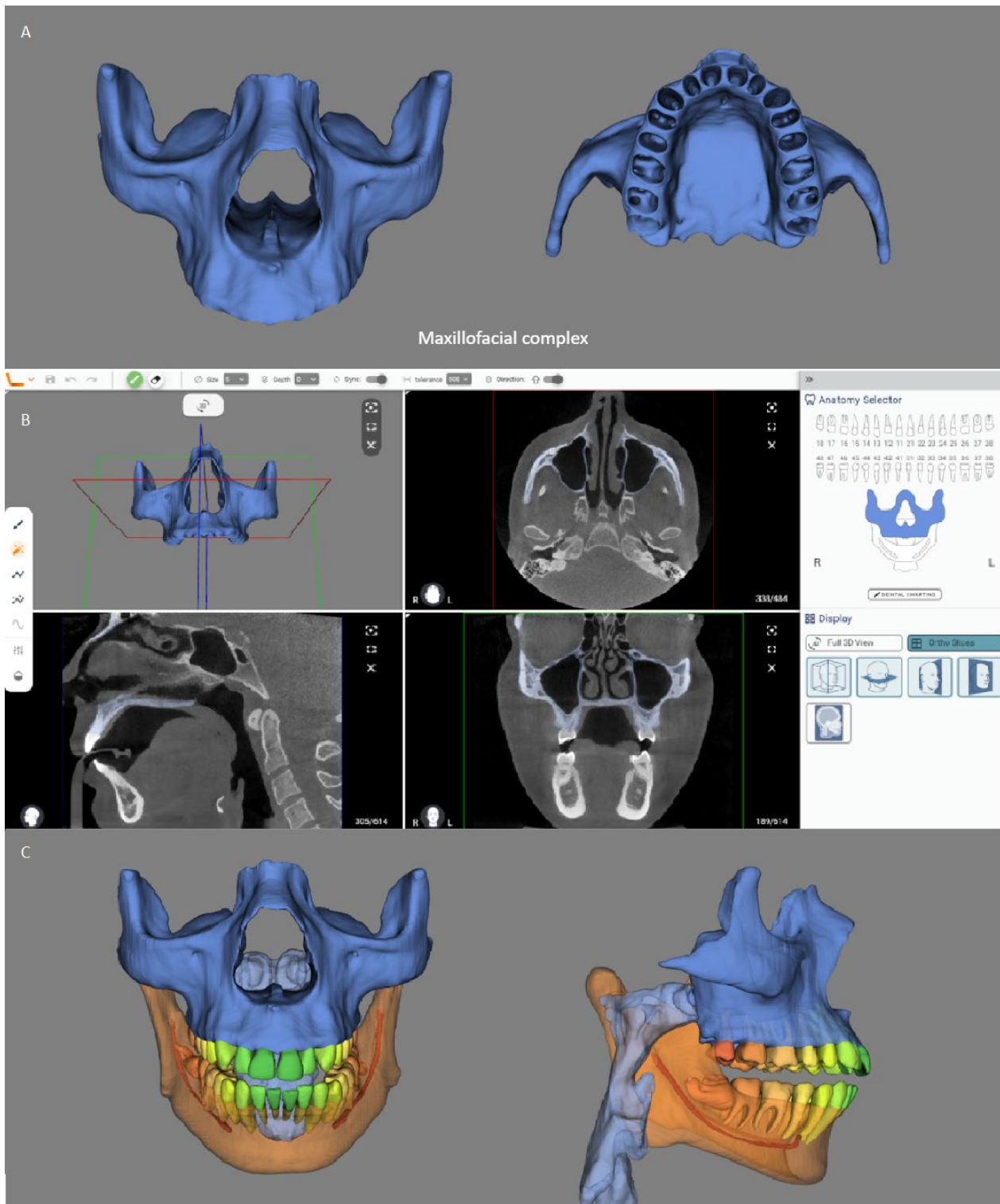


Fig. 3. Automated segmentation on the Virtual Patient Creator platform. A: segmentation of the maxillofacial complex, B: online tools for adjustment C: other structures of the dentomaxillofacial region available for segmentation on the platform.

2.5 Evaluation metrics

One operator manually segmented 12 CBCT scans with different FOVs from the testing dataset for comparison with the corresponding automated segmentation (AS). Additionally, semi-automatic segmentation (SA) was performed using Mimics software with thresholding from 500 to 700 and compared with the manual segmentation (Figure 1B, D). Two independent operators performed the needed corrections (CS) on the whole testing set (24 CBCT scans) and compared the outcomes with the AS.

2.5.1. Time

The time needed for the MS was calculated starting after the import of DICOM data in Mimics till exporting the STL file. For automated segmentation, the algorithm directly registered the time needed to build a full resolution binary segmentation. For corrected segmentation, the time taken by the CNN model and the time spent for manual correction were summed up.

2.5.2. Accuracy

A confusion matrix was used to compare the different types of segmentation at the voxel level using four variables: true positive (TP), true negative (TN), false positive (FP), and false negative (FN) voxels. The accuracy of the resultant automated segmentation was evaluated based on the following metrics^{32,33}:

Dice similarity coefficient (DSC) refers to the voxel overlap between volume A and B divided by their total number of voxels. A DSC equals 1 means complete overlap.

$$DSC(A, B) = \frac{2|A \cap B|}{|A| + |B|} = \frac{2TP}{2TP + FP + FN}$$

95% Hausdorff distance (HD): shows the maximum distance between all pairs of voxels belonging to volumes A and B. The 95% HD is used to avoid the impact of outliers.

$$95\% \text{ HD} = P_{95}(\min_{a \in A} \|B - A\|_2 \cup \min_{b \in B} \|A - B\|_2)$$

Intersection over union (IoU): refers to the voxel overlap between volume A and B divided by their union. An IoU equals 1 indicates complete overlap.

$$IoU(A, B) = \frac{|A \cap B|}{|A \cup B|} = \frac{TP}{TP + FP + FN}$$

For surface comparison, the STL files were imported to 3-matic software (Materialise NV, Leuven, Belgium), and part comparison analysis was applied to calculate the root mean square (RMS). This allowed measurement of the overlap difference between two surfaces. An RMS equals 0 mm implies a complete match.

$$RMS(x) = \sqrt{\frac{1}{n} (x_1^2 + x_2^2 + \dots + x_n^2)}$$

x = the distance (in millimeters) between the two surfaces' closest points.

2.5.3. Consistency

The trained CNN model was fully consistent as it performed a predefined set of mathematical operations. This enabled the model to keep producing identical segmentation every time it processed the same scan. Hence, the model was not assessed for its consistency. The inter-operator consistency was assessed by allowing two operators to perform the needed corrections of the testing set. Afterwards, the generated STL files were compared to each other.

2.6 Statistical analysis

Data were analysed with RStudio (Integrated Development Environment for R, version 1.3.1093, PBC, Boston, MA). The mean and standard deviation were calculated for all the evaluation metrics.

3. Results

3.1 Timing

The average time required for manual segmentation (12 CBCT scans) was 132.7 minutes, compared to the corresponding times of 39.07 seconds (203.8-fold time reduction) and 9.13 minutes (13.5-fold time reduction) for automated and corrected segmentation, respectively (Figure 4).

The average time needed for the manual correction of the testing set (24 CBCT scans) by the two operators was 9.33 minutes and 11.11 minutes, respectively. The corresponding average time for automated segmentation was 43.41 seconds.

3.2 Accuracy

Table 2 and Figure 5 illustrate the evaluation metrics for model accuracy compared to ground truth. The CNN model demonstrated a high DSC of 92.6% and a 95% HD of 0.62 mm, thereby confirming high similarity between automated and manually segmented 3D surfaces. For the comparison between semi-automated and manual segmentation, the accuracy metrics revealed a DSC of 68.7% and a 95% HD of 2.78 mm.

Timing for MS and AS

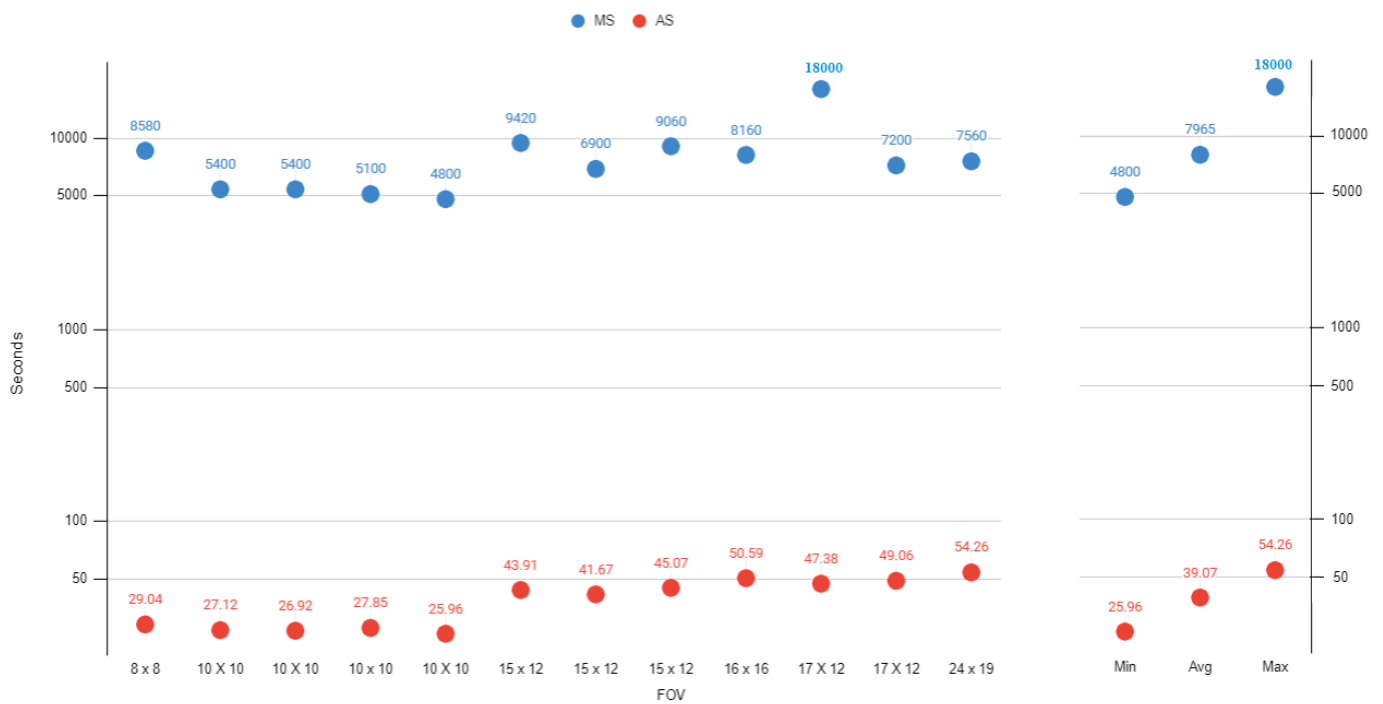


Fig. 4. Timing (in seconds) of manual segmentation (MS) and automated segmentation (AS).

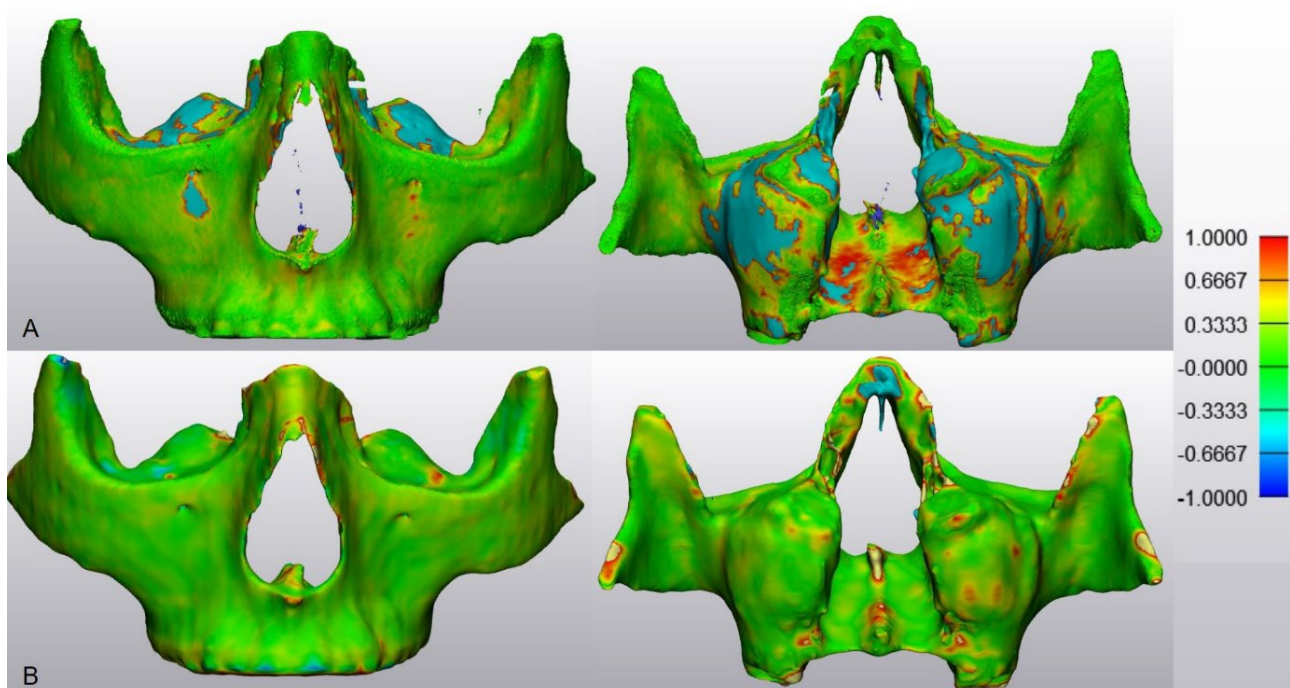


Fig. 5. STL comparison map between A) semi-automatic, B) automated segmentation versus manual segmentation.

Table 2. Evaluation metrics for accuracy.

Metric	Descriptive analysis	AS vs MS	SA vs MS
DSC	Mean	0.926	0.687
	SD	0.010	0.071
	Min	0.909	0.504
	Max	0.944	0.767
95%HD (mm)	Mean	0.621	2.78
	SD	0.126	0.404
	Min	0.447	2.2
	Max	0.823	3.56
IoU	Mean	0.862	0.527
	SD	0.017	0.078
	Min	0.834	0.337
	Max	0.894	0.622
RMS (mm)	Mean	0.5	1.76
	SD	0.137	0.267
	Min	0.296	1.46
	Max	0.741	2.26

AS: Automated segmentation, MS: Manual segmentation, SA: Semi-automatic segmentation, SD: Standard deviation, Min: Minimal value, Max: Maximal value, DSC: Dice Similarity Coefficient, HD: Hausdorff Distance, IoU: Intersection over Union, and RMS: root mean square.

3.3 Consistency

Table 3 presents the evaluation metrics for inter-operator consistency (for expert-based minor correction of the AS). According to the evaluation specifically designed by the authors for clinical appraisal, all AS scored a, b, or c, requiring minor to no corrections for errors of limited or no clinical impact. No segmentation was considered insufficient (d).

The comparison between automated and corrected segmentation showed an almost perfect overlap with a DSC of 99.8% and a 95% HD of 0% for both operators, indicating that minimal corrections were performed. An improved overlap was observed between automated and corrected segmentation compared to automated and manual segmentation. The inter-operator consistency also showed excellent DSC (99.7%) and 95% HD (0.009).

Table 3. Evaluation metrics for consistency.

Metric	Descriptive analysis	AS vs CS (operator 1)	AS vs CS (operator 2)	Inter-observer
DSC	Mean	0.998	0.998	0.997
	SD	0.003	0.002	0.003
	Min	0.988	0.994	0.989
	Max	0.999	0.999	0.999
95%HD (mm)	Mean	0	0	0.009
	SD	0	0	0.042
	Min	0	0	0
	Max	0	0	0.200
IoU	Mean	0.996	0.997	0.995
	SD	0.006	0.003	0.005
	Min	0.977	0.988	0.979
	Max	0.999	0.999	0.999
RMS (mm)	Mean	0.098	0.082	0.099
	SD	0.135	0.079	0.12
	Min	0.012	0.014	0.015
	Max	0.572	0.273	0.521

AS: Automated segmentation, CS: Corrected segmentation, SD: Standard deviation, Min: Minimal value, Max: Maximal value, DSC: Dice Similarity Coefficient, HD: Hausdorff Distance, IoU: Intersection over Union, and RMS: root mean square.

4. Discussion

An accurate segmentation of the maxillofacial complex from CBCT images is a prerequisite in the majority of dentomaxillofacial workflows for the creation of a 3D virtual patient model. The main clinical applications requiring segmented maxillofacial complex include orthognathic and reconstructive surgical treatment planning, designing of patient-specific implants, orthodontic virtual set-up and post-operative follow-up assessment of skeletal tissue³⁴⁻⁴².

Complete automatization and increasing the time-efficiency of the segmentation are necessary elements to consider which might have the ability to surpass the limitations of the currently available segmentation algorithms and software programs irrespective of the operator's experience. Therefore,

the current study proposed a fully automated deep learning CNN model for maxillofacial bone segmentation from CBCT images.

The generalizability of the proposed CNN model was ensured by using two CBCT devices with different scanning parameters and including scans with the presence of metal artifacts from implants, fillings, and orthodontic brackets. The model was able to segment the maxillofacial complex with an average time of less than one minute, which allowed a significant 204-fold decrease in the time required compared to manual segmentation. Moreover, the model showed high accuracy, comparable with the segmentation provided by clinical experts. This adds to the advantage of transferring the creator's expertise to all subsequent users through knowledge accumulation during the training phase. In contrast, manual segmentation is dependent on the operator's experience, suffers from a steep learning curve, and is prone to inter- and intra-operator variability, which could negatively impact the accuracy of the segmented region of interest. Additionally, the inconsistency between operators was quite minor, as observed by the classification based on the amount of required correction. However, both automated and corrected segmentation showed a perfect overlap because the mentioned corrections referred to a minimal region of the whole volume.

While using manual segmentation as a reference, the semi-automated approach revealed a 25% lower DSC score compared to the automated approach. This lower scoring could be attributed to the fact that the semi-automatic approach was unable to segment thin bony structures with the adjusted threshold level (Figure 1A, B). Furthermore, the ability of the proposed model to delineate the maxillofacial complex based on sutural limits could act as a viable tool for computer-assisted planning and follow-up assessment of maxillofacial reconstructive procedures.

Previous evidence related to CNN-based maxillofacial bone segmentation methodologies is heterogeneous, and no studies have reported on maxillofacial complex segmentation from CBCT images. Hence, the findings of the current study were compared to those assessing segmentation of the upper skull, with datasets derived from both CT and CBCT devices. Dot et al.⁴³ found a DSC value of 96% for the segmentation of the upper skull from CT images with an average time of 10 minutes using a U-Net framework. Yang and Su²⁴ applied AI-enabled segmentation in Mimics viewer for the segmentation of the upper skull from CT images and reported a DSC of 92.4%. Ham et al.⁴⁴ proposed a 3D U-Net based approach for the segmentation of craniofacial hard tissue structures from CBCT images and showed a DSC score of 82.8%. In comparison, the model presented in the current study showed a similar range of accuracy to a model originating from CT-derived data, whereas the model's performance was higher compared to those using CBCT datasets. As the contrast resolution of CT scan is higher with a homogenous intensity distribution, one might expect a more straightforward and accurate segmentation¹⁷. The same cannot be stated about the CBCT images,

where lower image quality and large intensity differences exist and vary between different regions of interest, scanning devices, and patients.

Furthermore, a comparison with existing studies in relation to the time required for segmentation was deemed difficult owing to the lack of reporting of this parameter. It should be noted that time is an important factor to consider in clinical dentistry, as one of the pillars of an optimal digital workflow is time-efficiency. Thereby, future studies applying artificial intelligence for segmentation should report time as a primary outcome to improve the level of evidence.

The main strength of the study was the inclusion of two CBCT devices with different acquisition parameters and metal artifacts for training, which enabled a more practical way to assess the performance of the model. However, further studies are warranted to assess the model performance based on the datasets from other CBCT devices and institutions for justifying its generalizability and applicability for regular clinical tasks. A limitation of the proposed method was the exclusion of nerve canals and crestal bone, for which further development of the model is currently under progress.

5. Conclusion

The proposed CNN model is an accurate, consistent, and time-efficient alternative to the conventional manual and semi-automated segmentation methods for the generation of a 3D maxillofacial complex model. An observer-independent 204-fold time reduction for the segmentation task compared to the manual approach and the integration of the model into an online platform can fit the current demands of clinical practice without the need of an experienced operator or a computer with high computational power.

References

1. T. Joda, M.M. Bornstein, R.E. Jung, M. Ferrari, T. Waltimo, N.U. Zitzmann, Recent Trends and Future Direction of Dental Research in the Digital Era, *Int. J. Environ. Res. Public Health*. 17 (2020) 1987. <https://doi.org/10.3390/ijerph17061987>.
2. G. Gopal, C. Suter-Crazzolara, L. Toldo, W. Eberhardt, Digital transformation in healthcare - Architectures of present and future information technologies, *Clin. Chem. Lab. Med.* 57 (2019) 328–335. <https://doi.org/10.1515/cclm-2018-0658>.
3. C.H.F. Hämmerle, L. Cordaro, N. van Assche, G.I. Benic, M. Bornstein, F. Gamper, K. Gotfredsen, D. Harris, M. Hürzeler, R. Jacobs, T. Kapos, R.J. Kohal, S.B.M. Patzelt, I. Sailer, A. Tahmaseb, M. Vercruyssen, D. Wismeijer, Digital technologies to support planning, treatment, and fabrication processes and outcome assessments in implant dentistry. Summary and consensus statements. The 4th EAO consensus conference 2015, *Clin. Oral Implants Res.* 26 (2015) 97–101. <https://doi.org/10.1111/clr.12648>.
4. S. Shujaat, M.M. Bornstein, J.B. Price, R. Jacobs, Integration of imaging modalities in digital dental workflows - possibilities, limitations, and potential future developments, *Dentomaxillofacial Radiol.* 50 (2021) 20210268. <https://doi.org/10.1259/dmfr.20210268>.
5. F. Renard, S. Guedria, N. De Palma, N. Vuillerme, Variability and reproducibility in deep learning for medical image segmentation, *Sci. Rep.* 10 (2020) 1–16. <https://doi.org/10.1038/s41598-020-69920-0>.
6. D.J. Withey, Z.J. Koles, Medical image segmentation: Methods and software, *Proc. 2007 Jt. Meet. 6th Int. Symp. Noninvasive Funct. Source Imaging Brain Hear. Int. Conf. Funct. Biomed. Imaging, NFSI ICFBI 2007*. (2007) 140–143. <https://doi.org/10.1109/NFSI-ICFBI.2007.4387709>.
7. J.K. Udupa, H.M. Hung, K.S. Chuang, Surface and volume rendering in three-dimensional imaging: A comparison, *J. Digit. Imaging*. 4 (1991) 159–168. <https://doi.org/10.1007/BF03168161>.
8. Q. Liu, H. Deng, C. Lian, X. Chen, D. Xiao, L. Ma, X. Chen, T. Kuang, J. Gateno, P.-T. Yap, J.J. Xia, SkullEngine: A Multi-stage CNN Framework for Collaborative CBCT Image Segmentation and Landmark Detection, in: *Lect. Notes Comput. Sci. (Including Subser. Lect. Notes Artif. Intell. Lect. Notes Bioinformatics)*, 2021: pp. 606–614. https://doi.org/10.1007/978-3-030-87589-3_62.
9. N. Boucher, M. Mupparapu, K. Matsumoto, Cone Beam Computerized Tomography Imaging for Orthodontic Diagnosis, in: *3D Diagnosis Treat. Plan. Orthod.*, Springer International Publishing, 2021: pp. 55–91. https://doi.org/10.1007/978-3-030-57223-5_4.
10. R. Pauwels, R. Jacobs, S.R. Singer, M. Mupparapu, CBCT-based bone quality assessment: Are Hounsfield units applicable?, *Dentomaxillofacial Radiol.* 44 (2015). <https://doi.org/10.1259/dmfr.20140238>.

11. Y.B. Chang, J.J. Xia, P. Yuan, T.H. Kuo, Z. Xiong, J. Gateno, X. Zhou, 3D segmentation of maxilla in cone-beam computed tomography imaging using base invariant wavelet active shape model on customized two-manifold topology, *J. Xray. Sci. Technol.* 21 (2013) 251–282. <https://doi.org/10.3233/XST-130369>.
12. L. Wang, Y. Gao, F. Shi, G. Li, K.C. Chen, Z. Tang, J.J. Xia, D. Shen, Automated segmentation of CBCT image with prior-guided sequential random forest, *Lect. Notes Comput. Sci. (Including Subser. Lect. Notes Artif. Intell. Lect. Notes Bioinformatics)*. 9601 LNCS (2016) 72–82. https://doi.org/10.1007/978-3-319-42016-5_7.
13. K. Hung, C. Montalvao, R. Tanaka, T. Kawai, M.M. Bornstein, The use and performance of artificial intelligence applications in dental and maxillofacial radiology: A systematic review, *Dentomaxillofacial Radiol.* 49 (2019). <https://doi.org/10.1259/dmfr.20190107>.
14. K. Hung, A.W.K. Yeung, R. Tanaka, M.M. Bornstein, Current applications, opportunities, and limitations of AI for 3D imaging in dental research and practice, *Int. J. Environ. Res. Public Health.* 17 (2020) 1–18. <https://doi.org/10.3390/ijerph17124424>.
15. Q. Liu, C. Lian, D. Xiao, L. Ma, H. Deng, X. Chen, Di. Shen, P.-T. Yap, J.J. Xia, Skull Segmentation from CBCT Images via Voxel-Based Rendering, in: *IEEE J. Biomed. Heal. Informatics*, 2021: pp. 615–623. https://doi.org/10.1007/978-3-030-87589-3_63.
16. J. Minnema, J. Wolff, J. Koivisto, F. Lucka, K.J. Batenburg, T. Forouzanfar, M. van Eijnatten, Comparison of convolutional neural network training strategies for cone-beam CT image segmentation, *Comput. Methods Programs Biomed.* 207 (2021) 106192. <https://doi.org/10.1016/j.cmpb.2021.106192>.
17. J. Minnema, M. van Eijnatten, W. Kouw, F. Diblen, A. Mendrik, J. Wolff, CT image segmentation of bone for medical additive manufacturing using a convolutional neural network, *Comput. Biol. Med.* 103 (2018) 130–139. <https://doi.org/10.1016/j.compbimed.2018.10.012>.
18. P. Lahoud, S. Diels, L. Niclaes, S. Van Aelst, H. Willems, A. Van Gerven, M. Quirynen, R. Jacobs, Development and validation of a novel artificial intelligence driven tool for accurate mandibular canal segmentation on CBCT, *J. Dent.* (2021) 103891. <https://doi.org/10.1016/j.jdent.2021.103891>.
19. P.-J. Verhelst, A. Smolders, T. Beznik, J. Meewis, A. Vandemeulebroucke, E. Shaheen, A. Van Gerven, H. Willems, C. Politis, R. Jacobs, Layered deep learning for automatic mandibular segmentation in cone-beam computed tomography, *J. Dent.* 114 (2021) 103786. <https://doi.org/10.1016/j.jdent.2021.103786>.
20. E. Shaheen, A. Leite, K.A. Alqahtani, A. Smolders, A. Van Gerven, H. Willems, R. Jacobs, A novel deep learning system for multi-class tooth segmentation and classification on cone beam computed tomography. A validation study, *J. Dent.* (2021) 103865. <https://doi.org/10.1016/j.jdent.2021.103865>.

21. P. Lahoud, M. EzEldeen, T. Beznik, H. Willems, A. Leite, A. Van Gerven, R. Jacobs, Artificial Intelligence for Fast and Accurate 3-Dimensional Tooth Segmentation on Cone-beam Computed Tomography, *J. Endod.* 47 (2021) 827–835. <https://doi.org/10.1016/j.joen.2020.12.020>.
22. S. Shujaat, O. Jazil, H. Willems, A. Van Gerven, E. Shaheen, C. Politis, R. Jacobs, Automatic segmentation of the pharyngeal airway space with convolutional neural network, *J. Dent.* 111 (2021) 103705. <https://doi.org/10.1016/j.jdent.2021.103705>.
23. N. Morgan, A. Van Gerven, A. Smolders, K. de Faria Vasconcelos, H. Willems, R. Jacobs, Convolutional neural network for automatic maxillary sinus segmentation on cone-beam computed tomographic images, *Sci. Rep.* 12 (2022) 7523. <https://doi.org/10.1038/s41598-022-11483-3>.
24. W. fa Yang, Y. xiong Su, Artificial intelligence-enabled automatic segmentation of skull CT facilitates computer-assisted craniomaxillofacial surgery, *Oral Oncol.* 118 (2021). <https://doi.org/10.1016/j.oraloncology.2021.105360>.
25. W. Scarfe, B. Azevedo, S. Toghyani, A. Farman, Cone Beam Computed Tomographic imaging in orthodontics, *Aust. Dent. J.* 62 (2017) 33–50. <https://doi.org/10.1111/adj.12479>.
26. F. Schwendicke, T. Singh, J.-H. Lee, R. Gaudin, A. Chaurasia, T. Wiegand, S. Uribe, J. Krois, Artificial intelligence in dental research: Checklist for authors, reviewers, readers, *J. Dent.* 107 (2021) 103610. <https://doi.org/10.1016/j.jdent.2021.103610>.
27. Y.M. Bichu, I. Hansa, A.Y. Bichu, P. Premjani, C. Flores-Mir, N.R. Vaid, Applications of artificial intelligence and machine learning in orthodontics: a scoping review, *Prog. Orthod.* 22 (2021). <https://doi.org/10.1186/s40510-021-00361-9>.
28. Ö. Çiçek, A. Abdulkadir, S.S. Lienkamp, T. Brox, O. Ronneberger, 3D U-Net: Learning Dense Volumetric Segmentation from Sparse Annotation, in: *Lect. Notes Comput. Sci. (Including Subser. Lect. Notes Artif. Intell. Lect. Notes Bioinformatics)*, 2016: pp. 424–432. https://doi.org/10.1007/978-3-319-46723-8_49.
29. Y. Wu, K. He, Group Normalization, *Int. J. Comput. Vis.* 128 (2020) 742–755. <https://doi.org/10.1007/s11263-019-01198-w>.
30. D.P. Kingma, J.L. Ba, Adam: A method for stochastic optimization, *3rd Int. Conf. Learn. Represent. ICLR 2015 - Conf. Track Proc.* (2015) 1–15.
31. C. Shorten, T.M. Khoshgoftaar, A survey on Image Data Augmentation for Deep Learning, *J. Big Data.* 6 (2019). <https://doi.org/10.1186/s40537-019-0197-0>.
32. D. Zhang, F. He, S. Han, L. Zou, Y. Wu, Y. Chen, An efficient approach to directly compute the exact Hausdorff distance for 3D point sets, *Integr. Comput. Aided. Eng.* 24 (2017) 261–277. <https://doi.org/10.3233/ICA-170544>.

33. A.A. Taha, A. Hanbury, Metrics for evaluating 3D medical image segmentation: Analysis, selection, and tool, *BMC Med. Imaging*. 15 (2015). <https://doi.org/10.1186/s12880-015-0068-x>.
34. K. Matsumoto, S. Sherrill-Mix, N. Boucher, N. Tanna, A cone-beam computed tomographic evaluation of alveolar bone dimensional changes and the periodontal limits of mandibular incisor advancement in skeletal Class II patients, *Angle Orthod*. 90 (2020) 330–338. <https://doi.org/10.2319/080219-510.1>.
35. J.M. Plooi, T.J.J. Maal, P. Haers, W.A. Borstlap, A.M. Kuijpers-Jagtman, S.J. Bergé, Digital three-dimensional image fusion processes for planning and evaluating orthodontics and orthognathic surgery. A systematic review, *Int. J. Oral Maxillofac. Surg.* 40 (2011) 341–352. <https://doi.org/10.1016/j.ijom.2010.10.013>.
36. H. Ma, J. Van Dessel, M. Bila, Y. Sun, C. Politis, R. Jacobs, Application of Three-Dimensional Printed Customized Surgical Plates for Mandibular Reconstruction: Report of Consecutive Cases and Long-Term Postoperative Evaluation, *J. Craniofac. Surg.* 32 (2021) e663–e667. <https://doi.org/10.1097/scs.00000000000007835>.
37. I. Azarmehr, K. Stokbro, R.B. Bell, T. Thygesen, Contemporary Techniques in Orbital Reconstruction: A Review of the Literature and Report of a Case Combining Surgical Navigation, Computer-Aided Surgical Simulation, and a Patient-Specific Implant, *J. Oral Maxillofac. Surg.* 78 (2020) 594–609. <https://doi.org/10.1016/j.joms.2019.11.005>.
38. B. Li, H. Wei, T. Jiang, Y. Qian, T. Zhang, H. Yu, L. Zhang, X. Wang, Randomized clinical trial of the accuracy of patient-specific implants versus cad/cam splints in orthognathic surgery, *Plast. Reconstr. Surg.* 148 (2021) 1101–1110. <https://doi.org/10.1097/PRS.00000000000008427>.
39. J. Uechi, Y. Tsuji, M. Konno, K. Hayashi, T. Shibata, E. Nakayama, I. Mizoguchi, Generation of virtual models for planning orthognathic surgery using a modified multimodal image fusion technique, *Int. J. Oral Maxillofac. Surg.* 44 (2015) 462–469. <https://doi.org/10.1016/j.ijom.2014.11.007>.
40. J.M. Palomo, H. El, N. Stefanovic, M. Bazina, Diagnostic Value of 3D Imaging in Clinical Orthodontics, in: *Craniofacial 3D Imaging*, Springer International Publishing, Cham, 2019: pp. 113–139. https://doi.org/10.1007/978-3-030-00722-5_7.
41. W. De Vos, J. Casselman, G.R.J. Swennen, Cone-beam computerized tomography (CBCT) imaging of the oral and maxillofacial region: A systematic review of the literature, *Int. J. Oral Maxillofac. Surg.* 38 (2009) 609–625. <https://doi.org/10.1016/j.ijom.2009.02.028>.
42. N. Mathew, S. Gandhi, I. Singh, M. Solanki, N.S. Bedi, 3D Models Revolutionizing Surgical Outcomes in Oral and Maxillofacial Surgery: Experience at Our Center, *J. Maxillofac. Oral Surg.* 19 (2020) 208–216. <https://doi.org/10.1007/s12663-019-01275-0>.
43. G. Dot, T. Schouman, G. Dubois, P. Rouch, L. Gajny, Fully automatic segmentation of craniomaxillofacial CT scans for computer-assisted orthognathic surgery planning using the nnU-Net framework, (2021) 1–17. <https://doi.org/https://doi.org/10.1101/2021.07.22.21260825>.

44. S. Ham, A. Lee, J. Park, B. Younghwa, S. Lee, M. Bae, N. Kim, Multi-structure Segmentation of Hard Tissues, Maxillary Sinus, Mandible, Mandibular Canals in Cone Beam CT of Head and Neck with 3D U-Net, (2018) 3–5.

Convolutional neural network for automatic maxillary sinus segmentation on cone-beam computed tomographic images

Morgan N. ^{1,2}

Van Gerven A.³

Smolders A.³

de Faria Vasconcelos K.¹

Willems H.³

Jacobs R.^{1,4}

¹ OMFS IMPATH Research Group, Department of Imaging & Pathology, Faculty of Medicine, KU Leuven & Oral and Maxillofacial Surgery, University Hospitals Leuven, Kapucijnenvoer33, BE-3000 Leuven, Belgium

² Department of Oral Medicine, Faculty of Dentistry, Mansoura University, 35516 Mansoura, Dakahlia, Egypt

³ Relu BV, Kapeldreef 60, BE-3000 Leuven, Belgium

⁴ Department of Dental Medicine, Karolinska Institutet, Box 4064, 141 04 Huddinge, Stockholm, Sweden

Published in *Scientific Reports* 2022 May 7;12(1):7523.

Abstract

An accurate 3D segmentation of the maxillary sinus is crucial for multiple diagnostic and treatment applications. Yet, it is challenging and time-consuming when manually performed on a cone-beam computed tomography (CBCT) dataset. Recently, convolutional neural networks (CNNs) have proven to provide excellent performance in the field of 3D image analysis. Hence, this study developed and validated an automated CNN-based methodology for the segmentation of the maxillary sinus using CBCT images. A dataset of 264 sinuses was acquired from 2 CBCT devices and randomly divided into 3 subsets: training, validation, and testing. A 3D U-Net architecture CNN model was developed and compared to semi-automatic segmentation in terms of time, accuracy, and consistency. The average time was significantly reduced ($p\text{-value} < 2.2e-16$) by automatic segmentation (0.4 min) compared to semi-automatic segmentation (60.8 min). The model accurately identified the segmented region with a dice similarity coefficient (DSC) of 98.4%. The inter-observer reliability for minor refinement of automatic segmentation showed an excellent DSC of 99.6%.

The proposed CNN model provided a time-efficient, precise, and consistent automatic segmentation which could allow the accurate generation of 3D models for diagnosis and virtual treatment planning.

1. Introduction

The maxillary sinus (*antrum of Highmore*) is the largest of the four paranasal sinuses, which are air-filled spaces located within the skull surrounding the nasal cavity¹. An adult's maxillary sinus has a pyramidal shape and lies in the body of the maxilla. It is bounded superiorly by the orbital floor, extending laterally into the zygomatic process of the maxilla and the zygomatic bone. On the medial side, it coincides with the lateral wall of the nasal cavity, communicating with it through the sinus ostium. The floor of the sinus is formed by the alveolar and palatine processes of the maxilla, which is in close proximity to the roots of the maxillary posterior teeth²⁻⁵.

Owing to the vital position of the sinus, its assessment is of paramount importance for maxillofacial surgeons, dentists, ENT surgeons, and dentomaxillofacial radiologists¹. An accurate three-dimensional (3D) segmentation of the sinus is crucial for multiple diagnostic and treatment applications, where evaluation of sinus changes, remodeling at follow-up, volumetric analysis^{6,7} or creation of 3D virtual models is required. Furthermore, the most relevant surgical procedures requiring sinus assessment include implant placement, sinus augmentation^{8,9} and orthognathic surgery.

Although the maxillary sinus is a well-delineated cavity, its 3-D segmentation is not a simple task. The close proximity of the maxillary sinus to the nasal passages and the teeth roots, along with its anatomical variations and frequently associated sinus thickening, makes the segmentation a challenging task. Such 3-D segmentations could be performed either by multi-slice (MSCT)¹⁰ or cone-beam computed tomography (CBCT). In oral health care, the maxillary sinus is mostly visualized using CBCT imaging for diagnosis and treatment planning¹¹⁻¹³. It provides a multiplanar sinus reconstruction, relatively lower radiation dose and isotropic volume resolution¹⁴. However, the segmentation of CBCT images still remains a challenging task due to the issues of image noise, low soft-tissue contrast, beam hardening artifacts, and a lack of absolute Hounsfield Unit¹⁵ (HU) calibration^{16,17}.

The manual segmentation of the maxillary sinus on CBCT images is time-consuming and dependent on the practitioner's experience with high inter- and intra-observer variability¹⁸. Other techniques, such as semi-automatic segmentation, improve the segmentation efficiency, yet they still require manual adjustments that can also induce error^{10,19}. Recently, artificial intelligence (AI) technologies have started to play a growing role in the field of dentomaxillofacial radiology^{20,21}. In particular, deep learning algorithms have gained much attention in the medical field for their ability to handle large and complex data, extract useful information, and allow automatic learning of feature hierarchies such as edges, shapes, and corners²².

Convolutional neural networks (CNNs) are one of the deep learning approaches that have shown excellent performance in the field of image analysis. It uses multi-layer neural computational connections for image processing tasks such as classification and segmentation²². The application of CNN for CBCT image segmentation could overcome the challenges associated with the other techniques by providing an efficient and consistent segmentation tool while maintaining anatomical accuracy. Therefore, the aim of this study was to develop and validate an automated CNN-based methodology for the segmentation of maxillary sinuses on CBCT images.

2. Materials and methods

This study was conducted in accordance with the standards of the Helsinki Declaration on medical research. Institutional ethical committee approval was obtained from the Ethical Review Board of the University Hospitals of Leuven (reference number: S57587). Informed consent was not required as patient-specific information was anonymized. The study plan and report followed the recommendations of Schwendicke et al.²³ for reporting on artificial intelligence in dental research.

2.1 Dataset

A sample of 132 CBCT scans (264 sinuses, 75 females and 57 males, mean age 40 years) from 2013 to 2021 with different scanning parameters was collected (Table 1). Inclusion criteria were patients with permanent dentition and maxillary sinus with/without mucosal thickening (shallow > 2mm, moderate > 4mm) and/or with semi-spherical membrane in one of the walls²⁴. Scans having dental restorations, orthodontic brackets and implants were also included. The exclusion criteria were patients with a history of trauma, sinus surgery, or the presence of pathologies affecting its contour.

Table 1. CBCT scanning parameters.

Device	Number of scans	Field of view (cm)	Voxel size (mm)
Newtom VGi evo (Cefla, Imola, Italy)	71	24 x 19	0.30
		16 x 16	0.25
		15 x 12	0.10
		10 x 10	
		8 x 8	
3D Accuitomo 170 (J. Morita, Kyoto, Japan)	61	17 x 12	0.25
		14 x 10	0.20
		10 x 10	0.125
		10 x 5	
		8 x 8	

The Digital Imaging and Communication in Medicine (DICOM) files of the CBCT images were exported anonymously. The dataset was further randomly divided into three subsets: 1. a training set (n = 83 scans) for training the CNN model based on the ground truth; 2. a validation set (n = 19 scans) for evaluation and selection of the best model; and 3. a testing set (n = 30 scans) for testing the model performance by comparison with ground truth.

2.2 Ground truth labelling

The ground truth datasets for training and testing of the CNN model were labelled by semi-automatic segmentation of the sinus using Mimics Innovation Suite (version 23.0, Materialise N.V., Leuven, Belgium). Initially, a custom threshold leveling was adjusted between (-1024 to -200 Hounsfield units (HU)) to create a mask of the air (Fig.1.a). Subsequently, the region of interest (ROI) was isolated from the rest of the surrounding structures. A manual delineation of the bony contours was performed using eclipse and the livewire function, and all contours were checked in coronal, axial, and sagittal orthogonal planes (Fig. 1.b). To avoid any inconsistencies in the ROI of different images, the segmentation region was limited to the early start of the sinus ostium from the sinus side before continuation into the infundibulum (Fig. 1.b). Finally, the edited mask of each sinus was exported separately as a standard tessellation language (STL) file. The segmentation was performed by a dentomaxillofacial radiologist (NM) with seven years of experience and subsequently re-assessed by two other radiologists (KFV&RJ) with 15 and 25 years of experience, respectively.

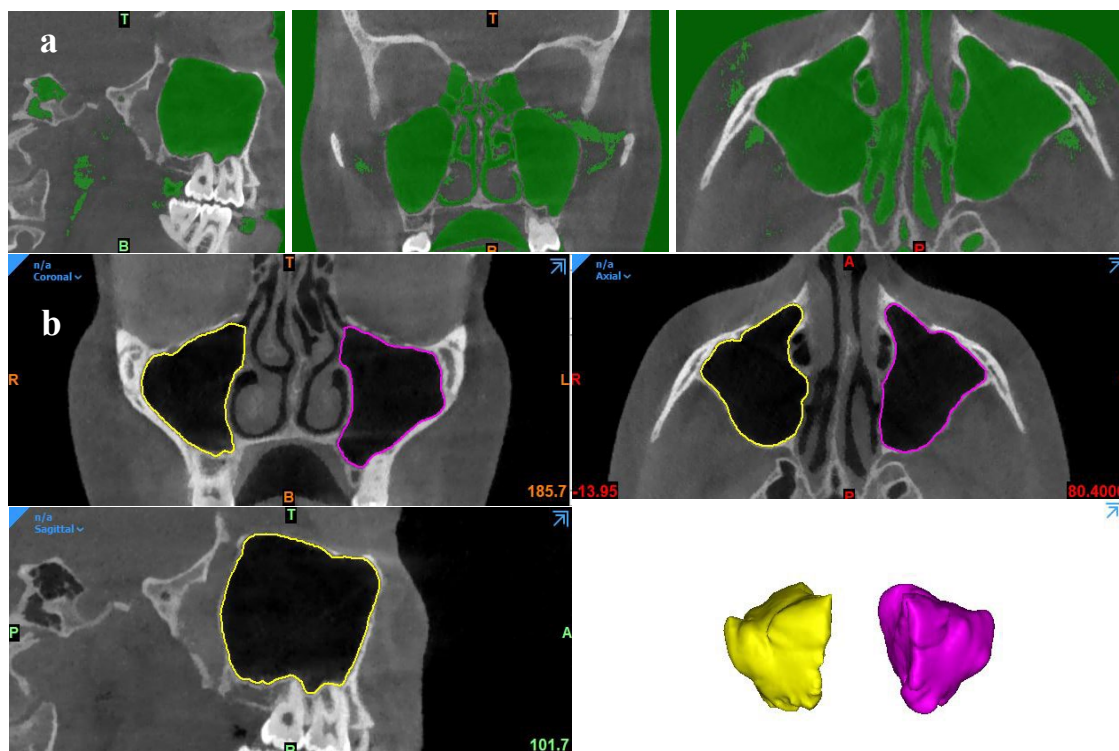


Figure 1. (a) Air mask creation using custom thresholding, (b) The edited mask with 3D reconstruction (version 23.0, Materialise N.V., Leuven, Belgium).

2.3 CNN model architecture and training

Two 3D U-Net architecture were used²⁵, both of which consisted of 4 encoder and 3 decoder blocks, 2 convolutions with a kernel size of 3x3x3, followed by a rectified linear unit (ReLU) activation and group normalization with 8 feature maps²⁶. Thereafter, max pooling with kernel size 2x2x2 by strides of two was applied after each encoder, allowing reduction of the resolution with a factor 2 in all dimensions. Both networks were trained as a binary classifier (0 or 1) with a weighted Binary Cross Entropy Loss:

$$L_{BCE} = y_n * \log(p_n) + (1 - y_n) * \log(1 - p_n)$$

for each voxel n with ground truth value $y_n = 0$ or 1 , and the predicted probability of the network = p_n

A two-step pre-processing of the training dataset was applied. First, all scans were resampled at the same voxel size. Thereafter, to overcome the GPU memory limitations, the full-size scan was down sampled to a fixed size.

The first 3D U-Net was used to provide roughly low-resolution segmentation for proposing 3D patches and cropped only those which belonged to the sinus. Later, those relevant patches were transferred to the second 3D U-Net where they were individually segmented and combined to create the full resolution segmentation map. Finally, binarization was applied, and only the largest connected part was kept, followed by the application of a marching cubes algorithm on the binary image. The resultant mesh was smoothed to generate a 3D model (Fig. 2).

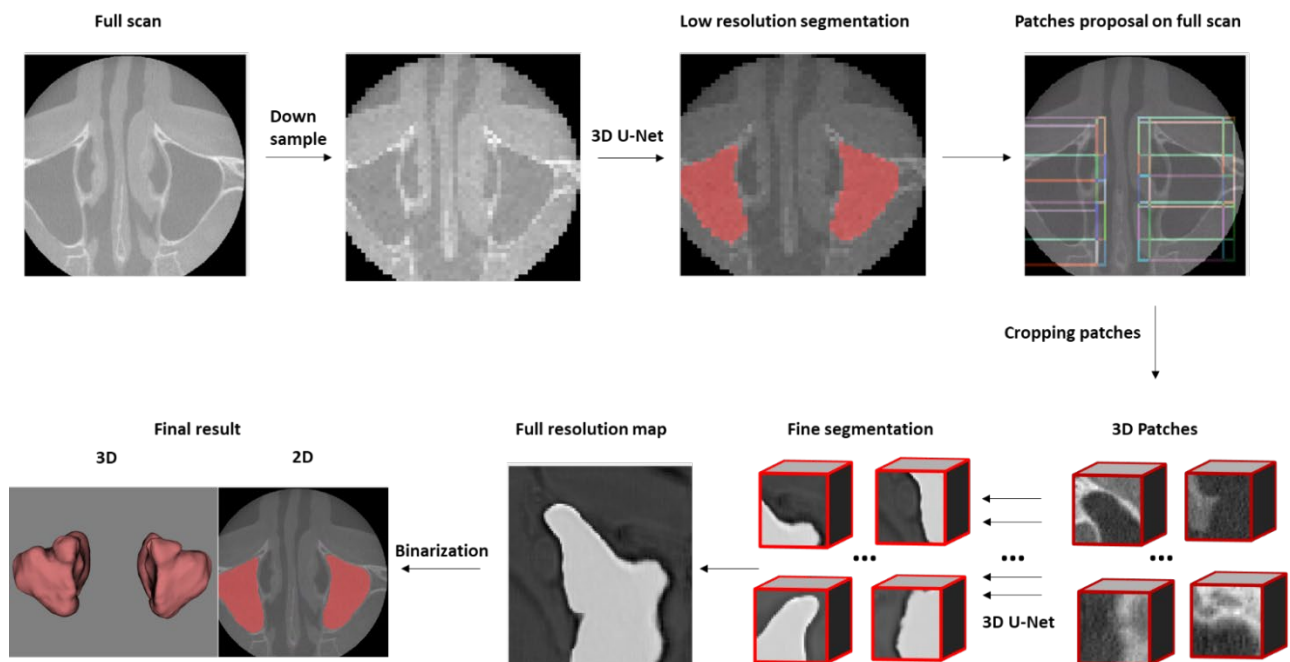


Figure 2. Working principle of the 3D U-Net based segmentation model.

The model parameters were optimized with ADAM²⁷ (an optimization algorithm for training deep learning models) having an initial learning rate of 1.25e-4. During training, random spatial augmentations (rotation, scaling, and elastic deformation) were applied. The validation dataset was used to define the early stopping, which indicates a saturation point of the model where no further improvement can be noticed by the training set and more cases will lead to data overfitting. The CNN model was deployed to an online cloud-based platform called “virtual patient creator” (creator.relu.eu, Relu BV, Version October 2021), where users could upload DICOM datasets and obtain an automatic segmentation of the desired structure.

2.4 Testing of AI pipeline

The testing of the CNN model was performed by uploading DICOM files from the test set to the virtual patient creator platform. The resulting automatic segmentation (Fig. 3) could be later downloaded in DICOM or STL file format. For clinical evaluation of the automatic segmentation, the authors developed the following classification criteria: A- perfect segmentation (no refinement was needed), B- very good segmentation (refinements without clinical relevance, slight over or under segmentation in regions other than the maxillary sinus floor), C- good segmentation (refinements that have some clinical relevance, slight over or under segmentation in the maxillary sinus floor region), D- deficient segmentation (considerable over or under segmentation, independent of the sinus region, with necessary repetition), and E- negative (the CNN model could not predict anything). Two observers (NM and KJV) evaluated all the cases, followed by an expert consensus (RJ). In cases where refinements were required, the STL file was imported into Mimics software and edited using the 3D tools tab. The resulting segmentation was denoted as “refined segmentation”.

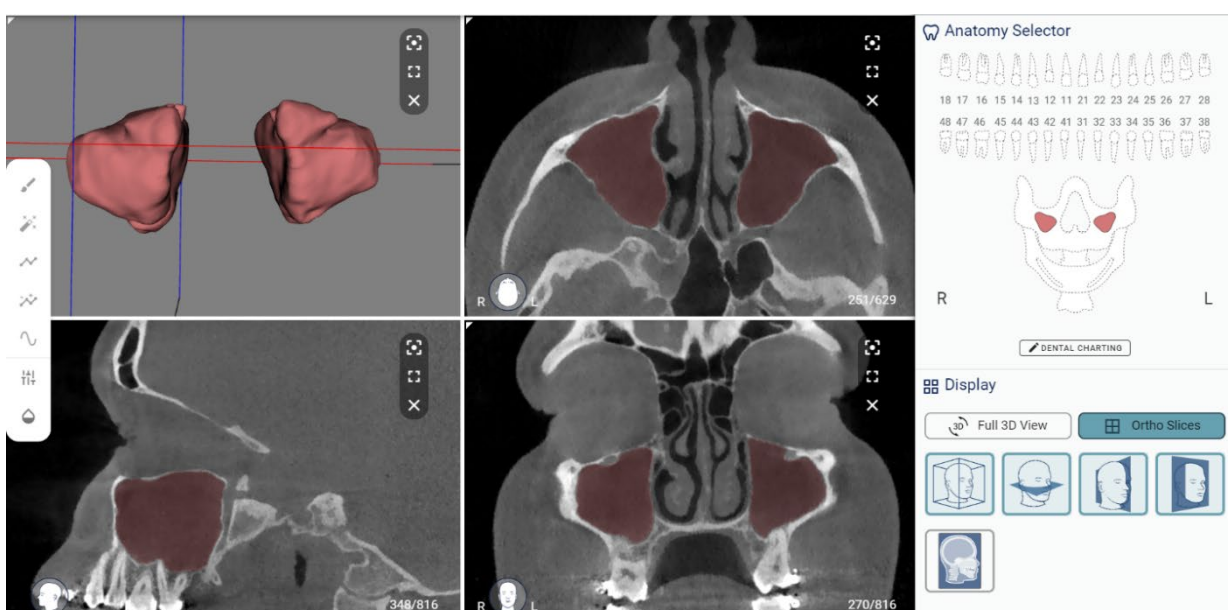


Figure 3. The resultant automatic segmentation on virtual patient creator online platform (creator.relu.eu, Relu BV, Version October 2021).

2.5 Evaluation metrics

The evaluation metrics^{28,29} are outlined in Table 2. The comparison of outcomes among the ground truth and automatic and refined segmentation was performed by the main observer on the whole testing set. A pilot of 10 scans was tested at first, which showed a Dice similarity coefficient (DSC) of 0.985 ± 0.004 , Intersection over union (IoU) of 0.969 ± 0.007 and 95% Hausdorff Distance (HD) of 0.204 ± 0.018 mm. Based on these findings, the sample size of the testing set was increased up to 30 scans according to the central limit theorem (CLT)³⁰.

Table 2. Metrics used for assessing accuracy and consistency.

Metric	Legend	Formula
Dice similarity coefficient (DSC)	represents the overlap of voxels between volume X and volume Y divided by the total number of voxels in both of them. A DSC of 1 indicates complete overlap.	$DSC(X, Y) = \frac{2 X \cap Y }{ X + Y } = \frac{2TP}{2TP + FP + FN}$
Intersection over Union (IoU)	represents also the overlap of voxels between volume X and volume Y divided by their union. An IoU of 1 means perfect overlapping segmentation.	$IoU(X, Y) = \frac{ X \cap Y }{ X \cup Y } = \frac{TP}{TP + FP + FN}$
95% Hausdorff distance (HD)	represents the maximal distance between all pairs of voxels in volume X and volume Y. A HD of 0 mm indicates a perfect segmentation. The 95 th percentile is used to eliminate the impact of a very small subset of outliers.	$d_{Hausdorff}(X, Y) = \max\{sup_{x \in X} inf_{y \in Y} d(x, y), sup_{y \in Y} inf_{x \in X} d(x, y)\}$ $95\%HD = (\min_{y \in Y} x - y _2 \cup \min_{x \in X} y - x _2)$
Root mean square distance (RMS)	measures the imperfections of the fit between two surfaces in mm. An RMS of 0 mm indicates a perfect match.	$RMS(x) = \sqrt{\frac{1}{n} (x_1^2 + x_2^2 + \dots + x_n^2)}$ <i>x = distance (mm) between two closest points of the two surfaces</i>

2.5.1 Time efficiency:

The time required for the semi-automatic segmentation was calculated starting from opening the DICOM files in Mimics software till export of the STL file. For automatic segmentation, the algorithm automatically calculated the time required to have a full resolution segmentation. The time for refined segmentation was calculated similarly to that of semi-automatic segmentation and later added to the initial automatic segmentation time. The average time for each method was calculated based on the testing set.

2.5.2 Accuracy:

A voxel-wise comparison amongst ground truth and automatic and refined segmentation of the testing set was performed by applying a confusion matrix with four variables: true positive (TP), true negative (TN), false positive (FP), and false negative (FN) voxels. Based on the aforementioned variables, the accuracy of the CNN model was assessed according to the metrics mentioned in Table 2.

2.5.3 Consistency:

To illustrate the consistency of the CNN model, one scan was uploaded twice on the platform, and the resultant STLs were compared. Intra- and inter-observer consistency were calculated for the semi-automatic and refined segmentation. The intra-observer reliability of the main observer was calculated by re-segmenting 10 scans from the testing set with different protocols. For the inter-observer reliability, two observers (NM and KfV) performed the needed refinements, then the STL files were compared with each other.

2.6 Statistical analysis

Data were analyzed with RStudio: Integrated Development Environment for R, version 1.3.1093 (RStudio, PBC, Boston, MA). The mean and standard deviation were calculated for all evaluation metrics. A paired-sample t-test was performed with a significance level ($p < 0.05$) to compare the timing required for semi-automatic and automatic segmentation of the testing set.

3. Results

3.1 Time efficiency:

The average time required for the semi-automatic segmentation was 60.8 minutes (3649.8 seconds) and 24.4 seconds for automatic segmentation, showing a significant reduction ($p\text{-value} < 2.2\text{e-}16$). Considering the refined data, around 30% of the testing set needed refinements (20% class B, 10% class C, no class D and E), with an average refinement time of 7.1 minutes (422.84 seconds). The automatic and refined segmentations were approximately 149 and 9 times faster than the semi-automatic segmentation, respectively.

3.2 Accuracy:

Table 3 provides an overview of the accuracy metrics for automatic segmentation. Overall, the automatic segmentation showed a DSC of 98.4% and a RMS of 0.21 mm in comparison to the ground truth, implying that the 3D volumes and models, along with the surfaces, were closely matched between them. (Fig. 4).

The comparison between automatic and refined segmentations showed a DSC of 99.6% and a RMS of 0.21 mm indicating perfect overlap between them. The minimal difference meant that minor refinements were needed.

Table 3. Accuracy assessment of automatic segmentation.

Metric	Descriptive analysis	Automatic vs ground truth	Automatic vs refined
DSC	Mean	0.984	0.996
	SD	0.004	0.004
	Min	0.962	0.983
	Max	0.991	0.999
IoU	Mean	0.968	0.992
	SD	0.008	0.007
	Min	0.926	0.967
	Max	0.983	0.998
95% HD (mm)	Mean	0.232	0.109
	SD	0.059	0.115
	Min	0.200	0
	Max	0.447	0.283
RMS (mm)	Mean	0.209	0.214
	SD	0.072	0.123
	Min	0.142	0.100
	Max	0.445	0.372

DSC dice similarity coefficient, IoU intersection over union, HD hausdorff distance, RMS root mean square, SD standard deviation, Min minimal value, Max maximal value.

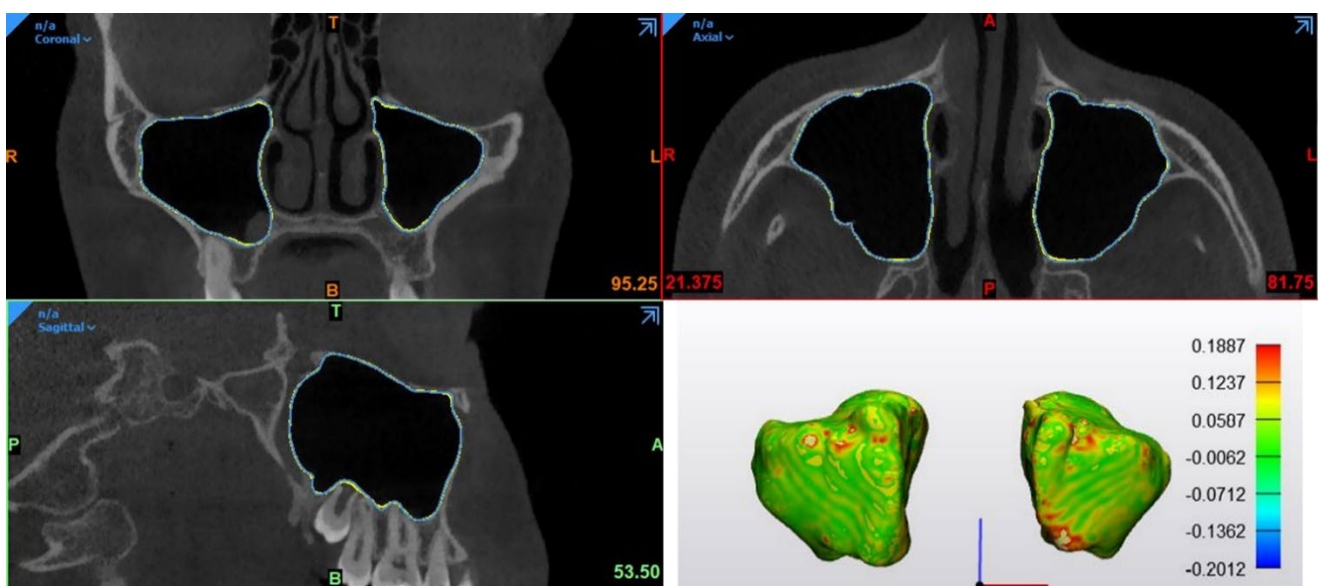
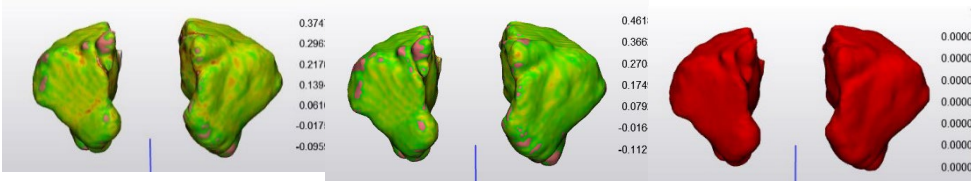


Figure 4. Overlap between automatic segmentation (yellow color) and ground truth (blue color) in 3 orthogonal planes, RMS in mm between STL surfaces illustrated with a color map.

3.3 Consistency:

Table 4 shows the metrics for intra- and inter-observer reliability with a DSC of 98.4% and 99.6%, respectively. For the CNN model test-retest reliability, it had, by default, an identical match with a DSC value of 100%.

Table 4. Mean and standard deviation for reliability assessment.

Metric	Descriptive analysis	Intra-observer	Inter-observer	CNN model test-retest
DSC	Mean	0.984	0.996	1
	SD	0.005	0.003	
	Min	0.974	0.987	
	Max	0.991	1	
IoU	Mean	0.969	0.993	1
	SD	0.008	0.006	
	Min	0.949	0.974	
	Max	0.982	1	
95% HD (mm)	Mean	0.200	0.113	0
	SD	0.021	0.121	
	Min	0.100	0	
	Max	0.321	0.346	
RMS (mm)	Mean	0.155	0.113	0
	SD	0.029	0.069	
	Min	0.100	0.010	
	Max	0.180	0.250	
STL map				
				

DSC dice similarity coefficient, IoU intersection over union, HD hausdorff distance, RMS root mean square, SD standard deviation, Min minimal value, Max maximal value.

4. Discussion

CBCT imaging has been widely employed in the field of oral and maxillofacial radiology for the visualization of orofacial structures, pre-surgical planning, and follow-up assessment¹¹⁻¹³. It allows for a 3D evaluation that is crucial for an accurate diagnosis and management of certain pathologies affecting the maxillofacial complex. Volumetric (3D) assessment of the maxillary sinus not only enhances the diagnostic process but also permits the creation of reconstructed virtual models for presurgical planning purposes, including implant placement, sinus floor elevation, removal of (impacted) posterior teeth and/or root remnants, and reconstructive and orthognathic surgical procedures. In this sense, an accurate segmentation of the sinus cavity is an essential step.

Manual segmentation is not a feasible task in a daily clinical practice since it is a time-consuming task and requires high operator experience. Semi-automatic segmentation techniques still require operator intervention for manual threshold selection. Additionally, the manual adjustments of segmented structures also require a considerable amount of time and may induce operator-based errors³¹. For overcoming the above-mentioned limitations and to provide a reproducible and consistent technique, the present study aimed to develop and validate an automated maxillary sinus segmentation methodology on CBCT images using a CNN-based model.

The model in the current study was trained using data acquired by 2 CBCT devices (NewTom VGi evo and 3D Accuitomo 170) with different scanning parameters. Furthermore, images both with and without metal artifacts were included. A comparison was performed between the CBCT devices using the CNN model versus the ground truth, and no significant differences were observed. Both devices showed a high DSC value of 98.37% (NewTom VGi evo) and 98.43% (3D Accuitomo 170). Hence, the whole dataset was treated as one sample.

When comparing the performance of the automatic versus the semi-automatic technique, the CNN-model showed remarkable results in relation to time, accuracy, and consistency. The automatic segmentation was approximately 149 times faster (24.4 seconds) than the semi-automatic approach (60.8 minutes). When considering all the evaluation metrics, the CNN model showed a high similarity to the ground truth (see Table 3).

Based on the proposed classification for the clinical evaluation of automatic segmentation, almost 70% of the testing set was classified as perfect segmentation (class A), with no refinements required. For cases classified as B or C, refinements were mainly associated with cases having mucosal thickening. No deficient or negative predictions were present. Moreover, the small difference between automatic and refined segmentations (see Table 3) suggested that minimal refinements were needed.

The inter-observer reliability for the refined segmentation showed a DSC of 99.6%, which implied consistency amongst observers. The models' performance was also 100% consistent during repeated segmentation of the same case, which is a great advantage to overcome human variability. As human performance will always be variable each time a segmentation is performed. Additionally, the developed model was fully automatic without the need for any human intervention, which also overcomes the issues of threshold leveling and grey scale variability.

To date, few researchers³²⁻³⁴ have investigated maxillary sinus segmentation from CBCT datasets with different study designs. Bui et al.³² investigated an automatic segmentation technique of the paranasal sinuses and the nasal cavity from 10 CBCT images. They applied a multi-step level of coarse to fine active contour modelling and reported a dice of 95.7% in comparison to manual segmentation by considering experts as a ground truth. Neelapu et al.³³ developed a knowledge-based algorithm for automatically segmenting the maxillary sinus from 15 CBCT imaging scans. The authors compared five segmentation techniques following automatic contour initialization and reported a dice ranging between 80-90% for all the segmentation methods. Ham et al.³⁴ proposed an automatic maxillary sinus segmentation technique using one 3D U-Net and found a DSC score of 92.8%. Even though a comparison with the aforementioned studies was difficult due to the variability in CBCT devices, scanning protocols, and study design, the currently proposed CNN model in the current study showed better results considering the metrics evaluated. Furthermore, the time needed for each segmentation method was clearly stated, and the sample size was justified, which have been rarely reported in previous studies. Recent studies^{35,36} have reported on automatic segmentation of sinus mucosal thickening and pathological lesions, yet this was not the focus of our study.

The limitations of this study were similar to the already present challenges of artificial intelligence in dentistry^{21,37}. Firstly, a lack of data heterogeneity and model generalizability exists, which could be solved by incorporating data from different CBCT devices having variable scanning parameters. Secondly, the online platform only allowed visualization and export of the automatic segmentation, and third-party software was required for performing the refinements. Recently, some editing tools have been added to the platform, and additional features will be added soon to overcome this issue. Finally, the CNN model enabled to extract the normal clear sinus and separate the bony borders in cases with sinus thickening, however, it cannot delineate the soft tissue. Future work will focus on the pathological conditions of the maxillary sinus.

5. Conclusions

A 3D U-Net architecture CNN model was developed and validated for automatic segmentation and 3D virtual model creation of the maxillary sinus from CBCT imaging. Owing to its promising performance in relation to time, accuracy, and consistency, it can represent a solid base for future studies by incorporation of pathological conditions. An additional benefit of the model is its deployment to an online web-based user-interactive platform, which could facilitate its application in clinical practice.

References

1. Whyte, A. & Boeddinghaus, R. The maxillary sinus: physiology, development and imaging anatomy. *Dentomaxillofacial Radiology* **48**, 20190205, doi:10.1259/dmfr.20190205 (2019).
2. Standring, S. *Gray's Anatomy : The Anatomical Basis of Clinical Practice*. 41st edn, (Elsevier Health Sciences, 2015).
3. James A. Duncavage, S. S. B. *The maxillary sinus: medical and surgical management*. (Thieme Medical Publishers, 2011).
4. Chanavaz, M. Maxillary sinus: anatomy, physiology, surgery, and bone grafting related to implantology--eleven years of surgical experience (1979-1990). *J Oral Implantol* **16**, 199-209 (1990).
5. Iwanaga, J. *et al*. Clinical anatomy of the maxillary sinus: application to sinus floor augmentation. *Anat Cell Biol* **52**, 17-24, doi:10.5115/acb.2019.52.1.17 (2019).
6. Andersen, T. N. *et al*. Accuracy and precision of manual segmentation of the maxillary sinus in MR images-a method study. *Br J Radiol* **91**, 20170663-20170663, doi:10.1259/bjr.20170663 (2018).
7. Giacomini, G. *et al*. Computed tomography-based volumetric tool for standardized measurement of the maxillary sinus. *PLoS One* **13**, e0190770, doi:10.1371/journal.pone.0190770 (2018).
8. Berberi, A. *et al*. Evaluation of Three-Dimensional Volumetric Changes After Sinus Floor Augmentation with Mineralized Cortical Bone Allograft. *J Maxillofac Oral Surg* **14**, 624-629, doi:10.1007/s12663-014-0736-3 (2015).
9. Starch-Jensen, T. & Jensen, J. D. Maxillary Sinus Floor Augmentation: a Review of Selected Treatment Modalities. *J Oral Maxillofac Res* **8**, e3-e3, doi:10.5037/jomr.2017.8303 (2017).
10. Xu, J. *et al*. Automatic CT image segmentation of maxillary sinus based on VGG network and improved V-Net. *International Journal of Computer Assisted Radiology and Surgery* **15**, 1457-1465, doi:10.1007/s11548-020-02228-6 (2020).
11. Venkatesh, E. & Elluru, S. V. Cone beam computed tomography: basics and applications in dentistry. *J Istanb Univ Fac Dent* **51**, S102-S121, doi:10.17096/jiufd.00289 (2017).
12. Carter, J. B., Stone, J. D., Clark, R. S. & Mercer, J. E. Applications of Cone-Beam Computed Tomography in Oral and Maxillofacial Surgery: An Overview of Published Indications and Clinical Usage in United States Academic Centers and Oral and Maxillofacial Surgery Practices. *Journal of Oral and Maxillofacial Surgery* **74**, 668-679, doi:<https://doi.org/10.1016/j.joms.2015.10.018> (2016).
13. Scarfe, W. C., Farman, A. G., Levin, M. D. & Gane, D. Essentials of maxillofacial cone beam computed tomography. *Alpha Omegan* **103**, 62-67, doi:10.1016/j.aodf.2010.04.001 (2010).

14. Bozdemir, E., Gormez, O., Yıldırım, D. & Aydogmus Erik, A. Paranasal sinus pathoses on cone beam computed tomography. *J Istanbul Univ Fac Dent* **50**, 27-34, doi:10.17096/jiufd.47796 (2016).
15. Pauwels, R., Jacobs, R., Singer, S. R. & Mupparapu, M. CBCT-based bone quality assessment: are Hounsfield units applicable? *Dentomaxillofac Radiol* **44**, 20140238-20140238, doi:10.1259/dmfr.20140238 (2015).
16. Chang, Y.-B. *et al.* 3D segmentation of maxilla in cone-beam computed tomography imaging using base invariant wavelet active shape model on customized two-manifold topology. *J Xray Sci Technol* **21**, 251-282, doi:10.3233/XST-130369 (2013).
17. Wang, L. *et al.* Automated segmentation of dental CBCT image with prior-guided sequential random forests. *Med Phys* **43**, 336-336, doi:10.1118/1.4938267 (2016).
18. Tingelhoff, K. *et al.* Analysis of manual segmentation in paranasal CT images. *Eur Arch Otorhinolaryngol* **265**, 1061-1070, doi:10.1007/s00405-008-0594-z (2008).
19. Tingelhoff, K. *et al.* Comparison between manual and semi-automatic segmentation of nasal cavity and paranasal sinuses from CT images. *Annu Int Conf IEEE Eng Med Biol Soc* **2007**, 5505-5508, doi:10.1109/iembs.2007.4353592 (2007).
20. Hung, K., Montalvao, C., Tanaka, R., Kawai, T. & Bornstein, M. M. The use and performance of artificial intelligence applications in dental and maxillofacial radiology: A systematic review. *Dentomaxillofac Radiol* **49**, 20190107-20190107, doi:10.1259/dmfr.20190107 (2020).
21. Hung, K., Yeung, A. W. K., Tanaka, R. & Bornstein, M. M. Current Applications, Opportunities, and Limitations of AI for 3D Imaging in Dental Research and Practice. *Int J Environ Res Public Health* **17**, 4424, doi:10.3390/ijerph17124424 (2020).
22. Lee, J. G. *et al.* Deep Learning in Medical Imaging: General Overview. *Korean J Radiol* **18**, 570-584, doi:10.3348/kjr.2017.18.4.570 (2017).
23. Schwendicke, F. *et al.* Artificial intelligence in dental research: Checklist for authors, reviewers, readers. *J Dent* **107**, 103610, doi:10.1016/j.jdent.2021.103610 (2021).
24. Bornstein, M. M. *et al.* An Analysis of Frequency, Morphology, and Locations of Maxillary Sinus Septa Using Cone Beam Computed Tomography. *Int J Oral Maxillofac Implants* **31**, 280-287, doi:10.11607/jomi.4188 (2016).
25. Çiçek, Ö., Abdulkadir, A., Lienkamp, S. S., Brox, T. & Ronneberger, O. in *Medical Image Computing and Computer-Assisted Intervention* (eds Sebastien Ourselin *et al.*) 424-432 (Springer International Publishing, Cham, 2016).
26. Wu, Y. & He, K. Group Normalization. *International Journal of Computer Vision* **128**, 742-755, doi:10.1007/s11263-019-01198-w (2020).

27. Kingma, D. P. & Ba, J. Adam: A Method for Stochastic Optimization. *CoRR* **abs/1412.6980** (2015).
28. Zhang, D. *et al.* An efficient approach to directly compute the exact Hausdorff distance for 3D point sets. *Integrated Computer-Aided Engineering* **24**, 261-277, doi:10.3233/ICA-170544 (2017).
29. Taha, A. A. & Hanbury, A. Metrics for evaluating 3D medical image segmentation: analysis, selection, and tool. *BMC Medical Imaging* **15**, 29, doi:10.1186/s12880-015-0068-x (2015).
30. Kwak, S. G. & Kim, J. H. Central limit theorem: the cornerstone of modern statistics. *Korean J Anesthesiol* **70**, 144-156, doi:10.4097/kjae.2017.70.2.144 (2017).
31. Cellina, M. *et al.* Segmentation procedures for the assessment of paranasal sinuses volumes. *The Neuroradiology Journal* **34**, 13-20, doi:10.1177/1971400920946635 (2021).
32. Bui, N. L., Ong, S. H. & Foong, K. W. C. Automatic segmentation of the nasal cavity and paranasal sinuses from cone-beam CT images. *International Journal of Computer Assisted Radiology and Surgery* **10**, 1269-1277 (2014).
33. Neelapu, B. C. *et al.* A pilot study for segmentation of pharyngeal and sino-nasal airway subregions by automatic contour initialization. *Int J Comput Assist Radiol Surg* **12**, 1877-1893, doi:10.1007/s11548-017-1650-1 (2017).
34. Sungwon Ham, A.-R. L., Jongha Park, Younghwa Byeon, & Sangwook Lee, M. B., Namkug Kim. in *Medical Imaging with Deep Learning* (Amsterdam, The Netherlands., 2018).
35. Hung, K. F. *et al.* Automatic detection and segmentation of morphological changes of the maxillary sinus mucosa on cone-beam computed tomography images using a three-dimensional convolutional neural network. *Clinical Oral Investigations*, doi:10.1007/s00784-021-04365-x (2022).
36. Jung, S. K., Lim, H. K., Lee, S., Cho, Y. & Song, I. S. Deep Active Learning for Automatic Segmentation of Maxillary Sinus Lesions Using a Convolutional Neural Network. *Diagnostics (Basel)* **11**, doi:10.3390/diagnostics11040688 (2021).
37. Schwendicke, F., Samek, W. & Krois, J. Artificial Intelligence in Dentistry: Chances and Challenges. *Journal of Dental Research* **99**, 769-774, doi:10.1177/0022034520915714 (2020).

Three-dimensional maxillary virtual patient creation by convolutional neural network-based segmentation on cone-beam computed tomography images

Nogueira-Reis F. ^{1,2}

Morgan N. ^{2,3}

Nomidis S. ⁴

Van Gerven A. ⁴

Oliveira-Santos N. ⁴

Jacobs R. ^{2,5}

Tabchoury CPM. ⁶

¹ Department of Oral Diagnosis, Division of Oral Radiology, Piracicaba Dental School, University of Campinas (UNICAMP), Av. Limeira 901, Piracicaba, São Paulo 13414-903, Brazil

² OMFS IMPATH Research Group, Department of Imaging & Pathology, Faculty of Medicine, KU Leuven & Oral and Maxillofacial Surgery, University Hospitals Leuven, Kapucijnenvoer33, BE-3000 Leuven, Belgium

³ Department of Oral Medicine, Faculty of Dentistry, Mansoura University, 35516 Mansoura, Dakahlia, Egypt

⁴ Relu BV, Kapeldreef 60, BE-3000 Leuven, Belgium

⁵ Department of Dental Medicine, Karolinska Institutet, Box 4064, 141 04 Huddinge, Stockholm, Sweden

⁶ Department of Biosciences, Division of Biochemistry, Piracicaba Dental School, University of Campinas (UNICAMP), Av. Limeira 901, Piracicaba, São Paulo 13414-903, Brazil

Published in *Clinical Oral Investigation*. 2022 Sep 17.

Abstract

Objective

To qualitatively and quantitatively assess the integrated segmentation of three convolutional neural network (CNN) models for the creation of a MVP from cone-beam computed tomography (CBCT) images.

Materials and methods

A dataset of 40 CBCT scans acquired with different scanning parameters was selected. Three previously validated individual CNN models were integrated to achieve a combined segmentation of the maxillary complex, maxillary sinuses, and upper dentition. Two experts performed a qualitative assessment, scoring-integrated segmentations from 0 to 10 based on the number of required refinements. Furthermore, experts executed refinements, allowing performance comparison between integrated automated segmentation (AS) and refined segmentation (RS) models. Inter-observer consistency of the refinements and the time needed to create a full resolution automatic segmentation were calculated.

Results

From the dataset, 85% scored 7–10, and 15% were within 3–6. The average time required for automated segmentation was 1.7 min. Performance metrics indicated an excellent overlap between automatic and refined segmentation with a dice similarity coefficient (DSC) of 99.3%. High inter-observer consistency of refinements was observed, with a 95% Hausdorff distance (HD) of 0.045 mm.

Conclusion

The integrated CNN models proved to be fast, accurate, and consistent, along with strong interobserver consistency in creating the MVP.

Clinical relevance

The automated segmentation of these structures simultaneously could act as a valuable tool in clinical orthodontics, implant rehabilitation, and any oral or maxillofacial surgical procedures, where visualization of MVP and its relationship with surrounding structures is a necessity for reaching an accurate diagnosis and patient-specific treatment planning.

Keywords: Computer simulation, Three-dimensional image, Artificial intelligence, Computational neural networks, Cone-beam computed tomography, Jaw bone, Tooth.

1. Introduction

One of the recent trends for diagnostics and pre-surgical planning in orthodontics, orthognathic surgery, and oral implant placement has been the introduction of simplified digital workflows¹. The solid basis of such workflows can often be accomplished by 3D imaging, mainly cone-beam computed tomography (CBCT), which offers volumetric anatomical data of orofacial structures.

Segmentation of the imaging data acquired from CBCT is essential for generating 3D models of patient-specific anatomical structures, which is a prerequisite for virtual treatment planning and 3D manufacturing¹. However, current segmentation techniques, either manual or semi-automatic, are time-consuming, suffer from human variability, and are hampered by metal and motion artifacts². Besides, segmentation of CBCT images requires more time than traditional multi-slice computed tomography (MSCT), as MSCT images have a superior contrast resolution and lower noise, which facilitate achieving a time-efficient segmentation²⁻⁴. However, CBCT acts as the modality of choice in oral healthcare, considering its low cost, relatively lower dose, and increased accessibility^{2, 5}.

Considering these limitations of CBCT imaging in relation to segmentation, there is a need for automation of the current digital workflows through the application of artificial intelligence (AI)-based techniques. Recently, convolutional neural network (CNN), a class of artificial neural networks, has dominated the field of medical image analysis, as it is specialized for processing data with defined, grid-like topology, such as 2D and 3D images^{6, 7}. CNNs have the ability to outperform standard image processing algorithms with high computational speed and correlate with other data, such as clinical information or response to therapy. This provides an improvement in the quality of image processing and helps clinicians to extract and analyze relevant information in a concise format⁷.

So far, the authors of several studies have focused on the segmentation of individual craniomaxillofacial anatomical structures using CNN models⁸⁻¹¹. However, no evidence exists about the integration of these multiple anatomical structures as a single unit. A combination of AI models specialized in segmenting different structures with variable densities simultaneously could pave the way towards the creation of a virtual patient with high performance in a time-efficient approach. This virtual patient could be applied for the digital virtual planning of several treatment procedures, not only in general dentistry but also in maxillofacial surgery, Ear, Nose and Throat (ENT), neurosurgery, and ophthalmology. Therefore, we aimed to assess the qualitative and quantitative performance of integrated CNN models of three previously validated individual networks for the creation of a segmented MVP consisting of the maxillary skeletal complex, maxillary sinuses, and teeth from CBCT images^{8, 12, 13}. We hypothesized that the three integrated CNN models would reveal a similar performance as the individuals' ones, along with a strong interobserver agreement in terms of time-efficiency and consistency for creating a segmented MVP.

2. Materials and Methods

This study was approved by the Research Ethics Committee of the University Hospitals of Leuven (reference number: S65708) and conducted in compliance with the World Medical Association Declaration of Helsinki on medical research. Patient-specific information was anonymized.

2.1 Dataset

The sample size was calculated based on previous comparable studies using a priori power analysis in G* power 3.1, with a power of 80% and a significance level of 5%^{9, 11}. In this way, a total dataset of 40 scans from two devices (20 *Accuitomo 3D*; 20 *Newtom VGi evo*) was selected, consisting of 560 teeth, 80 sinuses, and 40 maxillofacial complexes acquired with different scanning parameters (Table 1). Inclusion criteria were scans with permanent dentition, including teeth with coronal and/or root fillings. Patients with a history of maxillofacial trauma, orthognathic and maxillofacial reconstructive surgery, syndromic or degenerative diseases were excluded. Post-orthognathic surgery patients with mini-plates and screws and patients with presence of dental implants and missing teeth in proximity to the sinus floor were also excluded.

All CBCT images were saved in Digital Imaging and Communication in Medicine (DICOM) format and uploaded to an online cloud-based platform called “Virtual Patient Creator” (creator.relu.eu, version December 2021, Relu BV, Leuven, Belgium), which allowed combined automatic segmentation of the maxillary complex, maxillary sinuses, and teeth, referred to as MVP.

Table 1. CBCT scanning parameters of the sample.

	kV	mA	Voxel size (mm)	Field of view (cm)
Newtom VGi evo (Cefla, Imola, Italy)	110	3-8	0.2;0.25;0.3	24X19; 16X16; 12X8; 10X10
3D Accuitomo 170 (J. Morita, Kyoto, Japan)	90	5	0.25	17X12; 14X10; 10X10; 8X8

kVp: kilovoltage peak; *mA*: milliamperere.

2.2 Qualitative assessment

Two dentomaxillofacial radiologists (FNR and NM) clinically evaluated the automatic segmentation of the integrated structures by visually observing their corresponding colors on orthogonal planes of the CBCT images (Figure 1). The three individual CNN models of the maxillary complex, maxillary sinuses, and teeth have been previously validated, where they proved to be highly accurate, requiring only minor refinements (slight over or under segmentation in each structure) (Figure 2). Hence, a score from 0-10 was given for each segmentation based on the number of required minor refinements, where 0 represented ten refinements or more, 1 represented 9 refinements, 2 represented 8 refinements, and successively up to 10 that referred to a perfect segmentation without the need for any refinements. Inter-observer agreement was assessed for the scoring between the two observers. Additionally, needed refinements were performed for assessing the performance of the integrated models in comparison to the refined ones and assessing the consistency between observers.

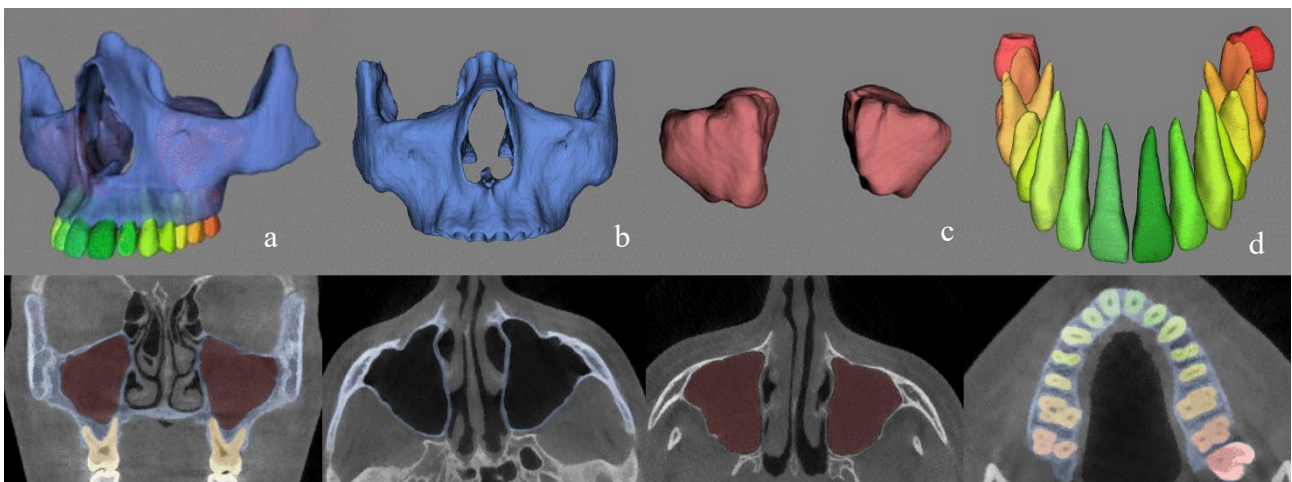


Fig.1 3D views and their respective colored segmentations on CBCT slices on Virtual Patient Creator (creator.relu.eu, Relu BV, Version December 2021): a) all structures combined showing the maxillary virtual patient, b) maxillofacial complex, c) maxillary sinuses, and d) upper dentition.

2.3 Smart correction tools

Following visual assessment, both observers performed the required refinements using the newly developed tools on the virtual patient creator platform: normal and smart brushes, contour, and livewire tools. The normal brush is a simple cylindrical brush which is used for adding brush strokes to refine small inadequacies between multiple image slices. The smart brush uses voxel intensities to group them by analysing the voxel's intensity below the cursor and selecting all voxels at a certain depth that have intensities within the selected voxel's tolerance range. Both tools are unidirectional, causing only the slices above or below to be changed. Hence, there was no issue of overwriting slices that had already been corrected.

The contour tool automatically interpolates the inter-slice region between upper and lower selected contours; however, if drastically different topology is observed between slices, then there is a risk of inaccurate interpolation, which could impact the final 3D shape. The livewire tool is an intelligent version of the contour tool, whose main principle of inter-slice interpolation remains the same. However, it connects the added points in a path that automatically follows the grey values of the image. Consequently, allowing the user to outline contours more quickly with a fewer number of points compared to a contour tool. Tutorials on how to use these tools are available as supplementary material (online resource 1-4).

2.4 Quantitative assessment

2.4.1 Timing

The time required to have a full resolution automatic segmentation (AS) was measured directly by an automated algorithm. As for the refined segmentation (RS), it was calculated by summing up the time required for automatic segmentation and refinements. Finally, the average time for each segmentation technique was calculated.

2.4.2 Automatic versus refined segmentations

The automatic segmentation was compared to the manual refined segmentation, and the metrics used to assess its similarity included the dice similarity coefficient (DSC), 95% Hausdorff distance (HD), and root mean square (RMS) (Table 2). The performance of the AI models for MVP segmentation was calculated using the following expression, where x is the comparison metric of interest (e.g., DSC) between automatic and refined segmentation.

$$\chi_{combined} = \frac{\langle x_{maxillofacial\ complex} \rangle + \langle x_{maxillary\ sinuses} \rangle + \langle x_{upper\ dentition} \rangle}{3}$$

The dentition metric was defined as the average over all individual tooth types:

$$\chi_{upper\ dentition} = \frac{\langle x_{tooth\ 11} \rangle + \langle x_{tooth\ 12} \rangle + \dots}{16}$$

2.4.3 Consistency of refined segmentations

The three CNN models have already proven to be 100% consistent at an individual level; hence, AI consistency was not further investigated. The interobserver consistency of refined segmentations was assessed by overlapping the DICOM and resultant STL files of the segmentations performed by each observer. Thereafter, corresponding evaluation metrics were calculated.

Table 2. Overview table of validation metrics used in the quantitative assessment.

Metrics	Definition	Formula
DSC	This ratio represents how similar the segmented region is to the ground truth.	$DSC(A, B) = \frac{2 A \cap B }{ A + B } = \frac{2TP}{2TP + FP + FN}$
95% HD	Indicator of the maximum difference between the limits of the automatic segmentation and the ground truth.	$95\% \text{ HD} = P_{95}(\min_{a \in A} \ B - A\ _2 \cup \min_{b \in B} \ A - B\ _2)$
RMS	Indicator of the imperfection of the fit between the STLs of the surface of interest and ground truth in mm.	$RMS(d) = \sqrt{\frac{1}{n} (d_1^2 + d_2^2 + \dots + d_n^2)}$

DSC Dice Similarity Coefficient, 95%HD 95% Hausdorff distance, RMS root mean square, A volumetric data of observer 1, B volumetric data of observer 2, TP true positives, TN true negatives, FP false positives, FN false negatives, P95 percentile 95.

2.5 Statistical analysis

Data were analysed with IBM SPSS version 28.0.1.0 software (Armonk, NY). The weighted Kappa test (95% CI) was performed for the inter-observer agreement of the qualitative assessment. For quantitative data, the mean value and standard deviation of each evaluation metric were calculated.

3. Results

3.1 Qualitative assessment

Based on the visual assessment, there was no overlap between the three structures. From the entire dataset, 85% showed a score of 7 or more by both observers, and 15% were within the range of 3-6. Furthermore, there were no cases with scores of 0-2 (Figure 2). In total, 40 scans required minor corrections, mainly due to mucosal thickening in the sinus, closed foramina and canals, small bone discontinuities in the palate and maxilla, and bone over-segmentation of zygomaticotemporal sutures (Table 3). Figure 3 illustrates some examples of the regions requiring refinements. The weighted Kappa test showed strong inter-observer agreement (K=0.832, 95% CI [0.704;0.960]) based on Landis and Koch's classification¹⁴.

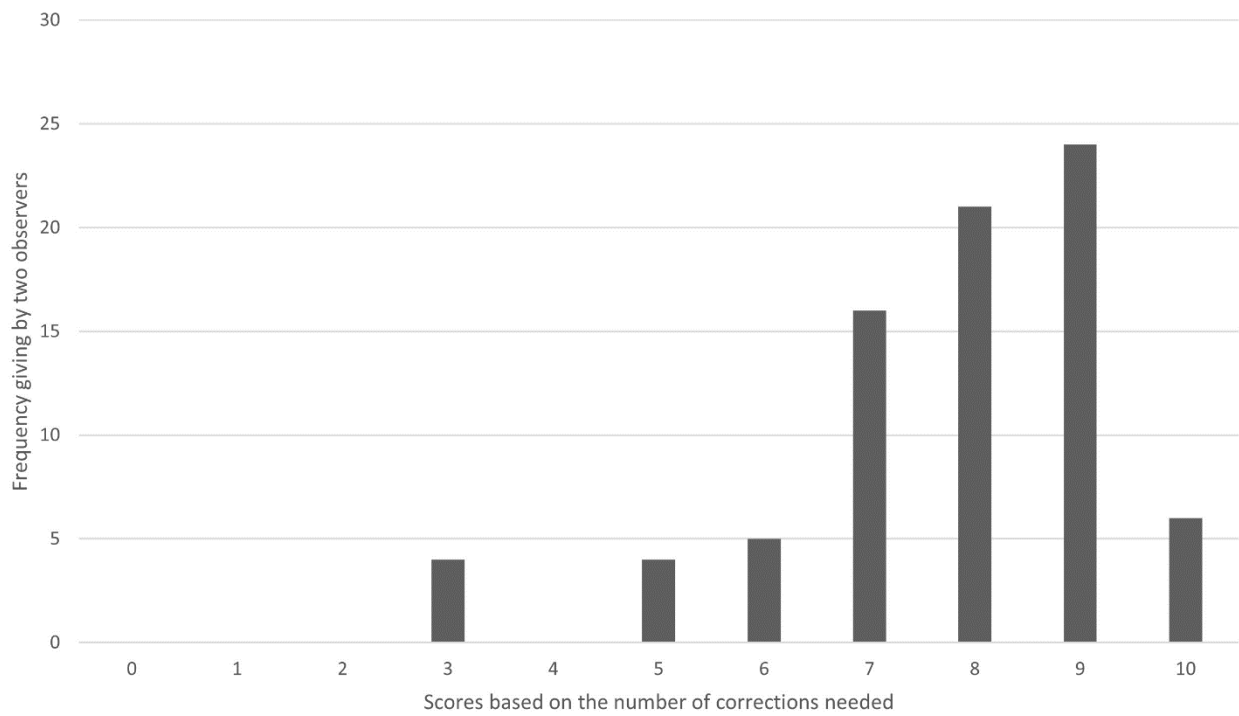


Fig. 2 Score frequency based on the number of corrections needed given by two observers (n = 80).

Table 3. Types of corrections required according to the structure with their description.

Structure refined	Correction type	Description
Upper dentition	Under segmentation	Small missing parts in the tooth contour
	Over segmentation	Not found
Maxillary sinuses	Under segmentation	Mucosal thickening, and air voids
	Over segmentation	Overextension in ethmoidal air sinus
Maxillofacial complex	Under segmentation	Bone discontinuities in medial wall and back of maxilla, and in the palate
	Over segmentation	Closed infraorbital and palatine foramina, nasopalatine canal, and overextension of zygomaticotemporal suture

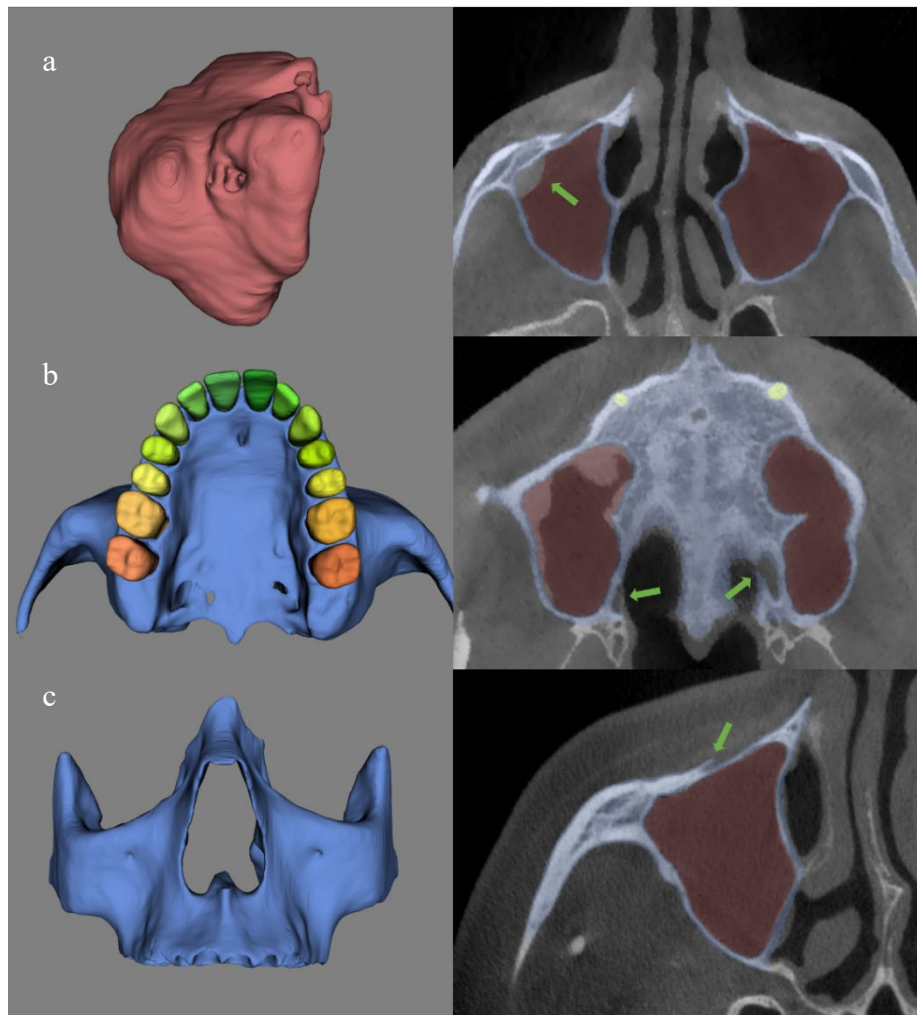


Fig. 3 3D models and axial sections of CBCT scans illustrating the necessary refinements most often detected in qualitative analysis. a) Mucosal thickening in the upper cortical of the right maxillary sinus. b) MVP in a view showing bone discontinuity around palatine foramina. c) Closed right infraorbital foramen in a lateral view of the MVP.

3.2 Quantitative assessment

The average time for the automated segmentation of 40 cases was 1.7 minutes, ranging from 1.1 to 2.4 minutes. The average time required for refinements by the first and second observers was 3.4 minutes (1.2 to 15 minutes) and 2.5 minutes (1.0 to 11 minutes), respectively.

The performance metrics (Table 4) indicated excellent overlap between automatic and refined segmentation, with a DSC of 99.3% for both observers, implying that minimal refinements were required. The RMS value was 0.289 mm and 0.286 mm, and the 95% HD was 0.210 mm and 0.228 mm for each observer, respectively.

Interobserver consistency of refinements (Table 4) showed a high DSC of 99.8%. A close to zero 95% HD of 0.045 was detected with a low RMS value of 0.053. Additionally, the STL overlap comparison map also observed a similar pattern. Hence, suggesting a substantial agreement between both observers.

Table 4. Evaluation metrics for comparison between automatic and refined segmentations.

Metric	Descriptive analysis	AS vs RS (Observer 1)	AS vs RS (Observer 2)	Inter-observer consistency
DSC	Mean	0.993	0.993	0.998
	SD	0.021	0.023	0.003
	Min	0.976	0.976	0.996
	Max	0.997	0.999	0.999
95%HD (mm)	Mean	0.210	0.228	0.045
	SD	1.004	1.006	0.067
	Min	0.000	0.000	0.000
	Max	1.004	1.006	0.067
RMS (mm)	Mean	0.289	0.286	0.053
	SD	0.462	0.467	0.099
	Min	0.167	0.167	0.000
	Max	0.629	0.634	0.099

AS: Automatic segmentation, RS: Refined segmentation, SD: Standard deviation, DSC: Dice Similarity Coefficient, 95%HD: Hausdorff Distance, and RMS: root mean square.

4. Discussion

An accurate 3D segmentation of orofacial structures is the first essential step in most digital dental workflows. It is crucial for precise delineation and outlining of normal anatomy, variations, differentiation from accompanied pathological lesions and volumetric estimation of anatomical structures. If segmentation of multiple anatomical structures is performed simultaneously, it provides a clinician with a complete picture and a focused approach towards studying the relationship with the

surrounding structures. Therefore, the present study investigated the performance of integrated CNN models for creating the MVP consisting of combined automatic segmentation of the maxillary complex, sinus, and teeth as a single unit.

For qualitative assessment, since only minor corrections were needed, the quality of integration was assessed based on the number of refinements and the required time. The results showed a strong agreement between both observers. A score equal to 7 or more (85% of the dataset) was considered a high-quality segmentation, while a score ranging from 3-6 (15% of the dataset) an above-average quality. Segmentations with a Table 3 illustrates the types of required refinements per segmented structure. According to previous validation studies ' classification^{12, 13}, minor refinements have no or slight clinical relevance, and the present qualitative analysis assumes that this clinical impact depends on the number of minor refinements needed. In daily practice, the clinical relevance of such refinements might differ depending on the task at hand, such as visualization, diagnosis, treatment planning, and patient education. Moreover, each type of refinement might be more relevant in a specific clinical specialty compared to another one. For instance, mucosal sinus thickness is more relevant for treatment planning in oral and maxillofacial surgical procedures involving maxillary sinus floor elevation¹⁵ compared to a routine dental examination or patient education.

The quantitative assessment revealed that the sum of the mean time required for automatic MVP segmentation (1.7 minutes) was slightly higher compared to the sum of the previously documented timing for each structure segmentation, which totaled 1.3 minutes (maxillofacial complex: 39.1, maxillary sinus: 24.4, all teeth: 13.7 seconds)^{8, 12, 13}. This minimal difference could be attributed to some technical variabilities, such as nonuser active processes, which impact the segmentation time even if the same AI tool is run several times, making it a challenge to keep the time constant¹⁶. Another reason could be the large field of view (FOV) of the included sample, which could have increased the processing time. The previous studies used fewer testing samples with large FOVs because they covered only one region of interest.

We did not investigate the clinical accuracy of automated segmentation, which has previously been reported to have a high DSC score (maxillary complex: 92.6%, maxillary sinus: 98.4%, teeth: 90%), when compared to the reference ground truth generated by skilled human operators using a manual or semi-automatic approach. Rather, the relevant performance of the combined structural segmentation was compared to the manually refined one. The findings showed no change in performance following post-integration. A DSC score of 99.3% was observed compared to refined segmentation for both observers. Hence, implying high segmentation quality even for scans requiring many refinements.

Additionally, the interobserver consistency showed almost perfect overlap with a DSC of 99.8%, indicating that the integrated model could provide an automated ground that increases consistency between observers, overcoming high observer variability in other segmentation techniques.

The presented CNN model overcame the issue of manual threshold selection required with semi-automatic approaches. Moreover, the main benefit of the model is the simultaneous segmentation of anatomical structures with different densities using a single platform, as shown in the coronal slice of Figure 1a. This type of combined segmentation is not possible with the available semi-automatic segmentation software programs, where each structure has a different threshold, requiring manual adjustment separately by the operator¹⁷. Clinically, this integrated segmentation could be a valuable tool in clinical orthodontics and maxillofacial surgical procedures, such as implant planning, bone grafting, and orthognathic and reconstructive surgery^{18–21}, where visualization of the MVP and its relationship with surrounding structures is a necessity for reaching an accurate diagnosis and patient-specific treatment planning.

An additional advantage of the proposed approach was that no third-party software was required to refine the automated segmentations, which was not the case in the previous individual CNN model-based validation studies. As newly developed tools have been employed on the platform, which also let the clinicians directly refine the segmentations. However, lack of data heterogeneity remains a limitation, and there is a need to incorporate data from other CBCT devices with varying scanning parameters to justify the generalizability of the tool. In the near future, we plan to integrate other validated individual anatomical regions, such as the mandible, inferior alveolar canal, and pharyngeal airway^{9–11}. It is also expected to expand the tool's ability by integrating data from intra-oral scanners and facial scanners for the creation of a complete virtual patient, which could enhance the delivery of personalized dental care²². Furthermore, additional CBCT scans from various institutions, CBCT scanner brands, as well as the variability of patient anatomy and pathology, should be integrated in the near future to increase the generalizability further. The application of AI tools and personalized data in clinical and research fields could support positive clinical protocols changes, help create predictive population models²³, and act as a visual educational tool for both clinicians and patients.

5. Conclusion

The three integrated CNN models proved to be fast and accurate for simultaneous segmentation of maxillary anatomical structures with different densities. Both the qualitative and the quantitative assessments revealed strong interobserver consistency. The integrated MVP could act as a feasible tool for visualization, diagnostics, and treatment planning in daily clinical practice.

References

1. Shujaat S, Bornstein MM, Price JB, Jacobs R (2021) Integration of imaging modalities in digital dental workflows - possibilities, limitations, and potential future developments. *Dentomaxillofacial Radiol* 50:20210268. <https://doi.org/10.1259/dmfr.20210268>
2. Jacobs R, Salmon B, Codari M, et al (2018) Cone beam computed tomography in implant dentistry: recommendations for clinical use. *BMC Oral Health* 18:88. <https://doi.org/10.1186/s12903-018-0523-5>
3. Minnema J, van Eijnatten M, Kouw W, et al (2018) CT image segmentation of bone for medical additive manufacturing using a convolutional neural network. *Comput Biol Med* 103:130–139. <https://doi.org/10.1016/j.compbimed.2018.10.012>
4. Vandenberghe B, Luchsinger S, Hostens J, et al (2012) The influence of exposure parameters on jawbone model accuracy using cone beam CT and multislice CT. *Dentomaxillofacial Radiol* 41:466–474. <https://doi.org/10.1259/dmfr/81272805>
5. Wang L, Chen KC, Gao Y, et al (2014) Automated bone segmentation from dental CBCT images using patch-based sparse representation and convex optimization. *Med Phys* 41:043503. <https://doi.org/10.1118/1.4868455>
6. Hagan MT, Demuth HB, Beale MH, de Jesús O (2006) *Neural Networks in a Softcomputing Framework*. Springer-Verlag, London
7. Leite AF, Vasconcelos K de F, Willems H, Jacobs R (2020) Radiomics and Machine Learning in Oral Healthcare. *PROTEOMICS – Clin Appl* 14:1900040. <https://doi.org/10.1002/prca.201900040>
8. Shaheen E, Leite A, Alqahtani KA, et al (2021) A novel deep learning system for multi-class tooth segmentation and classification on cone beam computed tomography. A validation study. *J Dent* 103865. <https://doi.org/10.1016/j.jdent.2021.103865>
9. Verhelst P-J, Smolders A, Beznik T, et al (2021) Layered deep learning for automatic mandibular segmentation in cone-beam computed tomography. *J Dent* 114:103786. <https://doi.org/10.1016/j.jdent.2021.103786>
10. Lahoud P, Diels S, Niclaes L, et al (2022) Development and validation of a novel artificial intelligence driven tool for accurate mandibular canal segmentation on CBCT. *J Dent* 116:103891. <https://doi.org/10.1016/j.jdent.2021.103891>
11. Shujaat S, Jazil O, Willems H, et al (2021) Automatic segmentation of the pharyngeal airway space with convolutional neural network. *J Dent* 111:103705. <https://doi.org/10.1016/j.jdent.2021.103705>

12. Morgan N, Van Gerven A, Smolders A, et al (2022) Convolutional neural network for automatic maxillary sinus segmentation on cone-beam computed tomographic images. *Sci Rep* 12:7523. <https://doi.org/10.1038/s41598-022-11483-3>
13. Preda F, Morgan N, Gerven A Van, et al (2022) Deep convolutional neural network-based automated segmentation of the maxillofacial complex from cone-beam computed tomography - A validation study. *J Dent* forthcoming
14. Landis JR, Koch GG (1977) The Measurement of Observer Agreement for Categorical Data. *Biometrics* 33:159. <https://doi.org/10.2307/2529310>
15. Hung KF, Ai QYH, King AD, et al (2022) Automatic detection and segmentation of morphological changes of the maxillary sinus mucosa on cone-beam computed tomography images using a three-dimensional convolutional neural network. *Clin Oral Investig*. <https://doi.org/10.1007/s00784-021-04365-x>
16. Nogueira PE, Matias R (2015) A quantitative study on execution time variability in computing experiments. In: 2015 Winter Simulation Conference (WSC). IEEE, pp 529–540
17. Friedli L, Kloukos D, Kanavakis G, et al (2020) The effect of threshold level on bone segmentation of cranial base structures from CT and CBCT images. *Sci Rep* 10:7361. <https://doi.org/10.1038/s41598-020-64383-9>
18. Ma H, Van Dessel J, Bila M, et al (2021) Application of Three-Dimensional Printed Customized Surgical Plates for Mandibular Reconstruction: Report of Consecutive Cases and Long-Term Postoperative Evaluation. *J Craniofac Surg* 32:e663–e667. <https://doi.org/10.1097/SCS.00000000000007835>
19. Li B, Wei H, Jiang T, et al (2021) Randomized clinical trial of the accuracy of patient-specific implants versus cad/cam splints in orthognathic surgery. *Plast Reconstr Surg* 148:1101–1110. <https://doi.org/10.1097/PRS.00000000000008427>
20. Mathew N, Gandhi S, Singh I, et al (2020) 3D Models Revolutionizing Surgical Outcomes in Oral and Maxillofacial Surgery: Experience at Our Center. *J Maxillofac Oral Surg* 19:208–216. <https://doi.org/10.1007/s12663-019-01275-0>
21. Palomo JM, El H, Stefanovic N, Bazina M (2019) Diagnostic Value of 3D Imaging in Clinical Orthodontics. In: *Craniofacial 3D Imaging*. Springer International Publishing, Cham, pp 113–139
22. Bornstein MM (2022) The crucial role of dentomaxillofacial radiology for AI research in dental medicine – why it's time for our specialty to lead the way! *Dentomaxillofac Radiol* 51:. <https://doi.org/10.1259/dmfr.20229001>
23. Joda T, Bornstein MM, Jung RE, et al (2020) Recent Trends and Future Direction of Dental Research in the Digital Era. *Int J Environ Res Public Health* 17:1987. <https://doi.org/10.3390/ijerph17061987>

Part 2

Clinical applications of automated segmentation

Three-dimensional quantification of skeletal midfacial complex symmetry

Morgan N. ^{1,2}

Shujaat S.¹

Jazil O.¹

Jacobs R.^{1,3}

¹ OMFS IMPATH Research Group, Department of Imaging & Pathology, Faculty of Medicine, KU Leuven & Oral and Maxillofacial Surgery, University Hospitals Leuven, Leuven, Belgium

² Department of Oral Medicine, Faculty of Dentistry, Mansoura University, 35516 Mansoura, Dakahlia, Egypt

³ Department of Dental Medicine, Karolinska Institutet, Stockholm, Sweden

Abstract

Purpose

Quantification of skeletal symmetry in a healthy population could have a strong impact on reconstructive surgical procedures where mirroring of the contralateral healthy side acts as a clinical reference for the restoration of unilateral defects. Hence, the aim of this study was to three-dimensionally assess the symmetry of the skeletal midfacial complex in skeletal class I patients.

Methods

A sample of 100 cone beam computed tomography (CBCT) scans (50 males, 50 females; age range: 19-40 years) was recruited. Automated segmentation of the skeletal midfacial complex was performed to create a 3D virtual model using a convolutional neural network (CNN)-based segmentation tool. Thereafter, the segmented model was mirrored and registered to quantify skeletal symmetry using a color-coded conformance mapping based on a surface part-comparison analysis.

Results

Overall, the mean and root mean square (RMS) differences between complete true and mirrored models were 0.14 ± 0.12 mm and 0.87 ± 0.21 mm, respectively. Female patients had a significantly more symmetrical midfacial complex (mean difference: 0.11 ± 0.1 mm, RMS: 0.81 ± 0.17 mm) compared to male patients (mean difference: 0.16 ± 0.13 mm, RMS: 0.94 ± 0.23 mm). No significant difference existed between the left and right sides, irrespective of the patient's gender.

Conclusion

The comparison between the true and mirrored complete and left/right split midfacial complex showed symmetry within a clinically acceptable range of 1 mm, which justifies the applicability of using the mirroring technique. The presented data could act as a reference guide for surgeons during the planning of reconstructive surgical procedures and outcome assessment at follow-up.

Keywords: midfacial complex- symmetry- automatic segmentation- CBCT- mirroring reconstructive surgeries- virtual surgical planning.

1. Introduction

The midfacial complex refers to the middle portion of the osseous facial architecture, which significantly contributes towards defining the facial form. It incorporates the maxilla, nasal skeleton, orbital rim, and zygoma (including the entire length of zygomatic arches), which are bounded by frontomaxillary, frontozygomatic, and frontonasal suture lines. The clinical relevance of the midfacial complex cannot be ignored, as it is one of the most commonly fractured regions requiring surgical correction, accounting for approximately 60% of all maxillofacial fractures¹⁻³. Furthermore, midfacial complex deformity correction is often performed through reconstructive surgery for improving facial esthetics and functionality. One of the main required outcomes of these surgical interventions is the restoration of facial symmetry following functional recovery.

With the advent of 3D CT/CBCT imaging, surface-based skeletal symmetry evaluation techniques have been widely applied for diagnostics, reconstructing symmetrical facial skeletal structures, and outcome assessment⁴⁻⁷. These 3D methodologies have replaced the conventional landmark-based assessment techniques^{8,9} which make the morphological assessment problematic owing to a high degree of human error, observer variability, and high time consumption¹⁰. In addition, the main steps involved in the 3D symmetry evaluation and virtual surgical planning for achieving a symmetrical skeletal outcome in patients with defects consist of surface segmentation followed by mirroring and superimposition of the normal region onto the defected side¹¹⁻¹³. These steps have been employed for quantifying the symmetry of orbital^{14,15} and zygomatic bones^{16,17} in a healthy population for the purpose of providing a reference benchmark which facilitates the surgical reconstruction of skeletal defects.

The most vital step for symmetry assessment involves segmentation or skeletal surface reconstruction for the creation of a virtual 3D model from CT/CBCT datasets. Any flaw in this step would contribute towards the accumulation of errors in the later steps. Studies assessing the symmetry of skeletal structures rely mainly on semi-automatic segmentation software programs, which are prone to certain limitations, such as threshold selection, observer variability, and over- or under-segmentation requiring time-consuming manual intervention¹⁸⁻²⁰, which in turn could lead to an inaccurate symmetry assessment. To overcome these limitations, convolutional neural network (CNN)-based deep learning algorithms have been applied for automated segmentation of dentomaxillofacial structures from CBCT images and have shown promising results²¹⁻²³. However, these artificial intelligence-based models still need to be applied for assessing the symmetry of skeletal structures.

To our knowledge limited evidence exists quantifying the midfacial complex symmetry in a healthy population group. Furthermore, no protocol exists for quantifying skeletal symmetry with the

application of CNN-based segmentation approaches¹⁰. Therefore, the following study was conducted to quantify the symmetry of the midfacial complex on CBCT images of skeletal class I patients using a recently validated CNN-based automated segmentation tool²⁴, which could act as a reference guide for mirroring reconstructive surgical procedures in patients with skeletal defects and asymmetry. The hypothesis behind this work was that the automation of the segmentation step and the provision of midfacial complex symmetry data would enhance the precision and time-efficiency of the symmetry evaluation process for further clinical applicability in patients requiring mirroring for reconstructive surgery.

2. Methods

This study was conducted in compliance with the World Medical Association Declaration of Helsinki on medical research. Ethical approval was obtained from the Ethical Review Board of the University Hospitals of Leuven (reference number: S57587).

2.1 Data collection

The sample size was calculated based on previous comparable studies^{11,14} using a priori power analysis in G*power software (version 3.1.9.4, University of Dusseldorf, Dusseldorf, Germany) to test the difference between two sample means at a power of 80%, an effect size of $d = 0.57$, and 0.05 level of significance.

A total sample of 100 CBCT scans (50 males and 50 females) were recruited during the period 2018–2020, from the radiological database of UZ Leuven Hospital, Leuven, Belgium. The scans were acquired with NewTom VGi evo CBCT device (NewTom, Verona, Italy) using a standardized scanning protocol (field of view: 24x19 cm, voxel size: 0.3 mm). The inclusion criteria were adult healthy patients aged 19-40 years with skeletal class I who underwent CBCT scanning for justified dental or maxillofacial indications. Patients with a history of maxillofacial trauma, odontological surgical interventions, reconstructive surgery, existing pathology, and skeletal deformity were excluded. All scans were saved in Digital Imaging and Communication in Medicine (DICOM) format for further processing.

2.2 Symmetry assessment protocol

2.2.1 Automatic segmentation

The segmentation of the skeletal midfacial complex was performed using a previously developed and validated CNN-based online cloud tool²⁴ known as the ‘Virtual Patient Creator’ (ReLu BV, Leuven, Belgium, Version October 2021).

The DICOM images were uploaded to the tool, which allowed automatic segmentation and generation of a virtual 3D model in Standard Tessellation Language (STL) file format. The segmented midfacial complex involved the palatine, maxillary, zygomatic, nasal, and lacrimal bones. The complex was bounded superiorly by replicating a Le Fort III fracture line which passed through the frontonasal suture, frontomaxillary suture, orbital wall, and frontozygomatic suture^{25,26}. Laterally and posteroinferiorly, it was limited till zygomaticotemporal and pterygomaxillary suture lines, respectively. Inferiorly, the complex extended up to the alveolar bone level. The teeth were automatically excluded from the segmented region as the CNN-based tool had been manually trained to specifically segment the skeletal complex and crop the dentition from the final segmentation output²⁴ (Figure 1).

Later, the STL files of the midfacial complex were imported into Mimics Innovation Suite (version 23.0, Materialise N.V., Leuven, Belgium) to confirm the visual quality of the segmentation. Visual inspection of the segmentation was performed by assessing the boundaries of the segmented midfacial complex overlapped onto the coronal, axial, and sagittal orthogonal planes of the CBCT images. If any minor discrepancy existed within the final segmentation, it was corrected manually using the 3D tools tab.

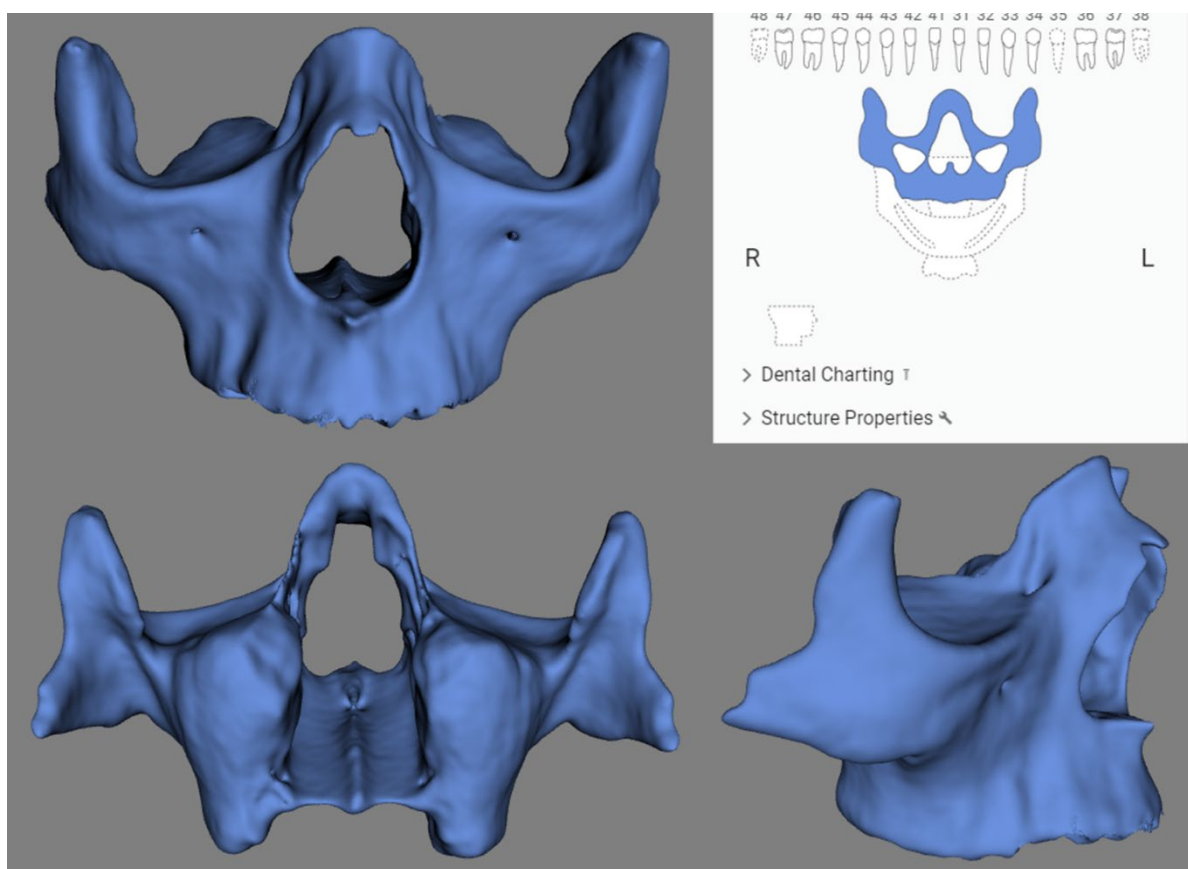


Figure 1. Automatic segmentation of midfacial complex: anterior, posterior, and side views (creator.relu.eu, ReLu BV, Version October 2021).

2.2.2 Mirroring and registration

Mirroring and registration were applied to quantify both the complete and unilateral left/right midfacial complex skeletal symmetry. The reasoning for that was to estimate the range of normal symmetry, which could act as an intuitive guide during the preoperative surgical planning phase and for analyzing residual postoperative asymmetry depending on the type of midfacial reconstructive surgery, i.e., either complete midfacial complex reconstruction or in cases where the normal contralateral side acts as a reference.

Firstly, the STL files of automated segmentation were imported into 3-matic software (version 15.0, Materialise N.V., Leuven, Belgium), where a mirrored model of the complete midfacial complex was created by a “mirror” command using an arbitrary midsagittal plane which was automatically determined by the software (Figure 2a). Thereafter, the mirrored model was registered onto the true model according to the least point-to-point distance between the two overlapped surfaces. This process was performed by applying global co-registration with enough iterations until the mean point-to-point distance for all point pairs reached its least value without any visible spatial changes (Figure 2b). The registration distance threshold was set at 10 mm for a gross overlap and was gradually changed up to 0.5 mm for fine tuning the final registration and maximizing the conformance.

Thereafter, morphological symmetry between the true and mirrored models was assessed using a color-coded conformance mapping based on the part-comparison function. This allowed quantitative calculation of the difference between true and mirrored midfacial complexes, depending on the degree of conformity or variation between both sites. Figure 3 illustrates an example of a case showing color-coded part comparison analysis of a complete midfacial complex symmetry.

In addition, a mirror model of the left and right sides of the segmented complex was created using a midsagittal plane based on the following landmarks: the posterior nasal spine, the anterior nasal spine, and the nasion. This plane has been found to be the most appropriate for assessing bilateral craniomaxillofacial symmetry^{27,28}. Each mirrored model was registered onto the opposing contralateral true model, i.e., the left mirrored model was registered onto the right true side, and vice versa, followed by registration and part-comparison as previously mentioned.

The entire procedure, starting from segmentation till part-comparison was performed blindly by two independent experts. Both observers repeated the assessment twice at an interval of 1 week for calculating intra- and inter-observer error and reliability.

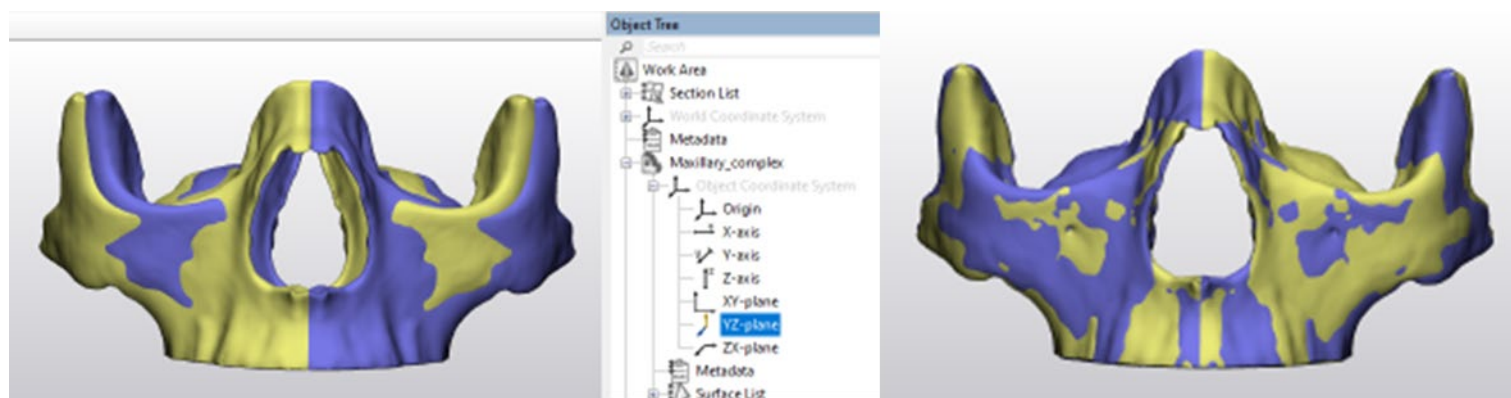


Figure 2. Mirroring and registration steps of complete midfacial complex. A. Mirroring of midfacial complex based on an arbitrary midsagittal plane, B. Global registration of original and mirrored models.

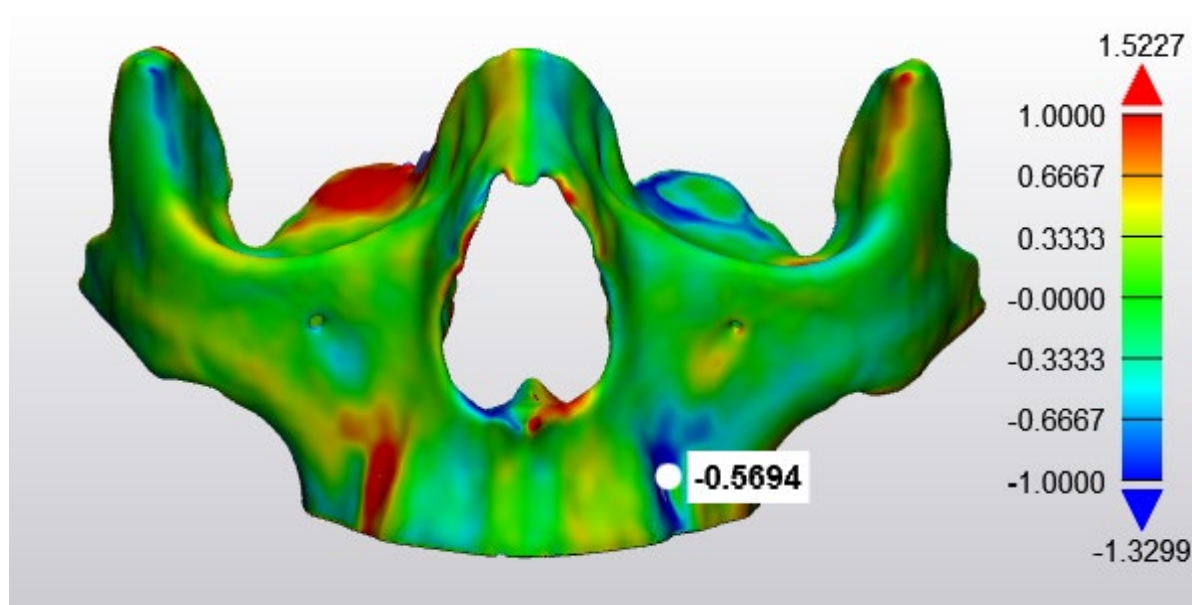


Figure 3. Color-coded part comparison analysis between complete true and mirrored midfacial complex.

Note: Green color (zero value) corresponds to no difference between the true and mirrored overlapped models, deviation towards blue color (negative values) correspond to under-estimation of true model, deviation towards red color (positive values) correspond to over-estimation of true model.

2.3 Statistical analysis

Data were analyzed using IBM SPSS Statistics for Windows, version 21.0 (IBM Corp., Armonk, NY, USA). The Shapiro–Wilk test was applied to assess the data for normal distribution and homoscedasticity was verified by conducting Levene’s test. The symmetry was presented as the mean and root mean square (RMS) difference between the true and mirrored models of the complete and unilateral midfacial complex. A t-test and two-way analysis of variance were applied for assessing the differences in symmetry of the complete and left/right split based on gender. The relative technical error of measurements (rTEM) was calculated for assessing the intra- and inter-observer error and classified into five categories (<1% = excellent, 1–3.9% = very good, 4–6.9% = good, 7–9.9% = moderate, >10% = poor)^{29,30}. Moreover, Intra-class Correlation Coefficient (ICC) was applied at a 95% confidence interval for evaluating the inter- and intra-observer reliability (where <0.50 = poor reliability; 0.50–0.75 = moderate reliability; 0.75–0.90 = good reliability; >0.90 = excellent reliability)³¹. A p-value of <0.05 was considered as statistically significant.

3. Results

All data presented a normal distribution and exhibited homoscedasticity. The visual examination of the segmentations revealed that 20% of the automatic segmentations required manual corrections. However, the corrections were minor and clinically insignificant in nature. The rTEM for both intra- and inter-observer error ranged from good to excellent, with the least amount of error observed when mirroring a complete midfacial complex compared to split left/right sides. Moreover, inter- and intra-observer reliability revealed an excellent ICC value (>0.99) for all parameters without any significant difference between observers (Table 1).

Table 1: Intra and inter observer error and reliability of complete and unilateral left/right midfacial complex skeletal symmetry.

		Complete true / mirrored		Right true /left mirrored		Left true /right mirrored	
		Mean	RMS	Mean	RMS	Mean	RMS
Intra-observer	rTEM	1.4%	0.18%	1.4%	0.24%	1.5%	0.35%
	ICC	0.999	0.999	0.999	0.999	0.998	0.999
Inter-observer	rTEM	1.8%	0.3%	5%	1.1%	6%	1.4%
	ICC	0.999	0.999	0.997	0.998	0.997	0.997

RMS: root mean square, rTEM: relative technical error measurements, ICC: Intra-class Correlation Coefficient.

Table 2 describes the symmetry of the complete midfacial complex based on part comparison analysis. Overall, the mean and RMS difference between complete true and mirrored models were $0.14 \pm 0.12 \text{ mm}$ and $0.87 \pm 0.21 \text{ mm}$, respectively. Male patients showed a higher complete midfacial complex asymmetry (mean difference: $0.16 \pm 0.13 \text{ mm}$, RMS: $0.94 \pm 0.23 \text{ mm}$) compared to the female patients (mean difference: $0.11 \pm 0.1 \text{ mm}$, RMS: $0.81 \pm 0.17 \text{ mm}$). Moreover, a significant mean ($p = 0.034$) and RMS difference ($p = 0.002$) existed based on the gender of patients, where female patients were found to be significantly more symmetrical compared to the male patients.

Table 3 demonstrates the overall and gender-based mean and RMS difference between the left/right true and mirrored sides. The comparison between the superimposed true right and mirrored left models showed similar values (mean: $0.13 \pm 0.11 \text{ mm}$, RMS: $0.82 \pm 0.22 \text{ mm}$) compared to the true left and mirrored right models (mean: $0.13 \pm 0.13 \text{ mm}$, RMS: $0.82 \pm 0.21 \text{ mm}$), with no significant mean ($F = 0.158$, $p = 0.692$) and RMS difference ($F = 0.017$, $p = 0.896$) existed between both sides. A significant difference existed between males and females either for the mean ($F = 6.6$, $p = 0.011$) or RMS value ($F = 22.06$, $p = <0.001$). Interaction between side and gender was negligible for both measurements (mean: $F = 0.069$, $p = 0.794$; RMS: $F = 0.232$, $p = 0.631$).

Table 2: Mean and root mean square (RMS) difference between true and mirrored midfacial complex.

Study population		Mean distance (mm)	RMS (mm)
Total	Mean	0.14	0.87
	SD	0.12	0.21
	Min	0.002	0.56
	Max	0.881	1.98
Male	Mean	0.16	0.94
	SD	0.13	0.23
	Min	0.005	0.59
	Max	0.881	1.98
Female	Mean	0.11	0.81
	SD	0.1	0.17
	Min	0.002	0.56
	Max	0.547	1.48

Table 3: Mean and root mean square (RMS) difference between true left/right and mirrored sides.

Study population		Mean right- left mirror (mm)	Mean left- right mirror (mm)	RMS right- left mirror (mm)	RMS left- right mirror (mm)
Total	Mean	0.13	0.13	0.82	0.82
	SD	0.11	0.13	0.22	0.21
	Min	0.003	0.004	0.546	0.49
	Max	0.872	0.902	2.08	1.87
Male	Mean	0.15	0.16	0.89	0.88
	SD	0.13	0.14	0.25	0.22
	Min	0.034	0.014	0.609	0.561
	Max	0.872	0.902	2.08	1.87
Female	Mean	0.11	0.11	0.74	0.76
	SD	0.07	0.12	0.15	0.19
	Min	0.003	0.004	0.546	0.49
	Max	0.349	0.62	1.27	1.43

4. Discussion

In a clinical practice, quantification of normal midfacial complex symmetry in a healthy population could have a strong impact on reconstructive surgical procedures where mirroring of the contralateral healthy part acts as a clinical reference for the restoration of unilateral defects. This quantification could provide a reference to the surgeons for achieving optimal treatment planning in terms of facial aesthetics and function and follow-up evaluation.

At present, mirroring techniques for craniomaxillofacial reconstructive surgery are based on the assumption that both the left and right sides are symmetrical. However, evidence suggests that a normal acceptable range of skeletal asymmetry exists, referred to as “fluctuating asymmetry”^{32,33}. This range has been mostly defined for skeletal structures such as the mandible, zygomatic bone, zygomaticomaxillary complex, and orbital region. To our knowledge, no study exists assessing the symmetry of the midfacial complex in a healthy population group. Hence, the following study was conducted to three-dimensionally quantify the average natural variation of its symmetry.

Recently, various 3D workflows have been established for the restoration of unilateral skeletal defects and assessing symmetry^{15-17, 34}. Although the mirroring and registration steps have been automated, the main limitation associated with these workflows has been the application of semi-automated skeletal segmentation tools, which might negatively impact the final expected outcome. Furthermore, the cortical bone of the midfacial complex is thin and fibrous in nature with a low bone mineral density, which makes segmentation challenging and prone to error and variability^{35,36}. Therefore, the current study applied a state-of-the-art CNN-based automated segmentation tool. At present, no completely automated workflow exists in the literature for mirroring reconstructive surgical procedures. The proposed tool not only allowed automatization of the 3D workflow for re-establishing the contralateral midfacial complex, but it could also act as a viable alternative for assessing symmetry by providing a consistent and time-efficient segmentation. Furthermore, the symmetry was assessed based on the geometric morphometry of the whole bone surface instead of relying on specific landmarks and linear/angular measurements, which could also offer a more realistic approach towards quantifying the site and magnitude of symmetry¹⁰.

A comparison with prior evidence was deemed difficult owing to the absence of studies evaluating the symmetry of the midfacial complex. Rather, the majority of studies focused towards the symmetry assessment of individual skeletal structures, such as the orbital bone^{14,15}, zygomatic arch^{16,17}, mandible^{37,38} and upper skull^{39,40}. It is noteworthy that the assessment of midfacial complex symmetry as a whole is equally important as individual anatomical structures for defining facial form and function, especially in major reconstructive surgical procedures where the whole unilateral complex region might require mirroring for reconstruction.

The findings of the present study showed that the overall asymmetry RMS value of the complete midfacial complex was comparable to that of zygomatic bone^{16,17} and orbital floor^{14,15}. On the contrary, the mean difference was found to be smaller compared to that of the upper skull. Based on gender variability, the present study showed a significant difference based on the mean and RMS values. These gender-based findings were contradictory to Gibelli et al¹⁶ study, where the authors reported no significant asymmetry of zygomatic bone for both types of values. In contrast, our findings were consistent with Ho et al¹⁷ study, which reported significantly higher asymmetry in male patients. Previous studies also suggest that female skulls are more symmetrical compared to male skulls, which could also apply to the midfacial complex region. Furthermore, Hingsammer et al⁴¹ reported a mean zygoma asymmetry of 1.6 mm, which was higher than the values obtained for the complex in the present study. This could be attributed to either the structural variability or the difference in methodology, where the authors relied on landmark-based linear measurements, which fail to provide the true 3D symmetry of an anatomical structure and are more prone to human error

and variability. In contrast, assessment of the entire skeletal structure using mirroring and part comparison provides more accurate and realistic information about symmetry.

Our findings also suggested no significant difference between the left and right sides, which was consistent with the studies evaluating the upper skull and orbital floor. The presence of a slight fluctuating asymmetry justifies mirroring reconstructive techniques in cases with unilateral defects and also confirms that no precipitating random difference exists on either side, which might impact the final treatment plan⁴².

The low magnitude of error and excellent observer reliability support the clinical applicability of the proposed methodology. The presented data suggested that the average amount of both complete and split midfacial complex asymmetry was within a clinically acceptable range of 1 mm, which signifies the rationale of using the contralateral unaffected side as an acceptable reference for performing unilateral reconstructive surgery of the midfacial complex in traumatic and oncologic patients. Although minimal differences existed based on the gender of the patient, female patients showed a significantly more symmetrical complete midfacial complex compared to male patients. Hence, implying that a surgeon should carefully examine any pre-existing asymmetry of the midfacial skeletal structures, especially in male patients, during the preoperative treatment planning phase. It should also be noted that the minimum and maximum values of asymmetry varied for each patient at an individual level. Thereby, a patient-specific or personalized approach should be applied for planning midfacial reconstructive surgery instead of relying on a traditional one-size-fits-all approach⁴³.

The main strengths of the study included the first-time reporting of the objective assessment of midfacial complex symmetry in a healthy population and the introduction of a reliable, accurate, and efficient segmentation tool which could further automatize the symmetry assessment task and overcome the negative impact of thresholding-based approaches. At the same instance, the study had certain limitations. Firstly, the amount of asymmetry associated with each individual anatomical structure was not evaluated, where one structure might influence the asymmetry more than the other; hence, requiring further studies to establish automated segmentation approaches of individual structures to increase the clinical feasibility of the approach. Secondly, the symmetry evaluation of the left versus right side was based on an operator-dependent landmark-based midsagittal plane. Although this plane has been documented to be clinically acceptable for assessing symmetry, there is still a need for further research to also automate this task to ensure an operator-free approach.

5. Conclusion

The comparison between the true and mirrored complete and split midfacial complex showed differences within a clinically acceptable range of 1 mm, which justifies the applicability of the mirroring technique. These presented data could act as a reference for surgeons when evaluating asymmetry and guide the decision-making process for restoring midfacial defects. Furthermore, the proposed automated approach could act as a viable alternative for a more precise diagnosis, surgical planning, and follow-up evaluation.

References

1. Yamamoto, K., Y. Matsusue, S. Horita, K. Murakami, T. Sugiura, and T. Kirita (2014) Clinical analysis of midfacial fractures. *Mater Sociomed*. 26: 21-5 [https://doi.org/ 10.5455/msm.2014.26.21-25](https://doi.org/10.5455/msm.2014.26.21-25).
2. Zaleckas, L., V. Pečiulienė, I. Gendvilienė, A. Pūrienė, and J. Rimkuvienė (2015) Prevalence and etiology of midfacial fractures: A study of 799 cases. *Medicina*. 51: 222-227 <https://doi.org/https://doi.org/10.1016/j.medici.2015.06.005>.
3. VandeGriend, Z.P., A. Hashemi, and M. Shkoukani (2015) Changing trends in adult facial trauma epidemiology. *J Craniofac Surg*. 26: 108-12 [https://doi.org/ 10.1097/scs.0000000000001299](https://doi.org/10.1097/scs.0000000000001299).
4. Schmelzeisen, R., N.C. Gellrich, R. Schoen, R. Gutwald, C. Zizelmann, and A. Schramm (2004) Navigation-aided reconstruction of medial orbital wall and floor contour in cranio-maxillofacial reconstruction. *Injury*. 35: 955-962 [https://doi.org/ https://doi.org/10.1016/j.injury.2004.06.005](https://doi.org/https://doi.org/10.1016/j.injury.2004.06.005).
5. Zizelmann, C., N.C. Gellrich, M.C. Metzger, R. Schoen, R. Schmelzeisen, and A. Schramm (2007) Computer-assisted reconstruction of orbital floor based on cone beam tomography. *British Journal of Oral and Maxillofacial Surgery*. 45: 79-80 <https://doi.org/https://doi.org/10.1016/j.bjoms.2005.06.031>.
6. Swennen, G.R.J. (2014) Timing of Three-Dimensional Virtual Treatment Planning of Orthognathic Surgery: A Prospective Single-Surgeon Evaluation on 350 Consecutive Cases. *Oral and Maxillofacial Surgery Clinics of North America*. 26: 475-485 <https://doi.org/https://doi.org/10.1016/j.coms.2014.08.001>.
7. Dubois, L., R. Schreurs, J. Jansen, T.J. Maal, H. Essig, P.J. Gooris, and A.G. Becking (2015) Predictability in orbital reconstruction: A human cadaver study. Part II: Navigation-assisted orbital reconstruction. *J Craniomaxillofac Surg*. 43: 2042-9 [https://doi.org/ 10.1016/j.jcms.2015.07.020](https://doi.org/10.1016/j.jcms.2015.07.020).
8. Gong, X., Y. He, Y. He, J.G. An, Y. Yang, and Y. Zhang (2014) Quantitation of zygomatic complex symmetry using 3-dimensional computed tomography. *J Oral Maxillofac Surg*. 72: 2053.e1-8 [https://doi.org/ 10.1016/j.joms.2014.06.447](https://doi.org/10.1016/j.joms.2014.06.447).
9. Mao, S.H., Y.H. Hsieh, P.Y. Chou, V.B. Shyu, C.T. Chen, and C.H. Chen (2016) Quantitative Determination of Zygomaticomaxillary Complex Position Based on Computed Tomographic Imaging. *Ann Plast Surg*. 76 Suppl 1: S117-20 [https://doi.org/ 10.1097/sap.0000000000000703](https://doi.org/10.1097/sap.0000000000000703).
10. Morgan, N., I. Suryani, S. Shujaat, and R. Jacobs (2021) Three-dimensional facial hard tissue symmetry in a healthy Caucasian population group: a systematic review. *Clin Oral Investig*. 25: 6081-6092 [https://doi.org/ 10.1007/s00784-021-04126-w](https://doi.org/10.1007/s00784-021-04126-w).

11. Khalifa, G.A., N.A. Abd El Moniem, S.A. Elsayed, and Y. Qadry (2016) Segmental Mirroring: Does It Eliminate the Need for Intraoperative Readjustment of the Virtually Pre-Bent Reconstruction Plates and Is It Economically Valuable? *J Oral Maxillofac Surg.* 74: 621-30 <https://doi.org/10.1016/j.joms.2015.09.036>.
12. Schramm, A., M.M. Suarez-Cunqueiro, M. Rücker, H. Kokemueller, K.H. Bormann, M.C. Metzger, and N.C. Gellrich (2009) Computer-assisted therapy in orbital and mid-facial reconstructions. *Int J Med Robot.* 5: 111-24 <https://doi.org/10.1002/rcs.245>.
13. Benazzi, S. and S. Senck (2011) Comparing 3-Dimensional Virtual Methods for Reconstruction in Craniomaxillofacial Surgery. *Journal of Oral and Maxillofacial Surgery.* 69: 1184-1194 <https://doi.org/https://doi.org/10.1016/j.joms.2010.02.028>.
14. Jozaghi, Y., H.H.L. Chan, J.C. Davies, and J.C. Irish (2019) Establishing Orbital Floor Symmetry to Support Mirror Imaging in Computer-Aided Reconstruction of the Orbital Floor. *J Craniofac Surg.* 30: 1888-1890 <https://doi.org/10.1097/scs.0000000000005368>.
15. Jansen, J., L. Dubois, R. Schreurs, P.J.J. Gooris, T.J.J. Maal, L.F. Beenen, and A.G. Becking (2018) Should Virtual Mirroring Be Used in the Preoperative Planning of an Orbital Reconstruction? *J Oral Maxillofac Surg.* 76: 380-387 <https://doi.org/10.1016/j.joms.2017.09.018>.
16. Gibelli, D., M. Cellina, S. Gibelli, A.G. Oliva, G. Termine, V. Pucciarelli, C. Dolci, and C. Sforza (2018) Assessing symmetry of zygomatic bone through three-dimensional segmentation on computed tomography scan and "mirroring" procedure: A contribution for reconstructive maxillofacial surgery. *J Craniomaxillofac Surg.* 46: 600-604 <https://doi.org/10.1016/j.jcms.2018.02.012>.
17. Ho, J., R. Schreurs, S. Aydi, R. Rezai, T.J.J. Maal, A.J. van Wijk, L.F.M. Beenen, L. Dubois, D.M.J. Milstein, and A.G. Becking (2017) Natural variation of the zygomaticomaxillary complex symmetry in normal individuals. *J Craniomaxillofac Surg.* 45: 1927-1933 <https://doi.org/10.1016/j.jcms.2017.09.017>.
18. Kavur, A.E., N.S. Gezer, M. Barış, Y. Şahin, S. Özkan, B. Baydar, U. Yüksel, Ç. Kılıkçier, Ş. Olut, G. Bozdağı Akar, G. Ünal, O. Dicle, and M.A. Selver (2020) Comparison of semi-automatic and deep learning-based automatic methods for liver segmentation in living liver transplant donors. *Diagnostic and interventional radiology (Ankara, Turkey).* 26: 11-21 <https://doi.org/10.5152/dir.2019.19025>.
19. Tingelhoff, K., A.I. Moral, M.E. Kunkel, M. Rilk, I. Wagner, K.G. Eichhorn, F.M. Wahl, and F. Bootz (2007) Comparison between manual and semi-automatic segmentation of nasal cavity and paranasal sinuses from CT images. *Annu Int Conf IEEE Eng Med Biol Soc.* 2007: 5505-8 <https://doi.org/10.1109/iembs.2007.4353592>.
20. Sozzi, D., D. Gibelli, G. Canzi, A. Tagliaferri, L. Monticelli, A. Cappella, A. Bozzetti, and C. Sforza (2018) Assessing the precision of posttraumatic orbital reconstruction through "mirror" orbital superimposition: A novel approach for testing the anatomical accuracy. *J Craniomaxillofac Surg.* 46: 1258-1262 <https://doi.org/10.1016/j.jcms.2018.05.040>.

21. Morgan, N., A. Van Gerven, A. Smolders, K. de Faria Vasconcelos, H. Willems, and R. Jacobs (2022)Convolutional neural network for automatic maxillary sinus segmentation on cone-beam computed tomographic images.Scientific Reports. 12: 7523 [https://doi.org/ 10.1038/s41598-022-11483-3](https://doi.org/10.1038/s41598-022-11483-3).
22. Shujaat, S., O. Jazil, H. Willems, A. Van Gerven, E. Shaheen, C. Politis, and R. Jacobs (2021)Automatic segmentation of the pharyngeal airway space with convolutional neural network.Journal of Dentistry. 111: 103705 [https://doi.org/ https://doi.org/10.1016/j.jdent.2021.103705](https://doi.org/10.1016/j.jdent.2021.103705).
23. Verhelst, P.-J., A. Smolders, T. Beznik, J. Meewis, A. Vandemeulebroucke, E. Shaheen, A. Van Gerven, H. Willems, C. Politis, and R. Jacobs (2021)Layered deep learning for automatic mandibular segmentation in cone-beam computed tomography.Journal of Dentistry. 114: 103786 [https://doi.org/ https://doi.org/10.1016/j.jdent.2021.103786](https://doi.org/10.1016/j.jdent.2021.103786).
24. Preda, F., N. Morgan, A. Van Gerven, F. Nogueira-Reis, A. Smolders, X. Wang, S. Nomidis, E. Shaheen, H. Willems, and R. Jacobs (2022)Deep convolutional neural network-based automated segmentation of the maxillofacial complex from cone-beam computed tomography:A validation study.Journal of Dentistry. 124: 104238 [https://doi.org/ https://doi.org/10.1016/j.jdent.2022.104238](https://doi.org/10.1016/j.jdent.2022.104238).
25. Hopper, R.A., S. Salemy, and R.W. Sze (2006)Diagnosis of Midface Fractures with CT: What the Surgeon Needs to Know.RadioGraphics. 26: 783-793 [https://doi.org/ 10.1148/rg.263045710](https://doi.org/10.1148/rg.263045710).
26. Mehta, N., P. Butala, and M.P. Bernstein (2012)The imaging of maxillofacial trauma and its pertinence to surgical intervention.Radiol Clin North Am. 50: 43-57 [https://doi.org/ 10.1016/j.rcl.2011.08.005](https://doi.org/10.1016/j.rcl.2011.08.005).
27. An, S., J.Y. Lee, C.J. Chung, and K.H. Kim (2017)Comparison of different midsagittal plane configurations for evaluating craniofacial asymmetry by expert preference.Am J Orthod Dentofacial Orthop. 152: 788-797 [https://doi.org/ 10.1016/j.ajodo.2017.04.024](https://doi.org/10.1016/j.ajodo.2017.04.024).
28. Elkenawy, I., L. Fijany, O. Colak, N.A. Paredes, A. Gargoum, S. Abedini, D. Cantarella, R. Dominguez-Mompell, L. Sfogliano, and W. Moon (2020)An assessment of the magnitude, parallelism, and asymmetry of micro-implant-assisted rapid maxillary expansion in non-growing patients.Progress in orthodontics. 21: 42-42 [https://doi.org/ 10.1186/s40510-020-00342-4](https://doi.org/10.1186/s40510-020-00342-4).
29. Andrade, L.M., A.M.B. Rodrigues da Silva, L.V. Magri, and M.A.M. Rodrigues da Silva (2017)Repeatability Study of Angular and Linear Measurements on Facial Morphology Analysis by Means of Stereophotogrammetry.Journal of Craniofacial Surgery. 28.
30. Camison, L., M. Bykowski, W.W. Lee, J.C. Carlson, J. Roosenboom, J.A. Goldstein, J.E. Losee, and S.M. Weinberg (2018)Validation of the Vectra H1 portable three-dimensional photogrammetry system for facial imaging.Int J Oral Maxillofac Surg. 47: 403-410 [https://doi.org/ 10.1016/j.ijom.2017.08.008](https://doi.org/10.1016/j.ijom.2017.08.008).
31. Koo, T.K. and M.Y. Li (2016)A Guideline of Selecting and Reporting Intraclass Correlation Coefficients for Reliability Research.J Chiropr Med. 15: 155-63 [https://doi.org/ 10.1016/j.jcm.2016.02.012](https://doi.org/10.1016/j.jcm.2016.02.012).

32. Gateño, J., T.L. Jones, S.G.F. Shen, K.C. Chen, A. Jajoo, T. Kuang, J.D. English, M. Nicol, J.F. Teichgraber, and J.J. Xia (2018) Fluctuating asymmetry of the normal facial skeleton. *International Journal of Oral and Maxillofacial Surgery*. 47: 534-540 [https://doi.org/ 10.1016/j.ijom.2017.10.011](https://doi.org/10.1016/j.ijom.2017.10.011).
33. Graham, J.H., S. Raz, H. Hel-Or, and E. Nevo (2010) Fluctuating Asymmetry: Methods, Theory, and Applications. *Symmetry*. 2: 466-540.
34. Davies, J.C., H.H.L. Chan, Y. Jozaghi, D.P. Goldstein, and J.C. Irish (2019) Analysis of simulated mandibular reconstruction using a segmental mirroring technique. *J Craniomaxillofac Surg*. 47: 468-472 [https://doi.org/ 10.1016/j.jcms.2018.12.016](https://doi.org/10.1016/j.jcms.2018.12.016).
35. Jacobs, R., B. Salmon, M. Codari, B. Hassan, and M.M. Bornstein (2018) Cone beam computed tomography in implant dentistry: recommendations for clinical use. *BMC Oral Health*. 18: 88 [https://doi.org/ 10.1186/s12903-018-0523-5](https://doi.org/10.1186/s12903-018-0523-5).
36. Wang, L., K.C. Chen, Y. Gao, F. Shi, S. Liao, G. Li, S.G. Shen, J. Yan, P.K. Lee, B. Chow, N.X. Liu, J.J. Xia, and D. Shen (2014) Automated bone segmentation from dental CBCT images using patch-based sparse representation and convex optimization. *Med Phys*. 41: 043503 [https://doi.org/ 10.1118/1.4868455](https://doi.org/10.1118/1.4868455).
37. Mendoza, L.V., C. Bellot-Arcís, J.M. Montiel-Company, V. García-Sanz, J.M. Almerich-Silla, and V. Paredes-Gallardo (2018) Linear and Volumetric Mandibular Asymmetries in Adult Patients With Different Skeletal Classes and Vertical Patterns: A Cone-Beam Computed Tomography Study. *Scientific Reports*. 8: 12319 [https://doi.org/ 10.1038/s41598-018-30270-7](https://doi.org/10.1038/s41598-018-30270-7).
38. Thiesen, G., M.P.M. Freitas, E.A. Araújo, B.F. Gribel, and K.B. Kim (2018) Three-dimensional evaluation of craniofacial characteristics related to mandibular asymmetries in skeletal Class I patients. *Am J Orthod Dentofacial Orthop*. 154: 91-98 [https://doi.org/ 10.1016/j.ajodo.2017.10.031](https://doi.org/10.1016/j.ajodo.2017.10.031).
39. Thiesen, G., M.P.M. Freitas, B.F. Gribel, and K.B. Kim (2019) Comparison of maxillomandibular asymmetries in adult patients presenting different sagittal jaw relationships. *Dental Press J Orthod*. 24: 54-62 [https://doi.org/ 10.1590/2177-6709.24.4.054-062.oar](https://doi.org/10.1590/2177-6709.24.4.054-062.oar).
40. Duran, G.S., F. Dindaroğlu, and P. Kutlu (2019) Hard- and soft-tissue symmetry comparison in patients with Class III malocclusion. *Am J Orthod Dentofacial Orthop*. 155: 509-522 [https://doi.org/ 10.1016/j.ajodo.2018.05.021](https://doi.org/10.1016/j.ajodo.2018.05.021).
41. Hingsammer, L., T. Seier, J.P. Johnner, M. Blumer, T. Gander, M. Rücker, and M. Wagner (2020) Does Zygomatic Complex Symmetry Differ Between Healthy Individuals and Surgically Treated Patients Using Intraoperative 3-Dimensional Cone Beam Computed Tomographic Imaging? *J Oral Maxillofac Surg*. 78: 798.e1-798.e7 [https://doi.org/ 10.1016/j.joms.2019.11.027](https://doi.org/10.1016/j.joms.2019.11.027).
42. Ekrami, O., P. Claes, J.D. White, S.M. Weinberg, M.L. Marazita, S. Walsh, M.D. Shriver, and S. Van Dongen (2020) A Multivariate Approach to Determine the Dimensionality of Human Facial Asymmetry. *Symmetry*. 12 [https://doi.org/ 10.3390/sym12030348](https://doi.org/10.3390/sym12030348).

43. Carrao, V., Tofigh, M., Greenberg, A.M (2018) Virtual Surgical Planning for Orthognathic Surgery. In: Greenberg, A. (eds) Digital Technologies in Craniomaxillofacial Surgery. Springer, New York, NY, pp 117-155 https://doi.org/10.1007/978-1-4939-1532-3_6

Artificial intelligence-assisted evaluation of volumetric bone graft changes following maxillary sinus augmentation

Morgan N. ^{1,2}

Cortellini S. ^{3,4}

Shujaat S. ^{1,5}

Nogueira-Reis F. ⁶

Temmerman A. ^{3,4}

Quirynen M. ^{3,4}

Jacobs R. ^{1,7}

¹ OMFS IMPATH Research Group, Department of Imaging & Pathology, Faculty of Medicine, KU Leuven & Oral and Maxillofacial Surgery, University Hospitals Leuven, Kapucijnenvoer33, BE-3000 Leuven, Belgium

² Department of Oral Medicine, Faculty of Dentistry, Mansoura University, 35516 Mansoura, Dakahlia, Egypt

³ Department of Oral Health Sciences, Section of Periodontology, KU Leuven, Leuven, Belgium

⁴ Dentistry, University Hospitals, KU Leuven, Leuven, Belgium

⁵ Department of Maxillofacial Surgery and Diagnostic Sciences, College of Dentistry, King Saud Bin Abdulaziz University for Health Sciences, Riyadh, Saudi Arabia

⁶ Department of Oral Diagnosis, Division of Oral Radiology, Piracicaba Dental School, University of Campinas (UNICAMP), Av. Limeira 901, Piracicaba, São Paulo 13414-903, Brazil

⁷ Department of Dental Medicine, Karolinska Institutet, Box 4064, 141 04 Huddinge, Stockholm, Sweden

Currently submitted to Journal of clinical periodontology.

Abstract

Aim

The purpose of the study was to propose and validate an artificial intelligence (AI) assisted approach for quantifying volumetric bone graft changes on cone-beam computed tomography (CBCT) images following sinus augmentation.

Materials and methods

A total of 19 patients (9 males, 10 females; mean age: 57 yrs.) were recruited who underwent sinus augmentation (n = 24, 5 bilateral, 14 unilateral) using the lateral window sinus floor elevation technique. Twelve sinuses were filled with deproteinized bovine bone mineral (DBBM), while the other 12 sinuses with a Leukocyte and Platelet Rich Fibrin (L-PRF) block prepared by mixing DBBM (50%) and L-PRF (50%). All patients had preoperative (T0), immediate postoperative (T1) and 6 months postoperative (T2) CBCT images. Maxillary sinus was automatically segmented from T0 and registered T1, and T2 scans using an AI-based platform. The volumetric difference of the sinus at T0-T1 provided the bone gain following augmentation, while the T1-T2 difference revealed graft resorption at 6 months follow-up. The accuracy of segmentation and reproducibility of the technique were assessed using the relative technical error of measurement (rTEM) and intra-class correlation coefficient (ICC), respectively.

Results

Based on rTEM values, the methodology was found to be highly accurate (0.2% to 0.25%), and ICC revealed excellent inter- and intra-observer reliability, ranging from 0.98 to 0.99. The average bone graft volumetric gain was $2.11 \pm 1.25 \text{ cm}^3$ (DBBM: $2.23 \pm 1.43 \text{ cm}^3$, L-PRF block: $1.63 \pm 0.7 \text{ cm}^3$). At follow-up, minor bone resorption of 5.3% was observed, where DBBM showed slightly lower resorption (4.3%) compared to L-PRF block (6.3%) without any significant difference.

Conclusion

With the assistance of AI-based segmentation, the proposed methodology provides a reliable, accurate, and time-efficient method for evaluating volumetric bone graft changes following a sinus augmentation procedure. This methodology could lay a platform for further simplifying follow-up assessment protocols, where both time and accuracy are of the essence for clinicians and researchers.

Keywords: artificial intelligence, volume change, grafting materials, sinus floor elevation, CBCT.

1. Introduction

Placement of dental implants in the maxillary posterior region is a challenging task in patients with severe bone loss due to alveolar bone atrophy and maxillary sinus pneumatization. The presence of insufficient bone volume could adversely impact the short- and long-term stability of a dental implant and lead to implant failure. In such patients, maxillary sinus augmentation, also referred as sinus floor elevation, is one of the most common surgical procedures performed for creating sufficient bone volume to allow for either simultaneous or delayed implant placement with optimal stability and a high survival rate. The procedure involves lifting the Schneiderian membrane from the underlying sinus wall and insertion of a bone graft inferior to the membrane. The two main approaches for sinus floor elevation include, a direct approach with the lateral window technique and indirectly with transalveolar approach¹⁻³.

To date, various graft materials have been successfully used alone or in combination⁴ for sinus augmentation, which could be broadly classified as autograft⁵⁻⁸, allograft⁹⁻¹¹, xenograft¹²⁻¹⁵, and alloplastic graft¹⁶⁻¹⁸. These grafts undergo natural resorption at varying rates¹⁹ depending on the type of material and other anatomical factors such as sinus angle, pressure exerted by the intra-sinus air during sinus re-pneumatization, and sinus width²⁰. This subsequent resorption could significantly impact the success of implant treatment outcome. Hence, an accurate quantification of the volumetric graft resorption is essential for ensuring that sufficient dimensional stability is maintained for facilitating the long-term success of implants.

Two-dimensional radiographic imaging, such as panoramic and periapical radiography, has been majorly applied for assessing graft dimensional changes over time²¹⁻²⁵. However, it has certain inherent limitations, such as image magnification, distortion, patient positioning error, and structural superimposition. All of which contribute towards a large margin of error, unreliable measurements, and the failure to provide information related to the third dimension. Owing to these limitations, 3D CBCT^{21,26,27} has become the radiographic standard for sinus lift treatment planning and follow-up of graft changes and resorption through the assessment of sinus volumetric differences²⁸⁻³¹. The CBCT images rely mostly on manual or semi-automatic segmentation algorithms for creating 3D surface-rendered volumetric models, which are then used to quantify the changes at follow-up. These segmentation processes either carry a high risk of observer variability, dependency on third-party software programs whose threshold leveling is standardized based on CT images rather than CBCT images, a requirement of manual post-processing or excessive time-consumption.

Recently, artificial intelligence (AI)-based convolutional neural networks (CNNs), a multilayer structure-learning algorithm have been applied for automated segmentation of maxillary sinus with outstanding performances³². However, these networks still need to be applied for assessing graft changes following sinus augmentation. We hypothesize that the application of AI for segmentation could not only overcome the limitations associated with other protocols for achieving a precise and consistent outcome but also lay a platform towards simplification of the digital workflow for graft follow-up assessment. Hence, the following study aimed to introduce and validate an AI-assisted approach for quantifying volumetric bone graft changes on cone-beam computed tomography (CBCT) images following sinus augmentation.

2. Material and methods

This retrospective pilot study was conducted in compliance with the World Medical Association Declaration of Helsinki on medical research. Ethical approval was obtained from the Ethical Review Board of the University Hospitals of Leuven, Belgium (reference number: S66689). Informed consent was not required as patient-specific information was anonymized.

2.1 Patients and radiographic examination

A total of 19 patients (9 males, 10 females; mean age: 57 yrs.) were recruited who underwent sinus augmentation procedures (n = 24, 5 bilateral, 14 unilateral) at the Department of Periodontology and Oral Microbiology, KU Leuven, Leuven, Belgium. Out of these, 16 sinus augmentation procedures presented with all missing posterior teeth, while the remaining 8 sinuses required rehabilitation of only the first molar region. Inclusion criteria were adult patients in whom lateral approach was indicated with delayed implant placement and the presence of preoperative (T0), immediate postoperative (T1), and 6 months postoperative (T2) CBCT scans. Exclusion criteria involved patients with immediate implant placement and scans having motion artifacts and/or insufficient coverage of the grafted region.

The total CBCT dataset consisted of 57 scans (T0: 19, T1: 19, T2: 19). All scans were acquired using NewTom VGI Evo® (QR, Verona, Italy) with scanning parameters of 0.3-0.15 mm voxel size, 8x5-10x10 field of view, 110 kV, and 3.4 mA. The scans were saved in Digital Imaging and Communications in Medicine (DICOM) format for further processing.

2.2 Surgical procedures

All surgical procedures were performed using the lateral window sinus floor elevation procedure by a single surgeon. Following delivery of local anesthesia (articaine hydrochloride 4% with adrenaline 1:100 000), a crestal incision was performed and a mucoperiosteal flap was raised. The lateral window was prepared using piezosurgery (Piezotome II™, Acteon, Merignac, France) and the Schneiderian membrane was detached from the sinus walls using hand instruments. Thereafter, trapdoor osteotomy was applied, where the superior osteotomy cut remained partially incomplete and the lateral window was rotated and pushed in an inward direction. Out of the total sinus augmentations, 12 were filled using deproteinized bovine bone mineral (DBBM; 0.25–1.0 mm particulate, 0.5 g; BioOss™, Geistlich®, Wolhusen, Switzerland), while the other 12 were filled with Leukocyte and Platelet Rich Fibrin (L-PRF) block prepared by mixing DBBM (50%) and L-PRF (50%).

2.3 Volumetric analysis

The DICOM files of CBCT datasets were imported into Amira software (version 2021.2, Thermo Fischer Scientific, Merignac, France), where voxel-based registration was applied to align and superimpose T1 and T2 scans onto the T0 scan. This allowed to bring the images in the same 3D space and standardize the superior limit of the sinuses at T1 and T2 time-points at the same level of T0 scan (Figure 1). The T0 and registered T1 and T2 DICOM datasets were then imported to an online cloud-based AI system, known as ‘Virtual Patient Creator’ (Relu BV, Leuven, Belgium), where automated segmentation of the maxillary sinus was performed and saved in standard tessellation language (STL) format (Figure 2). The CNN framework of this task was configured based on multiple 3D U-Net models and standardized based on CBCT datasets, which has been previously described and validated.

The STL files of sinus segmentations were then imported into Mimics Innovation Suite (version 23.0, Materialise N.V., Leuven, Belgium) for checking the visual quality of the segmentation, and refinements were performed if required. The software automatically generated the sinus volume at T0, T1, and T2 time-points. The graft volume was calculated as suggested by prior studies, where T0-T1 volumetric difference revealed the graft volume represented as bone gain and T1-T2 difference provided with the graft resorption at 6 months follow-up. Figure 3 illustrates the contours of the segmented sinus on CBCT images to visualize bone gain and resorption. Two maxillofacial radiologists with an experience of over 5 years (NM & FNR) performed the assessment independently and repeated the observations at an interval of 2 weeks for calculating the intra- and inter-observer reliability.

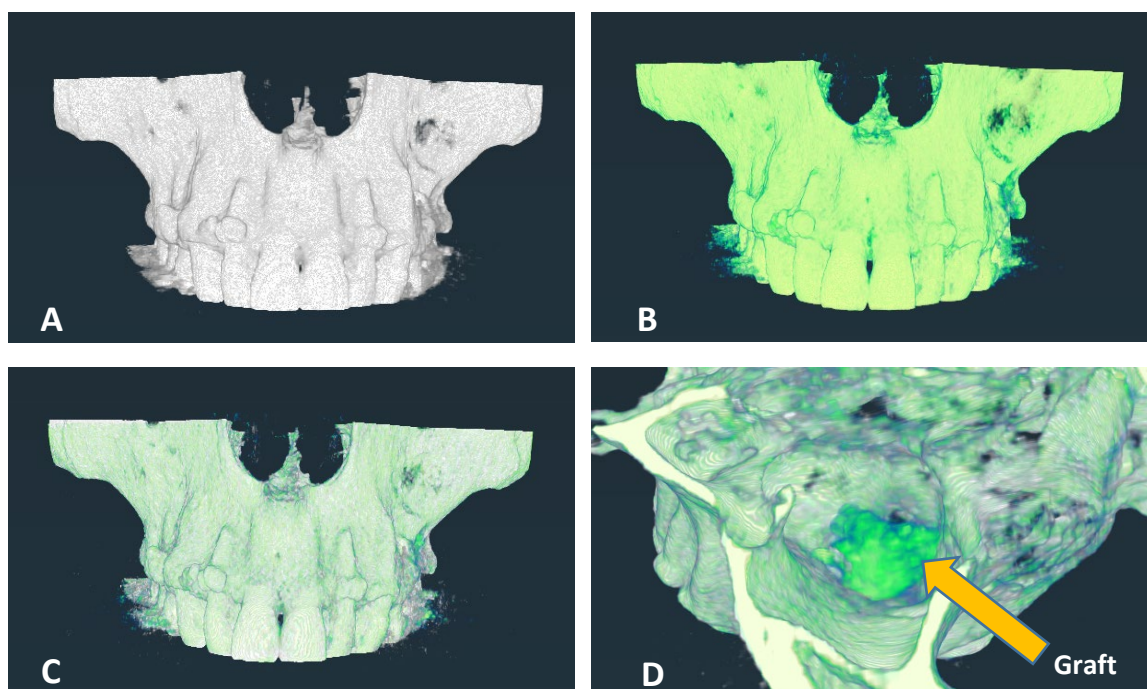


Figure 1. Voxel-based superimposition of cone-beam computed tomographic images. A. preoperative image (grey), B. immediate postoperative image (green), C. superimposed preoperative and immediate postoperative image, D. superior view showing bone graft on superimposed images.

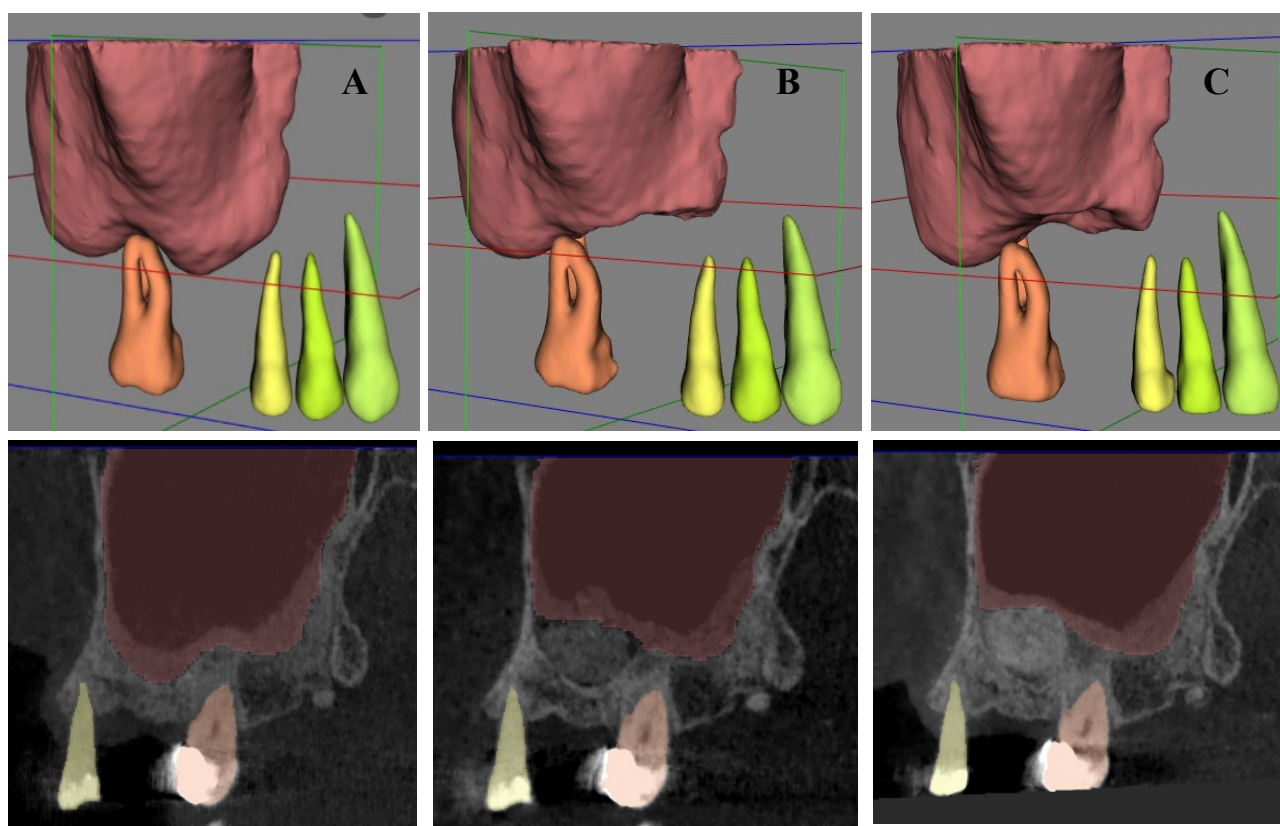


Figure 2. Automated segmentation of maxillary sinus on cone-beam computed tomographic images. A. preoperative image, B. immediate postoperative image, C. 6 months postoperative image.

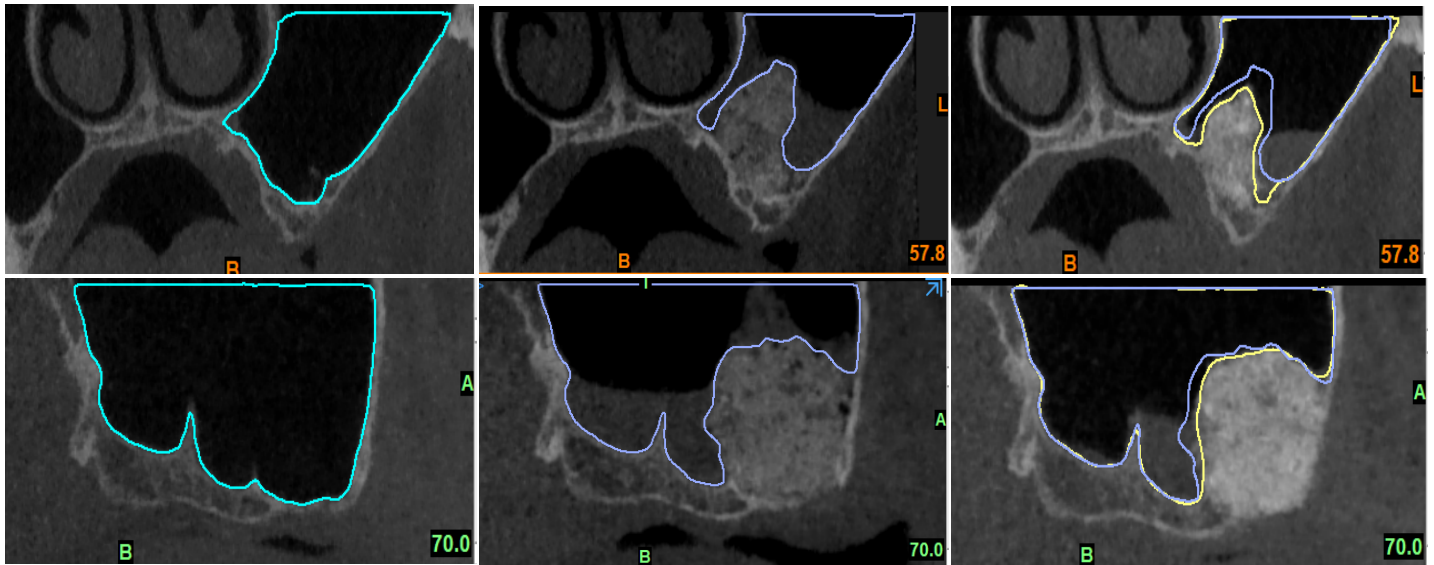


Figure 3. 3D maxillary sinus model contours on coronal and sagittal views of cone-beam computed tomographic images. A. preoperative image, B) immediate postoperative view (blue) showing sinus changes represented by bone gain following sinus augmentation, C. superimposed immediate (blue) and 6 months postoperative view (yellow) showing sinus changes represented by bone resorption.

2.4 Statistical analysis

Data were analyzed using IBM SPSS Statistics for Windows (version 21.0, IBM Corp., Armonk, NY, USA). The Shapiro–Wilk test and Levene’s test were conducted to assess data normality and homoscedasticity, respectively. The mean and standard deviation values were calculated for all the data. The accuracy of segmentation was assessed through calculation of relative technical error of measurement (rTEM) according to the scale proposed by Camison et al³³, based on which, <1% = excellent, 1–3.9% = very good, 4–6.9% = good, 7–9.9% = moderate, >10% = poor. Intra-Class Correlation Coefficient (ICC) was applied at a 95% confidence interval for assessing the inter- and intra- observer reliability of the methodology, where <0.50 = poor reliability; 0.50–0.75 = moderate reliability; 0.75–0.90 = good reliability; >0.90 = excellent reliability³⁴. One-way analysis of variance (ANOVA) was applied for assessing volumetric differences at T0-T1 and T1-T2 time intervals. A p-value of <0.05 was considered as statistically significant.

3. Results

Visual inspection of the automated segmentations revealed that no refinements were required for T0 models, while minor refinements were required for T1 and T2 models. Overall, the rTEM values were classified as excellent, ranging from 0.2% to 0.25%. In relation to the reproducibility of the methodology, both inter- and intra-observer ICC revealed excellent reliability for assessing volumetric differences at T0-T1 (intra-observer ICC: 0.99; inter-observer ICC: 0.98) and T1-T2 (intra-observer ICC: 0.99; inter-observer ICC: 0.98). **Figure 4** illustrates the variation in volumetric measurements for both observers at all time points. The findings showed an average sinus volume of $7.77 \pm 2.69 \text{ cm}^3$ at T0, $5.66 \pm 1.74 \text{ cm}^3$ at T1, and 5.78 ± 1.79 at T2.

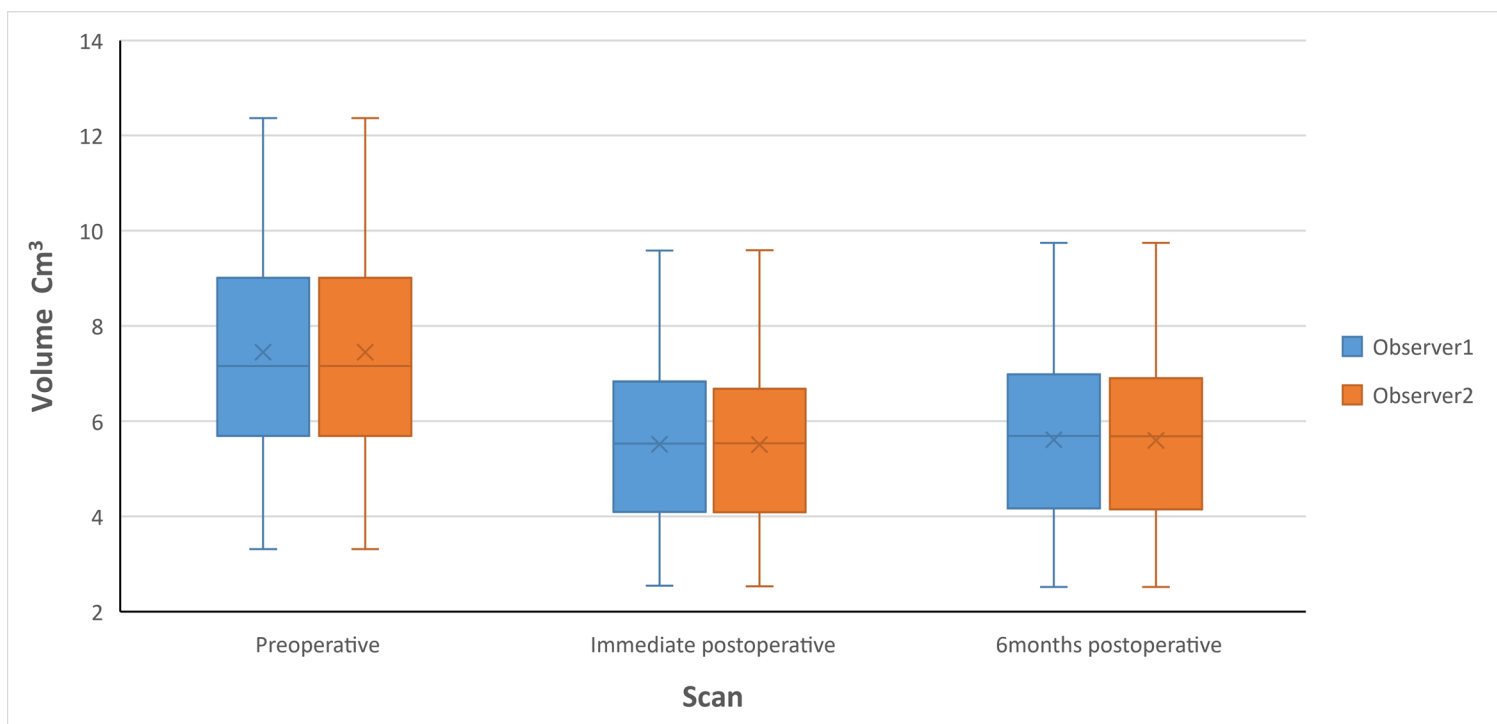


Figure 4. Variation in volumetric measurements for both observers at all time-points.

Table 1 describes the average bone gain (T0-T1) immediately after graft insertion and resorption at 6 months (T1-T2). The average volumetric bone gain was $2.11 \pm 1.25 \text{ cm}^3$ (DBBM: $2.23 \pm 1.43 \text{ cm}^3$, L-PRF block: $1.63 \pm 0.7 \text{ cm}^3$). At follow-up of 6 months, minor bone resorption of 5.3% was observed ($0.11 \pm 0.13 \text{ cm}^3$), where DBBM showed slightly lower resorption (4.3%) compared to L-PRF block (6.3%). The minimum and maximum resorption rates were 0.03 cm^3 (1.4%) and 0.4 cm^3 (14%), respectively. A significant volumetric difference existed between T0 and T1 ($p = 0.025$), whereas no significant difference was found at the T1-T2 interval ($p = 0.989$).

Table 1: Overview of average graft volume and graft remodeling.

Graft Material	Bone gain (Cm ³)	Bone change (Cm ³)
	2.11±1.25	0.11±0.13
Overall (mean ± SD)		
Bio-Oss (mean ± SD)	2.23±1.43	0.09±0.16
L-PRF block (mean ± SD)	1.63±0.7	0,1±0.1

4. Discussion

Three-dimensional post-surgical evaluation of the bone graft following sinus augmentation is essential for ensuring its optimal stability and a high success rate of implant treatment. Furthermore, the application of CNN-based AI models could further improve and simplify the follow-up assessment methodologies. Hence, the present study investigated the feasibility of applying AI-based automated segmentation for the volumetric assessment of bone graft resorption following sinus augmentation in the essence of improving the standard of follow-up assessment protocols.

The findings suggested that minor segmentation refinements were required, and the methodology offered a very small relative technical error and excellent observer reliability. These findings support the fact that automated segmentation has the ability to overcome limitations associated with both manual and semi-automatic segmentation software programs in terms of observer variability, human error, and time-consumption. Unlike these programs, the proposed segmentation approach was time-efficient (bilateral sinus segmentation: 24 seconds per scan) with 100% consistency, which meant that the AI platform was able to generate a similar segmented model independent of the number or experience of observers.

In the present study, the segmented maxillary sinus volumetric differences were used to assess the graft volume instead of directly segmenting the grafted bone. Even though previous studies^{35,36} have found manual segmentation of the graft on CBCT images to be accurate, the disadvantage of excessive time consumption for outlining the graft and dependency on observer experience cannot be ignored. It is also difficult to distinguish the graft from the host bone, especially following the healing period²⁶. Furthermore, semi-automatic graft segmentation^{28,37} has been proposed as an alternative solution. However, the outcome based on segmented model was negatively impacted as the selected threshold level for segmentation caused either over- or under-estimation²⁶ of the graft model and inaccurate volumetric representation due to the presence of neighboring bone with similar density.

Hence, relying on maxillary sinus segmentation and reflecting its volumetric changes to graft changes could offer a more standardized approach.

Based on the grafting material, autogenously derived bone has been regarded as the gold standard in sinus augmentation material. However, due to several limitations such as post-surgical complications at the donor site and increased risk of resorption and volume loss, other substitutes have been developed. Amongst these, DBBM, a well-known example of xenograft has been widely used for sinus augmentation due to its osteoconductive properties, angiogenesis enhancement, and bone neoformation³⁸⁻⁴¹. Several studies have reported successful clinical and histological outcomes⁴²⁻⁴⁴ while using it as a single graft material⁴⁵⁻⁴⁷. In addition, some studies^{48,49} have concluded that mixing L-PRF, an autogenous biomaterial,^{50,51} with DBBM might enhance bone regeneration and osseointegration. Our findings showed that the average resorption of DBBM was 4.3%, which was in accordance with the prior evidence. Lee et al.⁵² and Mazzocco et al.³⁷, reported graft volume contraction of 8% and 10% at follow-up of 6 months and 8-9 months, respectively. These findings confirm the slow resorption properties of DBBM and its ability to be used solely⁵³. The slight difference in bone resorption percentage compared to the aforementioned studies might be attributed to the differences in imaging modality, scanning parameters, methodology, sample size, and/or the follow-up duration. In contrast to our findings, Klein et al²⁸ found an increase of 9.1% in bone volume measured 8 months after the surgery. They justified their finding by pointing out the broad range of thresholds that could neglect some hyperdense particles of DBBM.

In cases treated with L-PRF/DBBM mixture, the resorption rate was comparable to that of DBBM alone without any significant difference. The selected ratio of the mixture was 50:50 which has been previously proven to be efficient for bone augmentation procedures⁵⁴. However, the addition of L-PRF did not impact the resorptive capacity of DBBM at 6 months which might be due to the fact that the bone substitute volume per tissue volume was similar for both types of augmentations. Only two studies^{55,56} were found investigating the application of L-PRF/DBBM mixture for sinus augmentation, which focused only on histological and histomorphometric comparisons and no studies existed assessing the radiographic changes. Hence, comparison with existing evidence was deemed difficult. Although 6 months follow-up period is considered sufficient for graft healing to support delayed implant⁵⁷⁻⁵⁹, it is necessary to quantify long-term volumetric graft resorption in future studies.

It is worth noting that several factors could impact the volumetric differences, such as: preoperative bone quality and quantity, physicochemical variation in sinus pneumatization, re-pneumatization, surgical technique, Schneiderian membrane reflection, graft condensation, and graft material properties²⁹. Furthermore, the graft material remodeling and resorption pattern have also been correlated to the features of the recipient region, such as volume of the recipient region, graft

thickness, surface area of the graft in contact with the basal bone and its projection into the sinus cavity⁶⁰. Hence, all these factors need to be considered in future prospective studies to reach a better conclusion.

The study had certain limitations. Firstly, the findings and statistical inferences of the present study should be interpreted with caution due to the limited sample size, and a follow-up period of 6 months might not be adequate for reaching a clinically-oriented outcome. However, the sample was enough for validating the methodology. Secondly, the grafted bone resorption was assessed without implant placement. Future studies with a large sample size and longer follow-up are required to assess if the graft remains stable over time and to investigate the impact of different implant placement protocols on bone resorption. It is also recommended to train AI-based models to automatically extract and segment bone grafts from CBCT images to further enhance the efficacy of the follow-up assessment protocols.

5. Conclusion

The proposed methodology proved to be reliable, accurate, and consistent for performing volumetric assessment of grafted bone changes with the assistance of automated AI-based sinus segmentation. It could provide a promising, simplified solution for clinicians to assess sinus augmentation outcomes and provide better insight into the 3D resorption phenomenon. This would further improve surgical outcomes and facilitate patient-specific planning. As for the amount of bone resorption, it was minimal at 6 months follow-up for both DBBM and DBBM/ L-PRF mixture. Future prospective studies are warranted to investigate both short- and long-term volumetric stability of different grafting materials.

References

1. Boyne, P. J. & James, R. A. Grafting of the maxillary sinus floor with autogenous marrow and bone. *J Oral Surg* **38**, 613-616 (1980).
2. Caudry, S. & Landzberg, M. Lateral window sinus elevation technique: managing challenges and complications. *J Can Dent Assoc* **79**, d101 (2013).
3. Tatum, H., Jr. Maxillary and sinus implant reconstructions. *Dent Clin North Am* **30**, 207-229 (1986).
4. Rickert, D., Slater, J. J., Meijer, H. J., Vissink, A. & Raghoobar, G. M. Maxillary sinus lift with solely autogenous bone compared to a combination of autogenous bone and growth factors or (solely) bone substitutes. A systematic review. *Int J Oral Maxillofac Surg* **41**, 160-167, doi:10.1016/j.ijom.2011.10.001 (2012).
5. Johansson, L. A., Isaksson, S., Lindh, C., Becktor, J. P. & Sennerby, L. Maxillary sinus floor augmentation and simultaneous implant placement using locally harvested autogenous bone chips and bone debris: a prospective clinical study. *J Oral Maxillofac Surg* **68**, 837-844, doi:10.1016/j.joms.2009.07.093 (2010).
6. Klijn, R. J., Meijer, G. J., Bronkhorst, E. M. & Jansen, J. A. A meta-analysis of histomorphometric results and graft healing time of various biomaterials compared to autologous bone used as sinus floor augmentation material in humans. *Tissue Eng Part B Rev* **16**, 493-507, doi:10.1089/ten.TEB.2010.0035 (2010).
7. Nkenke, E. & Stelzle, F. Clinical outcomes of sinus floor augmentation for implant placement using autogenous bone or bone substitutes: a systematic review. *Clin Oral Implants Res* **20 Suppl 4**, 124-133, doi:10.1111/j.1600-0501.2009.01776.x (2009).
8. Schmitt, C. M. *et al.* Histological results after maxillary sinus augmentation with Straumann® BoneCeramic, Bio-Oss®, Puros®, and autologous bone. A randomized controlled clinical trial. *Clin Oral Implants Res* **24**, 576-585, doi:10.1111/j.1600-0501.2012.02431.x (2013).
9. Annibali, S. *et al.* Human maxillary sinuses augmented with mineralized, solvent-dehydrated bone allograft: a longitudinal case series. *Implant Dent* **20**, 445-454, doi:10.1097/ID.0b013e31823420a4 (2011).
10. Bavetta, G. & Licata, M. E. The use of human allogenic graft (HBA) for maxillary bone regeneration: review of literature and case reports. *Curr Pharm Des* **18**, 5559-5568, doi:10.2174/138161212803307572 (2012).
11. Irinakis, T. Efficacy of injectable demineralized bone matrix as graft material during sinus elevation surgery with simultaneous implant placement in the posterior maxilla: clinical evaluation of 49 sinuses. *J Oral Maxillofac Surg* **69**, 134-141, doi:10.1016/j.joms.2010.07.028 (2011).

12. Özkan, Y., Akoğlu, B. & Kulak-Özkan, Y. Maxillary sinus floor augmentation using bovine bone grafts with simultaneous implant placement: a 5-year prospective follow-up study. *Implant Dent* **20**, 455-459, doi:10.1097/ID.0b013e3182386cbc (2011).
13. Scarano, A., Piattelli, A., Perrotti, V., Manzon, L. & Iezzi, G. Maxillary sinus augmentation in humans using cortical porcine bone: a histological and histomorphometrical evaluation after 4 and 6 months. *Clin Implant Dent Relat Res* **13**, 13-18, doi:10.1111/j.1708-8208.2009.00176.x (2011).
14. Sivoilella, S., Bressan, E., Gnocco, E., Berengo, M. & Favero, G. A. Maxillary sinus augmentation with bovine bone and simultaneous dental implant placement in conditions of severe alveolar atrophy: a retrospective analysis of a consecutively treated case series. *Quintessence Int* **42**, 851-862 (2011).
15. Testori, T. *et al.* High temperature-treated bovine porous hydroxyapatite in sinus augmentation procedures: a case report. *Int J Periodontics Restorative Dent* **32**, 295-301 (2012).
16. Boyne, P. J. *et al.* De novo bone induction by recombinant human bone morphogenetic protein-2 (rhBMP-2) in maxillary sinus floor augmentation. *J Oral Maxillofac Surg* **63**, 1693-1707, doi:10.1016/j.joms.2005.08.018 (2005).
17. Laurencin, C., Khan, Y. & El-Amin, S. F. Bone graft substitutes. *Expert Rev Med Devices* **3**, 49-57, doi:10.1586/17434440.3.1.49 (2006).
18. Triplett, R. G. *et al.* Pivotal, randomized, parallel evaluation of recombinant human bone morphogenetic protein-2/absorbable collagen sponge and autogenous bone graft for maxillary sinus floor augmentation. *J Oral Maxillofac Surg* **67**, 1947-1960, doi:10.1016/j.joms.2009.04.085 (2009).
19. Hatano, N., Shimizu, Y. & Ooya, K. A clinical long-term radiographic evaluation of graft height changes after maxillary sinus floor augmentation with a 2:1 autogenous bone/xenograft mixture and simultaneous placement of dental implants. *Clin Oral Implants Res* **15**, 339-345, doi:10.1111/j.1600-0501.2004.00996.x (2004).
20. Hürzeler, M. B., Kirsch, A., Ackermann, K. L. & Quiñones, C. R. Reconstruction of the severely resorbed maxilla with dental implants in the augmented maxillary sinus: a 5-year clinical investigation. *Int J Oral Maxillofac Implants* **11**, 466-475 (1996).
21. Hallman, M., Hedin, M., Sennerby, L. & Lundgren, S. A prospective 1-year clinical and radiographic study of implants placed after maxillary sinus floor augmentation with bovine hydroxyapatite and autogenous bone. *J Oral Maxillofac Surg* **60**, 277-284; discussion 285-276, doi:10.1053/joms.2002.30576 (2002).
22. Szabó, G. *et al.* A prospective multicenter randomized clinical trial of autogenous bone versus beta-tricalcium phosphate graft alone for bilateral sinus elevation: histologic and histomorphometric evaluation. *Int J Oral Maxillofac Implants* **20**, 371-381 (2005).

23. Ozyuvaci, H., Bilgiç, B. & Firatli, E. Radiologic and histomorphometric evaluation of maxillary sinus grafting with alloplastic graft materials. *J Periodontol* **74**, 909-915, doi:10.1902/jop.2003.74.6.909 (2003).
24. Reinert, S., König, S., Bremerich, A., Eufinger, H. & Krimmel, M. Stability of bone grafting and placement of implants in the severely atrophic maxilla. *Br J Oral Maxillofac Surg* **41**, 249-255, doi:10.1016/s0266-4356(03)00078-0 (2003).
25. Diss, A., Dohan, D. M., Mouhyi, J. & Mahler, P. Osteotome sinus floor elevation using Choukroun's platelet-rich fibrin as grafting material: a 1-year prospective pilot study with microthreaded implants. *Oral Surg Oral Med Oral Pathol Oral Radiol Endod* **105**, 572-579, doi:10.1016/j.tripleo.2007.08.021 (2008).
26. Dellavia, C., Speroni, S., Pellegrini, G., Gatto, A. & Maiorana, C. A new method to evaluate volumetric changes in sinus augmentation procedure. *Clin Implant Dent Relat Res* **16**, 684-690, doi:10.1111/cid.12058 (2014).
27. Klijn, R. J., Meijer, G. J., Bronkhorst, E. M. & Jansen, J. A. Sinus floor augmentation surgery using autologous bone grafts from various donor sites: a meta-analysis of the total bone volume. *Tissue Eng Part B Rev* **16**, 295-303, doi:10.1089/ten.TEB.2009.0558 (2010).
28. Klein, G. G. *et al.* Bone Volume Changes After Sinus Floor Augmentation with Heterogenous Graft. *Int J Oral Maxillofac Implants* **31**, 665-671, doi:10.11607/jomi.3948 (2016).
29. Berberi, A. *et al.* Evaluation of Three-Dimensional Volumetric Changes After Sinus Floor Augmentation with Mineralized Cortical Bone Allograft. *J Maxillofac Oral Surg* **14**, 624-629, doi:10.1007/s12663-014-0736-3 (2015).
30. Kim, E. S., Moon, S. Y., Kim, S. G., Park, H. C. & Oh, J. S. Three-dimensional volumetric analysis after sinus grafts. *Implant Dent* **22**, 170-174, doi:10.1097/ID.0b013e31827f3576 (2013).
31. Temmerman, A. *et al.* Volumetric changes of grafted volumes and the Schneiderian membrane after transcresal and lateral sinus floor elevation procedures: A clinical, pilot study. *J Clin Periodontol* **44**, 660-671, doi:10.1111/jcpe.12728 (2017).
32. Morgan, N. *et al.* Convolutional neural network for automatic maxillary sinus segmentation on cone-beam computed tomographic images. *Sci Rep* **12**, 7523, doi:10.1038/s41598-022-11483-3 (2022).
33. Camison, L. *et al.* Validation of the Vectra H1 portable three-dimensional photogrammetry system for facial imaging. *Int J Oral Maxillofac Surg* **47**, 403-410, doi:10.1016/j.ijom.2017.08.008 (2018).
34. Koo, T. K. & Li, M. Y. A Guideline of Selecting and Reporting Intraclass Correlation Coefficients for Reliability Research. *J Chiropr Med* **15**, 155-163, doi:10.1016/j.jcm.2016.02.012 (2016).
35. Kirmeier, R. *et al.* Evaluation of three-dimensional changes after sinus floor augmentation with different grafting materials. *Clin Oral Implants Res* **19**, 366-372, doi:10.1111/j.1600-0501.2007.01487.x (2008).

36. Klijn, R. J. *et al.* Predictive value of ridge dimensions on autologous bone graft resorption in staged maxillary sinus augmentation surgery using Cone-Beam CT. *Clin Oral Implants Res* **23**, 409-415, doi:10.1111/j.1600-0501.2011.02342.x (2012).
37. Mazzocco, F. *et al.* Three-dimensional volume change of grafted bone in the maxillary sinus. *Int J Oral Maxillofac Implants* **29**, 178-184, doi:10.11607/jomi.3236 (2014).
38. Testori, T. *et al.* Effect of xenograft (ABBM) particle size on vital bone formation following maxillary sinus augmentation: a multicenter, randomized, controlled, clinical histomorphometric trial. *Int J Periodontics Restorative Dent* **33**, 467-475, doi:10.11607/prd.1423 (2013).
39. Dos Anjos, T. L. *et al.* Implant stability after sinus floor augmentation with deproteinized bovine bone mineral particles of different sizes: a prospective, randomized and controlled split-mouth clinical trial. *Int J Oral Maxillofac Surg* **45**, 1556-1563, doi:10.1016/j.ijom.2016.09.004 (2016).
40. de Molon, R. S. *et al.* A randomized clinical trial evaluating maxillary sinus augmentation with different particle sizes of demineralized bovine bone mineral: histological and immunohistochemical analysis. *International Journal of Oral and Maxillofacial Surgery* **48**, 810-823, doi:<https://doi.org/10.1016/j.ijom.2018.09.003> (2019).
41. Chackartchi, T. *et al.* Sinus floor augmentation using large (1-2 mm) or small (0.25-1 mm) bovine bone mineral particles: a prospective, intra-individual controlled clinical, micro-computerized tomography and histomorphometric study. *Clin Oral Implants Res* **22**, 473-480, doi:10.1111/j.1600-0501.2010.02032.x (2011).
42. Fickl, S. *et al.* Dimensional Evaluation of Different Ridge Preservation Techniques: A Randomized Clinical Study. *Int J Periodontics Restorative Dent* **37**, 403-410, doi:10.11607/prd.2629 (2017).
43. Kuchler, U. *et al.* DBBM shows no signs of resorption under inflammatory conditions. An experimental study in the mouse calvaria. *Clin Oral Implants Res* **31**, 10-17, doi:10.1111/clr.13538 (2020).
44. Kuchler, U. *et al.* Impact of DBBM Fragments on the Porosity of the Calvarial Bone: A Pilot Study on Mice. *Materials (Basel)* **13**, doi:10.3390/ma13214748 (2020).
45. Corbella, S., Taschieri, S., Weinstein, R. & Del Fabbro, M. Histomorphometric outcomes after lateral sinus floor elevation procedure: a systematic review of the literature and meta-analysis. *Clin Oral Implants Res* **27**, 1106-1122, doi:10.1111/clr.12702 (2016).
46. Browaeys, H., Bouvry, P. & De Bruyn, H. A literature review on biomaterials in sinus augmentation procedures. *Clin Implant Dent Relat Res* **9**, 166-177, doi:10.1111/j.1708-8208.2007.00050.x (2007).
47. Jensen, T., Schou, S., Stavropoulos, A., Terheyden, H. & Holmstrup, P. Maxillary sinus floor augmentation with Bio-Oss or Bio-Oss mixed with autogenous bone as graft: a systematic review. *Clin Oral Implants Res* **23**, 263-273, doi:10.1111/j.1600-0501.2011.02168.x (2012).

48. Castro, A. B. *et al.* Regenerative potential of leucocyte- and platelet-rich fibrin. Part B: sinus floor elevation, alveolar ridge preservation and implant therapy. A systematic review. *J Clin Periodontol* **44**, 225-234, doi:10.1111/jcpe.12658 (2017).
49. Oliveira, M. R. *et al.* Influence of the association between platelet-rich fibrin and bovine bone on bone regeneration. A histomorphometric study in the calvaria of rats. *Int J Oral Maxillofac Surg* **44**, 649-655, doi:10.1016/j.ijom.2014.12.005 (2015).
50. Dohan Ehrenfest, D. M. *et al.* Classification of platelet concentrates (Platelet-Rich Plasma-PRP, Platelet-Rich Fibrin-PRF) for topical and infiltrative use in orthopedic and sports medicine: current consensus, clinical implications and perspectives. *Muscles Ligaments Tendons J* **4**, 3-9 (2014).
51. Fujioka-Kobayashi, M. *et al.* Optimized Platelet-Rich Fibrin With the Low-Speed Concept: Growth Factor Release, Biocompatibility, and Cellular Response. *J Periodontol* **88**, 112-121, doi:10.1902/jop.2016.160443 (2017).
52. Lee, J. S., Shin, H. K., Yun, J. H. & Cho, K. S. Randomized Clinical Trial of Maxillary Sinus Grafting using Deproteinized Porcine and Bovine Bone Mineral. *Clin Implant Dent Relat Res* **19**, 140-150, doi:10.1111/cid.12430 (2017).
53. Galindo-Moreno, P. *et al.* Slow resorption of anorganic bovine bone by osteoclasts in maxillary sinus augmentation. *Clin Implant Dent Relat Res* **15**, 858-866, doi:10.1111/j.1708-8208.2012.00445.x (2013).
54. Cortellini, S. *et al.* Leucocyte- and platelet-rich fibrin block for bone augmentation procedure: A proof-of-concept study. *J Clin Periodontol* **45**, 624-634, doi:10.1111/jcpe.12877 (2018).
55. Zhang, Y. *et al.* Effects of Choukroun's platelet-rich fibrin on bone regeneration in combination with deproteinized bovine bone mineral in maxillary sinus augmentation: a histological and histomorphometric study. *J Craniomaxillofac Surg* **40**, 321-328, doi:10.1016/j.jcms.2011.04.020 (2012).
56. Nizam, N., Eren, G., Akcalı, A. & Donos, N. Maxillary sinus augmentation with leukocyte and platelet-rich fibrin and deproteinized bovine bone mineral: A split-mouth histological and histomorphometric study. *Clinical Oral Implants Research* **29**, 67-75, doi:<https://doi.org/10.1111/clr.13044> (2018).
57. Wood, G. A. Osseointegration and Autogenous Onlay Bone Grafts: Reconstruction of the Edentulous Atrophic Maxilla: Per-Ingvar Branemark, Kerstin Grondahl and Philip Worthington. Quintessence Books, 2001. Price £84, 160 pp. 359 illustrations. ISBN 0-86715-398-9 (Hardback). *British Journal of Oral and Maxillofacial Surgery* **40**, 352-353, doi:10.1016/S0266-4356(02)00118-3 (2002).
58. Chrcanovic, B. R., Albrektsson, T. & Wennerberg, A. Reasons for failures of oral implants. *J Oral Rehabil* **41**, 443-476, doi:10.1111/joor.12157 (2014).

59. Borges, F. L. *et al.* Simultaneous sinus membrane elevation and dental implant placement without bone graft: a 6-month follow-up study. *J Periodontol* **82**, 403-412, doi:10.1902/jop.2010.100343 (2011).
60. Sbordone, C. *et al.* Volume Changes of Grafted Autogenous Bone in Sinus Augmentation Procedure. *Journal of Oral and Maxillofacial Surgery* **69**, 1633-1641, doi:<https://doi.org/10.1016/j.joms.2010.12.004> (2011).

General discussion, conclusions, and future perspectives

Morgan N.^{1,2}

¹OMFS-IMPATh Research Group, Department of Imaging and Pathology, Faculty of Medicine, KU Leuven, and Department of Oral and Maxillofacial Surgery, University Hospitals Leuven, Leuven, Belgium.

²Department of Oral Medicine, Faculty of Dentistry, Mansoura University, Mansoura, Dakahlia, Egypt.

General discussion

Accurate segmentation of midfacial structures such as skeletal structures and the maxillary sinus, is a prerequisite in the majority of dentomaxillofacial workflows for creating a 3D virtual model. The main clinical applications where the midfacial virtual skeletal model is utilized include diagnostics, treatment planning, and follow-up evaluation of orthodontic treatment and reconstructive surgical procedures¹⁻⁵. In addition, virtual modeling of the maxillary sinus is beneficial for presurgical planning of surgical tooth extraction, implant placement, sinus augmentation^{6, 7}, and reconstructive surgical procedures⁸.

When considering the segmentation process, automatization of this task through the integration of CNN-based models is an important factor to consider for overcoming the inherent limitations associated with manual or semi-automated segmentation algorithms. Thereby, allowing to increase the time-efficiency and precision regardless of the operator's experience. Recently, 3D U-Net based deep learning models have been successfully applied for the segmentation of various craniomaxillofacial anatomical structures such as mandible^{9, 10}, mandibular canal^{11, 12}, pharyngeal airway space¹³, and teeth^{14, 15}. However, no evidence has been reported related to the application of CNNs for segmentation of midfacial structures. Therefore, the present thesis builds on well-established research aims and questions, going from the validation of CNN-based automated approaches for segmentation of the midfacial skeletal complex and maxillary sinus to the deployment of these networks within specific clinical workflows. This integration of automated segmentation in digital workflows could decrease a surgeon's load and improve the precision of diagnostics, treatment planning, and follow-up evaluation of patients where the midfacial region is involved, such as in orthognathic surgery, reconstructive surgery, traumatology, and dental implant surgery.

Firstly, CNN-based models were validated, and their performance was evaluated for the automated segmentation of midfacial structures. In **article 1**, we investigated the performance of a deep CNN-based model for the automated segmentation of the midfacial skeletal complex on CBCT images. Based on the performance metrics, the average time required for automated segmentation was 39.07s, compared to the corresponding manual time of 132.7 min. The CNN model demonstrated a high DSC value of 92.6%, thereby confirming high similarity between automated and manual segmentation. The qualitative visual examination of automated segmentation revealed that corrections were required to improve the final segmentation. At the same instance, a DSC value of 99.8% existed between automated and refined models, which confirmed a high degree of similarity between them and indicated that minor corrections were required.

In **article 2**, we investigated the accuracy, consistency, and time-efficiency of a deep CNN-based model for automated maxillary sinus segmentation on CBCT images in comparison to semi-automated segmentation as the reference standard. Based on performance metrics, the average time required for automated segmentation (for both sinuses) was 24.4s, compared to 60.8 min with semi-automated approach. The CNN model showed a high DSC of 98.4%, indicating that minimal corrections were required. Based on the visual examination of automated segmentations, 70% of the testing set was categorized as perfect segmentation requiring no refinements, while the remaining 30% required minor corrections. Intra- and inter-observer reliability showed excellent consistency, with DSC values of 98.4% and 99.6%, respectively. The models in both articles were able to generate identical segmentation results if a similar scan was processed, thereby confirming their consistency and independence from observer's experience-based variabilities. Furthermore, the models were trained using two CBCT devices with different scanning parameters and presence of metallic artifacts for ensuring its generalizability.

The architecture pipeline of CNN models in both **article 1** and **article 2** was similar, as illustrated in Figure 1, yet minor differences existed related to their performance metrics and time-efficiency. The average timing for sinus segmentation was slightly less than for the midfacial skeletal complex. This might be attributed to the difference in FOV and complexity of the datasets, where midfacial skeletal data had a larger FOV and complex anatomy, requiring more time for data processing. Considering the segmentation performance, the maxillary sinus showed a higher DSC value than the midfacial complex. Unlike the maxillary skeletal region, the sinus is a well-defined structure with distinct surrounding borders, which makes it easier for the CNN to learn the features. However, it should be kept in mind that certain cases were prone to lower performance. For instance, the CNN model was not able to appreciate the margins of the skeletal complex where narrow or ill-defined sutures existed. In addition, performance dropped in cases where mucosal thickening was observed in the sinus region. Hence, incorporating larger heterogenous datasets might lead to higher performance.

The findings of both articles were in accordance with our hypothesis that CNN models offered an accurate, consistent, and time-efficient segmentation approach compared to manual or semi-automated approaches. The proposed CNN models could allow for accurate 3D virtual model creation in clinical digital workflows for diagnostics and treatment planning. More importantly, the CNN model was integrated into an interactive online platform that fits the current demand of a clinical practice by offering a user-friendly approach without the need of an experienced operator or a computer with high computational power. However, both articles shared main limitations, such as a lack of data heterogeneity and the need for a third-party software program for performing required corrections as the online platform lacked a correction service. In addition, the model in **article 1** was

only able to segment the midfacial complex as a whole, not individual skeletal structures. On the other hand, the model in **article 2** was only able to delineate the sinus bony borders without considering the sinus mucosal thickening.

Individual anatomical structures segmentation is important for defining the normal anatomy, differentiating it from pathological conditions, and 3D evaluation of specific regions of interest. On the other hand, multi-structural segmentation is equally important for providing a complete picture of the patient and for investigating relationship with the surrounding structures. Therefore, in **article 3**, we assessed the qualitative and quantitative performance of an integrated tri-CNN model for the creation of a segmented MVP consisting of the midfacial complex, maxillary sinuses, and teeth from CBCT images. The main focus of this study was to observe the number of refinements required to achieve a perfect segmentation of a virtual patient, which could further allow to know the deficiencies and improve the model performance. As the clinical relevance of such refinements might vary depending on the task at hand, for example, diagnostics and treatment planning require more refined segmentation compared to visualization and patient education. Moreover, each type of refinement might be more relevant in a specific clinical specialty compared to another one. The qualitative assessment based on visual inspection revealed no overlap between the three anatomical structures. On a scale of 0 to 10, representing the number of refinements required (where 0 = ten or more refinements, 10 = no refinement), 85% of the dataset showed a score of 7 or more, and 15% were within the range of 3-6. Regarding the quantitative assessment, the average time required for automated segmentation was 1.7 min. A DSC of 99.3% existed between automated and refined segmentation, implying that minimal refinements were required. Interobserver consistency of the refinements also showed a high DSC value of 99.8%, suggesting a substantial agreement between observers. Furthermore, in this study, one of the previously mentioned limitations of using third-party software programs for refinements was solved by incorporating smart correction tools into the online platform. On the basis of these findings, the integrated CNN models could act as a clinically viable tool for multiple applications in orthodontics and reconstructive surgery, where analyzing both the segmented structures and their relationship with the surrounding tissue is essential for reaching an accurate diagnosis and patient-specific treatment planning.

Even though the CNN-based deep learning algorithms showed promising performance, it is still vital to assess their performance and technical errors for different clinical applications involving segmentation of the midfacial structures. In **article 4**, we used the validated tool in **article 1** to quantify the symmetry of the midfacial complex on CBCT images of skeletal class I patients. We hypothesized that the automation of the segmentation step would improve the precision and time-efficiency of the symmetry evaluation process in combination with automated mirroring and

registration. This could improve clinical outcomes in patients requiring reconstructive surgical planning through mirroring. The visual assessment of the automated segmentations showed that 20% of the whole dataset required minor correction. The rTEM values ranged from good to excellent for both intra- and inter-observer error, thereby supporting the clinical applicability of the proposed methodology. Overall, mean and root mean square differences between true and mirrored models were within a range of 1mm, and no significant difference existed between left and right sides. Hence, further justifying the applicability of the proposed technique for mirroring reconstructive surgical techniques. Moreover, female patients showed higher midfacial complex symmetry than male patients. This could be attributed to the differences in growth patterns, facial proportions, and masticatory frequencies^{16, 17}. The presented findings could be used as a reference guide by surgeons when evaluating asymmetry and help with the decision-making for restoring midfacial defects. Furthermore, the proposed automated approach could be a viable alternative for achieving a precise diagnosis, surgical planning, and follow-up evaluation.

It should be noted that the proposed methodology for symmetry assessment was in accordance with the currently applied computer-assisted surgical planning methodologies for restoration of unilateral facial defects¹⁸. However, in cases with severe asymmetry, the closest point from one surface to another is not guaranteed to be an anatomically corresponding point, which might generate a strong underestimation of the actual asymmetry¹⁹. Hence, further studies are required to investigate alternative approaches for implementation in the surgical planning of such patients. Claes et al.¹⁹ proposed a spatially-dense and robust 3D facial asymmetry assessment protocol utilizing a weighted least squares superimposition that proved to be accurate when applied to subjects with both typical and disordered growth patterns. Besides, it allowed for quantifying a percentage of asymmetrical facial areas. Implementation of such methodology within the surgical planning protocols would be beneficial for pre- and post-surgical symmetry evaluation, especially for asymmetric cases. Furthermore, it could enhance the precision of mirroring reconstructive surgical procedures.

In **article 5**, the tool validated in **article 2** was used to quantify volumetric bone graft changes on CBCT images following lateral window sinus augmentation at three time points: T0 (presurgical), T1 (immediate postsurgical), and T2 (6 months postsurgical). This quantification is essential to ensure graft stability and predictability of success rates following implant placement. Visual inspection of the automated segmentations revealed that no refinements were required for cases at T0 time-points, while minor refinements were required for models generated at T1 and T2 time-points. Overall, rTEM values were classified as excellent, ranging from 0.2% to 0.25%. Both inter- and intra-observer ICC revealed excellent reliability for assessing volumetric differences, implying the reproducibility of the methodology.

Based on the findings of articles 4 and 5, automated segmentation proved to be clinically applicable for the assessment of skeletal symmetry and maxillary sinus changes. Further studies should be conducted to observe the performance and accuracy of automated segmentation in other clinical workflows and to determine whether it could act as a more accurate, reliable, and simplified alternative compared to conventional techniques.

Conclusions

The creation of a 3D virtual model through segmentation of dentomaxillofacial structures on CBCT images lies at the realm of various digital dental workflows. Integration between AI algorithms and dentomaxillofacial imaging has the ability to revolutionize clinical practice. Hence, this doctoral thesis focused on the value that AI can bring to the field of dentomaxillofacial radiology in the form of automated segmentation. The following conclusions can be drawn:

- The proposed CNN models proved to be highly time-efficient with optimal performance for the segmentation of midfacial structures, including the maxillary skeletal complex, maxillary sinus, and teeth.
- The CNN models could act as a plausible alternative to conventional manual and semi-automated segmentation approaches, and have the ability to improve the final treatment outcome and further enhance the level of patient care.
- The implementation of these automated tools in digital workflows for symmetry assessment and sinus changes confirmed their clinical applicability.
- The deployment of CNN models on an online cloud-based platform overcomes the need for high-performance computers; hence, reducing the costs for AI implementation in hospital settings.

Future perspectives

- Generally, artificial intelligence-based models have limited value in a daily clinical practice owing to the lack of model generalizability and data heterogeneity. There is still room for improvement before these models can be applied at a global level by incorporating training datasets acquired from different CBCT devices with various scanning parameters.

- Future studies should not only aim to develop models for the segmentation of normal anatomical structures but also focus on adding pathological cases, such as pathological sinus conditions, bone lesions, dentomaxillofacial fractures and craniofacial anomalies. The addition of such conditions in the training dataset could improve the standard of patient care. It is also essential to incorporate the validated individual and multi-structural segmentation approaches in different dentomaxillofacial planning workflows to assess their clinical applicability. Additionally, further studies should consider a combination of data from CBCT images, intra-oral scanner and/or facial scanners to enhance the delivery of personalized dental care.
- Further improvement of the online platform is required. In addition to smart tools for correction, extra tools for performing measurements, analysis, and boolean operations should be incorporated. Besides, it is also recommended to later implement algorithms for achieving automated treatment planning of various dentomaxillofacial procedures without the need for human intervention.
- Although U-net is most widely used for medical images, further studies should compare the performance of different networks²⁰ for the segmentation task on CBCT images, which has not been thoroughly investigated. At present, models lack standardization, CE certification, and medical device regulation (MDR) compliance, which should be considered going forward before their implementation in clinical practice. Furthermore, the cost–benefit ratio and cost effectiveness of AI need to be established.
- In relation to symmetry the assessment protocol, studies are required to establish automated segmentation approaches for individual structural segmentation and to evaluate the impact of these structures on the overall facial symmetry. Furthermore, future studies should investigate alternative approaches for surface registration taking the closest points as the corresponding points between the two surfaces.
- For sinus graft follow-up, further studies with a large sample size and longer follow-up are required to assess if the graft remains stable over time and to investigate the impact of different implant placement protocols on bone resorption. It is also recommended to train AI-based models to automatically extract and segment bone grafts from CBCT images to further enhance the efficacy of the follow-up assessment protocols.

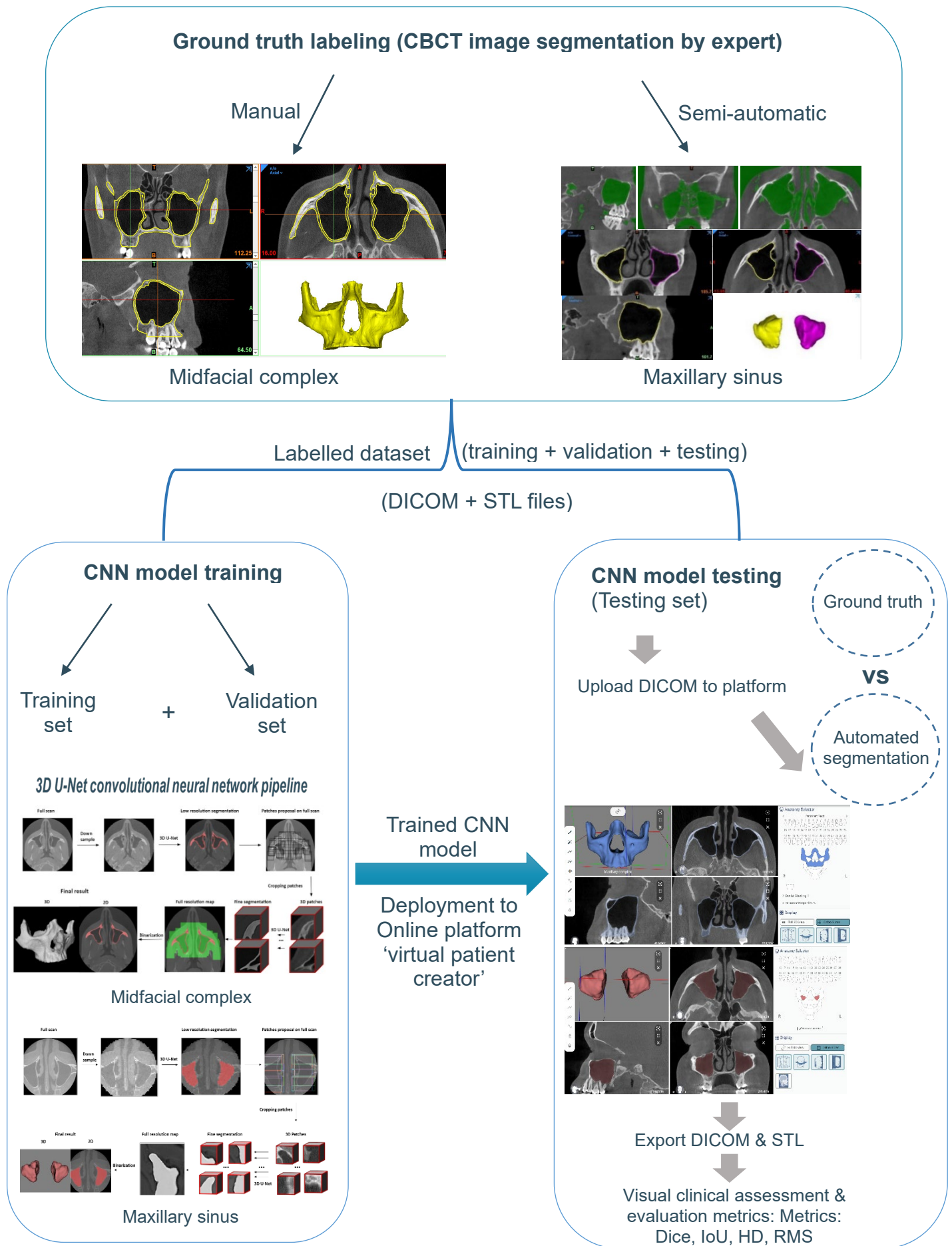


Figure 1. Flowchart of proposed methodology in article 1 & 2.

References

1. Ma, H., J. Van Dessel, M. Bila, Y. Sun, C. Politis, and R. Jacobs, *Application of Three-Dimensional Printed Customized Surgical Plates for Mandibular Reconstruction: Report of Consecutive Cases and Long-Term Postoperative Evaluation*. Journal of Craniofacial Surgery, 2021. **32**(7): p. e663-e667.
2. Matsumoto, K., S. Sherrill-Mix, N. Boucher, and N. Tanna, *A cone-beam computed tomographic evaluation of alveolar bone dimensional changes and the periodontal limits of mandibular incisor advancement in skeletal Class II patients*. The Angle Orthodontist, 2020. **90**(3): p. 330-338.
3. Azarmehr, I., K. Stokbro, R.B. Bell, and T. Thygesen, *Contemporary Techniques in Orbital Reconstruction: A Review of the Literature and Report of a Case Combining Surgical Navigation, Computer-Aided Surgical Simulation, and a Patient-Specific Implant*. Journal of Oral and Maxillofacial Surgery, 2020. **78**(4): p. 594-609.
4. Plooi, J.M., T.J.J. Maal, P. Haers, W.A. Borstlap, A.M. Kuijpers-Jagtman, and S.J. Bergé, *Digital three-dimensional image fusion processes for planning and evaluating orthodontics and orthognathic surgery. A systematic review*. International Journal of Oral and Maxillofacial Surgery, 2011. **40**(4): p. 341-352.
5. Uechi, J., Y. Tsuji, M. Konno, K. Hayashi, T. Shibata, E. Nakayama, and I. Mizoguchi, *Generation of virtual models for planning orthognathic surgery using a modified multimodal image fusion technique*. International Journal of Oral and Maxillofacial Surgery, 2015. **44**(4): p. 462-469.
6. Berberi, A., L. Bouserhal, N. Nader, R.B. Assaf, N.B. Nassif, J. Bouserhal, and Z. Salameh, *Evaluation of Three-Dimensional Volumetric Changes After Sinus Floor Augmentation with Mineralized Cortical Bone Allograft*. Journal of maxillofacial and oral surgery, 2015. **14**(3): p. 624-629.
7. Starch-Jensen, T. and J.D. Jensen, *Maxillary Sinus Floor Augmentation: a Review of Selected Treatment Modalities*. Journal of oral & maxillofacial research, 2017. **8**(3): p. e3-e3.
8. Morgan, N., A. Van Gerven, A. Smolders, K. de Faria Vasconcelos, H. Willems, and R. Jacobs, *Convolutional neural network for automatic maxillary sinus segmentation on cone-beam computed tomographic images*. Scientific Reports, 2022. **12**(1): p. 7523.
9. Egger, J., B. Pfarrkirchner, C. Gsaxner, L. Lindner, D. Schmalstieg, and J. Wallner, *Fully Convolutional Mandible Segmentation on a valid Ground- Truth Dataset*. Annu Int Conf IEEE Eng Med Biol Soc, 2018. **2018**: p. 656-660.
10. Verhelst, P.-J., A. Smolders, T. Beznik, J. Meewis, A. Vandemeulebroucke, E. Shaheen, A. Van Gerven, H. Willems, C. Politis, and R. Jacobs, *Layered deep learning for automatic mandibular segmentation in cone-beam computed tomography*. Journal of Dentistry, 2021. **114**: p. 103786.
11. Kwak, G.H., E.J. Kwak, J.M. Song, H.R. Park, Y.H. Jung, B.H. Cho, P. Hui, and J.J. Hwang, *Automatic mandibular canal detection using a deep convolutional neural network*. Sci Rep, 2020. **10**(1): p. 5711.

12. Lahoud, P., S. Diels, L. Niclaes, S. Van Aelst, H. Willems, A. Van Gerven, M. Quirynen, and R. Jacobs, *Development and validation of a novel artificial intelligence driven tool for accurate mandibular canal segmentation on CBCT*. Journal of Dentistry, 2022. **116**: p. 103891-103891.
13. Shujaat, S., O. Jazil, H. Willems, A. Van Gerven, E. Shaheen, C. Politis, and R. Jacobs, *Automatic segmentation of the pharyngeal airway space with convolutional neural network*. Journal of Dentistry, 2021. **111**: p. 103705.
14. Xu, X., C. Liu, and Y. Zheng, *3D Tooth Segmentation and Labeling Using Deep Convolutional Neural Networks*. IEEE Trans Vis Comput Graph, 2019. **25**(7): p. 2336-2348.
15. Lahoud, P., M. EzEldeen, T. Beznik, H. Willems, A. Leite, A. Van Gerven, and R. Jacobs, *Artificial Intelligence for Fast and Accurate 3-Dimensional Tooth Segmentation on Cone-beam Computed Tomography*. Journal of Endodontics, 2021. **47**(5): p. 827-835.
16. Ferrario, V.F., C. Sforza, G. Pizzini, G. Vogel, and A. Miani, *Sexual dimorphism in the human face assessed by euclidean distance matrix analysis*. J Anat, 1993. **183 (Pt 3)**(Pt 3): p. 593-600.
17. Thornhill, R. and S.W. Gangestad, *Facial sexual dimorphism, developmental stability, and susceptibility to disease in men and women*. Evolution and Human Behavior, 2006. **27**(2): p. 131-144.
18. Ho, J., R. Schreurs, S. Aydi, R. Rezai, T.J.J. Maal, A.J. van Wijk, L.F.M. Beenen, L. Dubois, D.M.J. Milstein, and A.G. Becking, *Natural variation of the zygomaticomaxillary complex symmetry in normal individuals*. J Craniomaxillofac Surg, 2017. **45**(12): p. 1927-1933.
19. Claes, P., M. Walters, D. Vandermeulen, and J.G. Clement, *Spatially-dense 3D facial asymmetry assessment in both typical and disordered growth*. J Anat, 2011. **219**(4): p. 444-55.
20. Siddique, N., S. Paheding, C.P. Elkin, and V. Devabhaktuni, *U-Net and Its Variants for Medical Image Segmentation: A Review of Theory and Applications*. IEEE Access, 2021. **9**: p. 82031-82057.

Summary

The integration of digital technology within each step of a dental workflow has transformed dentistry, as it can render the dental procedures in a more efficient way, saving time, increasing accuracy, facilitating the treatments, and improving the outcome to meet rising patient demands.

The first and most essential step in the majority of digital dental workflows is image segmentation in order to generate 3D models of the dentomaxillofacial structures, any flaw in this step would contribute towards accumulation of error in the later steps.

Considering the limitations of the conventional segmentation methods, recent application of deep convolutional neural networks (CNNs) has outperformed the previously available algorithms for modelling of the dentomaxillofacial region. These CNNs have been successfully applied with promising results for the CBCT-based automated segmentation of the teeth, pharyngeal airway space, inferior alveolar nerve canal, and mandible. However, a lack of evidence exists related to the CNN-based automated segmentation of the midfacial structures.

Hence, The overall aim of the PhD project is twofold. Firstly, to develop a tool for automatic segmentation of the midfacial structures (bone and air) on CBCT images. Secondly, to incorporate these automated virtual 3D models in clinical applications to assess its performance in the digital workflow. The hypothesis behind this work is that a deep CNN approach could offer a more accurate, consistent, and time-efficient segmentation compared to the present conventional approaches. Besides, it could deliver accurate and ready-to-print 3D models that are essential to patient-specific digital treatment planning.

In **articles 1,2** we investigated the performance of a deep CNN-based model for the automated midfacial complex bone and maxillary sinus segmentation from CBCT images. Based on the findings of both articles, the proposed CNN models provided fast, accurate, and consistent CBCT based automated segmentation, which could allow accurate 3D virtual models creation for diagnosis and treatment planning.

In **article 3**, we assessed the qualitative and quantitative performance of an integrated tri-CNN models for the creation of a segmented MVP consisting of midfacial complex, maxillary sinuses, and teeth from CBCT images. On the basis of the findings of this study, the integrated CNN models could provide a clinical valuable tool for multiple applications in orthodontics and maxillofacial surgery, where studying both the individual structure and its surrounding is essential to reach accurate diagnosis and patient-specific treatment planning.

In **article 4**, we used the developed tool in **article 1** to quantify the symmetry of midfacial complex on CBCT images of skeletal class I patients. The rTEM ranged from good to excellent for both intra- and inter observer error supporting the clinical applicability of the proposed methodology. The overall mean and RMS differences between true and mirrored models were within a range of 1mm, and no significant difference existed between left and right sides, which justifies the applicability of mirroring reconstructive surgical techniques. Based on the results of this study, the proposed automated approach could be a viable alternative for more precise diagnosis, surgical planning, and follow-up evaluation.

In **article 5**, the developed tool in **article 2** was used to assist for quantifying volumetric bone graft changes on CBCT images following lateral window sinus augmentation at three time points T0 (presurgical), T1 (immediate postsurgical), and T2 (6 months postsurgical). This quantification is essential to ensure the graft stability and predictability of high success rate after implant placement. The average bone gain immediately after graft insertion was $2.11 \pm 1.25 \text{ cm}^3$, while at follow-up of 6 months, minor bone resorption of 5.3% was observed ($0.11 \pm 0.13 \text{ cm}^3$). The overall rTEM values were classified as excellent, ranging from 0.2% to 0.25%. Both inter- and intra-observer ICC revealed excellence reliability for assessing volumetric differences, implying the reproducibility of the methodology.

The findings of this doctoral thesis showed that the proposed CNN models proved to be fast, accurate, and consistent, alternative to the conventional manual and semi-automated segmentation methods, rendering the clinical procedures in more efficient and easier way for the operator as well as improving the final outcome for the patients.

Samenvatting

De integratie van digitale technologie in elke stap van een tandheelkundige workflow heeft de tandheelkunde veranderd, omdat het de tandheelkundige procedures op een efficiëntere manier kan weergeven, tijd bespaart, de nauwkeurigheid verhoogt, de behandelingen vergemakkelijkt en het resultaat verbetert om aan de toenemende eisen van de patiënt te voldoen.

De eerste en meest essentiële stap in de meeste digitale tandheelkundige workflows is beeldsegmentatie om 3D-modellen van de dentomaxillofaciale structuren te genereren.

Gezien de beperkingen van de conventionele segmentatiemethoden heeft de recente toepassing van diepe convolutionele neurale netwerken (CNN's) de eerder beschikbare algoritmen voor de modellering van het dentomaxillofaciale gebied overtroffen. Deze CNN's zijn met succes toegepast met veelbelovende resultaten voor de CBCT-gebaseerde automatische segmentatie van de tanden, de faryngeale luchtwegruimte, het nervus alveolaris inferior en de onderkaak. Er is echter een gebrek aan bewijs met betrekking tot de CNN-gebaseerde automatische segmentatie van de midfaciale structuren.

De algemene doelstelling van het doctoraatsproject is dan ook tweeledig. Ten eerste, het ontwikkelen van een tool voor automatische segmentatie van de midfaciale structuren (bot en lucht) op CBCT beelden. Ten tweede, het opnemen van deze geautomatiseerde virtuele 3D-modellen in klinische toepassingen om de prestaties ervan in de digitale workflow te beoordelen. De hypothese achter dit werk is dat een diepe CNN-benadering een nauwkeurigere, consistentere en tijdsefficiëntere segmentatie kan bieden dan de huidige conventionele benaderingen. Bovendien zou het nauwkeurige en printklare 3D-modellen kunnen opleveren die essentieel zijn voor patiënt-specifieke digitale behandelplanning.

In **artikels 1,2** onderzochten wij de prestaties van een diep CNN-gebaseerd model voor de geautomatiseerde segmentatie van het middengehemeltecomplex en de sinus maxillaris uit CBCT-beelden. Uit de bevindingen van beide artikelen blijkt dat de voorgestelde CNN-modellen een snelle, nauwkeurige en consistente CBCT-gebaseerde automatische segmentatie opleveren, waarmee nauwkeurige virtuele 3D-modellen kunnen worden gemaakt voor diagnose en behandelplanning.

In **artikel 3** evalueerden wij de kwalitatieve en kwantitatieve prestaties van een geïntegreerd tri-CNN model voor het maken van een gesegmenteerd MVP bestaande uit het middengezichtscomplex, de maxillaire sinussen en de tanden op basis van CBCT beelden. Op basis van de bevindingen van deze studie zouden de geïntegreerde CNN-modellen een klinisch waardevol hulpmiddel kunnen vormen voor meerdere toepassingen in de orthodontie en de maxillofaciale chirurgie, waar het bestuderen van zowel de individuele structuur als de omgeving ervan essentieel is om tot een nauwkeurige diagnose en patiënt-specifieke behandelplanning te komen.

In **artikel 4** hebben wij het in **artikel 1** ontwikkelde instrument gebruikt om de symmetrie van het middengezichtscomplex te kwantificeren op CBCT-beelden van skeletklasse I-patiënten. De rTEM varieerde van goed tot uitstekend voor zowel intra- als interobservatiefouten, wat de klinische toepasbaarheid van de voorgestelde methode ondersteunt. De totale gemiddelde en RMS-verschillen tussen ware en gespiegelde modellen lagen binnen een bereik van 1 mm, en er was geen significant verschil tussen linker- en rechterzijde, wat de toepasbaarheid van spiegelende reconstructieve chirurgische technieken rechtvaardigt. Op basis van de resultaten van deze studie zou de voorgestelde geautomatiseerde aanpak een haalbaar alternatief kunnen zijn voor een nauwkeuriger diagnose, chirurgische planning en follow-up evaluatie.

In **artikel 5** werd het in **artikel 2** ontwikkelde instrument gebruikt als hulpmiddel voor het kwantificeren van volumetrische veranderingen in het bottransplantaat op CBCT-beelden na een sinusaugmentatie op drie tijdstippen: T0 (vóór de operatie), T1 (onmiddellijk na de operatie) en T2 (6 maanden na de operatie). Deze kwantificering is essentieel voor de stabiliteit van het transplantaat en de voorspelbaarheid van een hoog succespercentage na plaatsing van het implantaat. De gemiddelde botwinst onmiddellijk na het inbrengen van het transplantaat was $2,11 \pm 1,25$ cm³, terwijl bij de follow-up van 6 maanden een geringe botresorptie van 5,3% werd waargenomen ($0,11 \pm 0,13$ cm³). De totale rTEM-waarden werden geclassificeerd als uitstekend, variërend van 0,2% tot 0,25%. Zowel de inter- als intra-observer ICC toonde een uitstekende betrouwbaarheid voor de beoordeling van volumetrische verschillen, hetgeen de reproduceerbaarheid van de methodologie impliceert.

De bevindingen van dit proefschrift toonden aan dat de voorgestelde CNN-modellen een snel, accuraat en consistent alternatief bleken te zijn voor de conventionele manuele en semi-automatische segmentatiemethoden, waardoor de klinische procedures efficiënter en gemakkelijker verlopen voor de operator en het eindresultaat voor de patiënten verbeterd.

SCIENTIFIC ACKNOWLEDGEMENTS

This work could not have successfully reached its completion without the scientific contribution from certain individuals whom I would like to extend my gratitude.

Article 1: I would like to thank **Flavia Preda** for being the first shared author of this study, providing equal contributions to me as well as coordinating responsibility for the research execution. Thanks to the efforts of **Fernanda Nogueira-Reis** and **Xiaotong Wang** for their valuable contributions in data labeling and clinical validation.

Article 2: Thanks to the efforts of **Karla de Faria Vasconcelos** for her valuable contribution as a second observer of this study.

Article 3: I would like to thank **Fernanda Nogueira-Reis** for her help in designing the protocol of this study and providing data visualization.

Article 1-3: I would like to thank **ReLu team (Adriaan Van Gerven, Andreas Smolders, Stefanos Nomidis, and Holger Willems)** for the help to build and train the related networks and for providing computing resources.

Article 4: I would like to thank **Sohaib Shujaat and Kevin Dotremont** for their help in designing the protocol of this study and checking the clinical and technical aspects of the manuscript, respectively. Thanks to the efforts of **Omid Jazil** for his valuable contribution as a second observer of this study.

Article 5: I would like to thank **Simone Cortellini** for providing research data. Thanks to **Sohaib Shujaat** for his help in preparing the published work. Thanks to the efforts of **Fernanda Nogueira-Reis** for her valuable contribution as a second observer of this study.

Lastly, I would like to sincerely acknowledge my promoter, **Prof. Dr. Reinhilde Jacobs** for her scientific support and contributions throughout the duration of the PhD.

PERSONAL CONTRIBUTIONS

The author, **Nermin Morgan**, devised the projects and the main conceptual ideas, collected patients' clinical and radiological data, performed the experiments, analyzed data, and took the lead in writing the (peer-reviewed) manuscripts with scientific support from her promoter, Prof. Dr. Reinhilde Jacobs. The detailed personal contributions for each article are as follows:

Article 1 (*shared first authorship*): Conceptualization, Methodology (dataset segmentation/clinical evaluation), Validation, formal analysis, investigation, Data Curation, Writing – original draft, Writing – review & editing, Visualization.

Article 2 (*first author*): Conceptualization, Methodology (dataset segmentation/clinical evaluation), Validation, formal analysis, investigation, Data Curation, Writing – original draft, Writing – review & editing, Visualization, Project administration.

Article 3 (*second author*): Conceptualization, Methodology (segmentation refinements/clinical evaluation), Validation, formal analysis, investigation, Writing – original draft, Writing – review & editing.

Article 4 (*first author*): Conceptualization, Methodology, Validation, formal analysis, investigation, Data Curation, Writing – original draft, Writing – review & editing, Visualization, Project administration.

Article 5 (*first author*): Conceptualization, Methodology, Validation, formal analysis, investigation, Data Curation, Writing – original draft, Writing – review & editing, Visualization, Project administration.

CONFLICTS OF INTEREST

The author, Nermin Morgan, declares that Adriaan Van Gerven, Andreas Smolders, Stefanos Nomidis, and Holger Willems have professional relationships with Relu BV (ownership, development, and commercial interests), which may be considered as potential competing interests.



CURRICULUM VITAE

Nermin Morgan

Born on September 20th, 1990, in Dakahliya, Egypt

Education

- | | |
|------|--|
| 2022 | Postgraduate studies in advanced medical imaging, KU Leuven, Belgium |
| 2021 | Equivalence to the Flemish degree of "Master of Science in Dentistry" recognized by NARIC-Vlaanderen, Belgium |
| 2017 | Master of Oral Diagnosis and Radiology (MSc) Faculty of Dentistry, Mansoura University, Egypt |
| 2012 | Bachelor of Dental Surgery (B.D.S) Faculty of Dentistry, Mansoura University, Egypt |

Experience

- | | |
|----------------|---|
| 2019 – Present | Doctoral researcher at OMFS-IMPACT research group, KU Leuven (Image analysis and segmentation- academic research writing- collaboration with RELU company) |
| 2017 - Present | Teaching assistant of Oral Radiology and diagnostic sciences Faculty of Dentistry, Mansoura University, Egypt |
| 2013 - 2019 | General Dentist
Outpatient clinics, Mansoura University Dental Hospital, Egypt |
| 2013 - 2017 | Clinical demonstrator of Oral Radiology and diagnostic sciences Faculty of Dentistry, Mansoura University, Egypt |

Publications

- **Morgan N**, Shujaat S, Jazil O, Jacobs R. Three-dimensional quantification of skeletal midfacial complex symmetry. Int J CARS (2022). <https://doi.org/10.1007/s11548-022-02775-0>
- Nogueira-Reis F, **Morgan N**, Nomidis S, Van Gerven A, Oliveira-Santos N, Jacobs R, Tabchoury CPM. Three-dimensional maxillary virtual patient creation by convolutional neural network-based segmentation on cone-beam computed tomography images. Clin Oral Investig. 2022 Sep 17. doi: 10.1007/s00784-022-04708-2. Epub ahead of print. PMID: 36114907.
- Preda F, **Morgan N**, Van Gerven A, Nogueira-Reis F, Smolders A, Wang X, Nomidis S, Shaheen E, Willems H, Jacobs R. Deep convolutional neural network-based automated segmentation of the maxillofacial complex from cone-beam computed tomography - A validation study. J Dent. 2022 Jul 21:104238. doi: 10.1016/j.jdent.2022.104238. Epub ahead of print. PMID: 35872223.
- **Morgan, N.**, Van Gerven, A., Smolders, A. et al. Convolutional neural network for automatic maxillary sinus segmentation on cone-beam computed tomographic images. Sci Rep 12, 7523 (2022). <https://doi.org/10.1038/s41598-022-11483-3>
- Alqahtani KA, Shaheen E, **Morgan N**, Shujaat S, Politis C, Jacobs R. Impact of orthognathic surgery on root resorption: A systematic review. J Stomatol Oral Maxillofac Surg. 2022 Apr 25:S2468-7855(22)00100-8. doi: 10.1016/j.jormas.2022.04.010. Epub ahead of print. PMID: 35477011.
- **Morgan N**, Suryani I, Shujaat S, Jacobs R. Three-dimensional facial hard tissue symmetry in a healthy Caucasian population group: a systematic review. Clin Oral Investig. 2021 Aug 13. doi: 10.1007/s00784-021-04126-w. Epub ahead of print. PMID: 34386858.
- Aboelmaaty, W., **Morgan, N.**, Abdelfadil, E. & Ashmawy, M. Accuracy of QuickScan Imaging Protocols of iCAT FLX CBCT in Assessment of Peri-implant Bone Defects. Egyptian Dental Journal 64, 2327-2336, doi:10.21608/edj.2018.76810 (2018).

International Presentation

- **E-poster, “Automated prediction of graft volume for maxillary sinus augmentation”, European Association of Osseointegration Annual Congress**
Geneva, Switzerland - From 29th September to -1st October 2022
- **E-presentation, “Automated Segmentation of Midfacial Structures on CBCT Images Using Deep Convolutional Neural Network”, 18th European Congress of DentoMaxilloFacial Radiology**
Lublin, Poland - From 8-10th June 2022

- **Webinar presentation, “Automated CBCT Image Segmentation of the Maxillary Sinus”, The Department of Oral Medicine and Diagnostic Sciences at the King Saud University College of Dentistry**

Riyadh, Saudi Arabia – on 28th June 2021

- **E-poster presentation, “Automatic Segmentation of Maxillary Sinus”, 23rd International Congress of DentoMaxilloFacial Radiology**

Gwangju, South Korea - From 28th April to 1st May 2021

- **Chair session & Oral presentation, “Accuracy of Low Dose Imaging Protocols of CBCT in Assessment of Peri-implant Bone Defects”, 33rd International Congress on Computer Assisted Radiology and Surgery**

Rennes, France - From 17-21 June 2019

- **Oral presentation, " Assessment of dental implants by various radiographic techniques", Egyptian Dental Syndicate International Congress**

Cairo, Egypt - From 13-15 September 2017

- **Oral presentation, “Detection of various width and depth of peri-implant crestal bone defects with different imaging modalities”, 31st International Congress on Computed Assisted Radiology and Surgery**

Barcelona, Spain – From 20-24 June 2017

- **Oral presentation, “Clinical accuracy of pre-bending of titanium reconstructive plates on 3D printed models from CBCT for mandibular defects”, 30th International Congress on Computed Assisted Radiology and Surgery**

Heidelberg, Germany – From 21-25 June 2016

Awards

- **1st prize oral presentation, 18th European Congress of DentoMaxilloFacial Radiology (2022)**

*The author of this PhD manuscript, **Nermin Morgan**, obtained her degree in Bachelor of Dental Surgery (B.D.S.) from the Faculty of Dentistry, Mansoura University, Egypt (2007–2012), followed by an internship year at the faculty clinics. After her graduation, she worked there as a teaching assistant in the department of Oral radiology and Diagnostic sciences (2013–2019). Meanwhile, she has earned her master's degree of Oral Diagnosis and Radiology (2017). The same year, she became a radiology specialist at the Ministry of Health in Cairo, Egypt. Her research work has focused on Cone Beam CT (CBCT) and its different clinical applications in the maxillofacial region.*

From June 2019 till December 2022, she was a PhD researcher in the OMFS-IMPACT research group, with Prof. Dr. Reinhilde Jacobs as her scientific promoter. The research topic for her PhD was focused towards automated segmentation of midfacial structures on CBCT images and its applications in clinical practice. During her PhD studies, she also achieved her degree in Postgraduate studies in advanced medical imaging at KU Leuven, Belgium.

The first and most essential step in the majority of digital dental workflows is image segmentation in order to generate 3D models of the dentomaxillofacial structures; any flaw in this step would contribute towards the accumulation of error in the later steps. This doctoral thesis aimed, firstly, to develop a CNN-based deep learning tool for automated 3D segmentation of the midfacial structures on CBCT images. Secondly, to incorporate these automated virtual 3D models in clinical applications to assess their performance in the digital workflow. The outcomes of this thesis showed that the CNN models could act as a plausible alternative to conventional manual and semi-automated segmentation approaches and have the ability to improve the final treatment outcome and further enhance the level of patient care.



KU LEUVEN